DEVELOPMENT, VALIDATION, AND USE OF A

QUANTITATIVE THEORY OF IN VIVO DOPAMINE DYNAMICS

by

Seth Holt Walters

B.S. Cellular & Molecular Biology, Ohio University, 2006

Submitted to the Graduate Faculty of the

Kenneth P. Dietrich School of Arts and Sciences in partial fulfillment

of the requirements for the degree of

Doctor of Philosophy

University of Pittsburgh

2016

UNIVERSITY OF PITTSBURGH

DIETRICH SCHOOL OF ARTS AND SCIENCES

This dissertation was presented

by

Seth Holt Walters

It was defended on

August 11th, 2016

and approved by

Steven G. Weber, Professor, Department of Chemistry

Shigeru Amemiya, Associate Professor, Department of Chemistry

Amy K. Wagner, Associate Professor, Physical Medicine and Rehabilitation

Dissertation Advisor: Adrian C. Michael, Professor, Department of Chemistry

DEVELOPMENT, VALIDATION, AND USE OF A QUANTITATIVE THEORY OF DOPAMINE DYNAMICS

Seth Walters, PhD

University of Pittsburgh, 2016

Since the early 1980s, fast scan cyclic voltammetry (FSCV) has been used to detect changes in dopamine's presence in the brain's extracellular space. The dopamine signals detected result from several simultaneous biophysical processes. Because these processes currently cannot be directly measured, a mathematical model which quantitatively explains FSCV data is necessary to describe their natures and magnitudes. I have created a simple mathematical model which posits that diffusion of dopamine in the brain follows a unidirectional first order kinetic scheme from its source. The model, using just three parameters, produces excellent fits to dopamine responses evoked by short electrical stimuli. These parameters are: R_p (release), k_U (uptake) and k_T (mass transport). When longer stimulations are performed, the addition of a term k_R, which modifies R_p by an exponential, is adequate to fit nearly all observed dopamine responses in the anaesthetized rat brain.

To complement this work, I have determined that the ubiquitous failure of dopamine concentration changes as measured by FSCV to return to baseline, called hang-up, is an artifact caused by a form of long duration adsorption to the carbon fiber electrodes commonly used to measure dopamine. I have developed a mathematical correction for this artifact. In addition, I have experimentally determined that the observed first order behavior of the mass transport parameter k_T arises essentially entirely from the brain itself, rather than the adsorption kinetics of dopamine at the electrode.

Finally, having established a sound theoretical framework for understanding the biological and instrumental origins of dopamine signals in the brain, I have used this model to study both anatomical differences in dopamine signaling, as well as the biophysical effects of the drug bupropion, an antidepressant. These studies have found that the density of dopamine signaling is greatest in the dorsolateral striatum, and that this high density of signaling is enabled by high rates of dopamine uptake, which attenuate the spatial range of dopamine signaling. I anticipate that this work is a necessary step towards the comprehensive mechanistic dissection of cellular signaling, and I hope it will prove invaluable to future progress.

TABLE OF CONTENTS

LIST OF TABLES

LIST OF FIGURES

LIST OF EQUATIONS

PREFACE

The search for knowledge is older than recorded history. This text is an accounting of my contribution to that search. It is important to acknowledge the contributions that others have made that have allowed this work to come to fruition. I must first thank Professor Adrian Michael for uncounted hours of discussion, for teaching me how to write code, and for all the advice he has given me. Adrian has had an interest in kinetic modeling of brain processes for quite some time, and has not been afraid or hesitant to question old ideas throughout the latest chapter of his efforts to shed light on dopamine dynamics in the brain. This is not an easy path to take, but it is a necessary one, and I am grateful to have had a mentor with his attitude and inclinations. Without Adrian's mentorship and support I would not have had the freedom to conduct the work that I did, and I believe that our work will stand the test of time as an important step forward in understanding of brain function. I am therefore grateful for having had the opportunity to learn from and work with him.

I also wish to acknowledge all of my coworkers, and especially the coworkers with whom I worked closely. Drs. Mitch Taylor and Zhan Shu taught me how to do surgery, and also provided me with reams of data which was of invaluable help in developing the model presented in this work. Many hours of conversation with both of them helped guide me to the quantitative ideas I eventually developed. I also worked closely with Elaine Robbins, a graduate student two

1.0   INTRODUCTION

The study of the function of brains is one of the most important fields of scientific inquiry. One can imagine a full and complete understanding of the operational principles of brains, coupled with advances in molecular biology and hardware engineering, conferring the ability both to repair and enhance the function of existing brains, and to design, build, and operate new brains in biological, electronic, and various other operating media. Such advances should help to drive the efficient conversion of energy into cognition, which has the potential to cause an unsurpassed economic paradigm shift.

While our understanding of how brains operate currently remains incomplete, substantial detail is known. In particular, brains can be understood as networks of cells which engage in electrical and chemical communication with one another, and which can preserve persistent memory. The feeding of informational inputs into this network and the interaction of these inputs with the memory allows for a brain to generate an effective response output to any given input. The exchange of this information within the cellular network is mediated by chemicals known as neurotransmitters, of which there are on the order of 10^2, and which have several different modes of action. In many cases, neurotransmitters act on a subsecond time scale, and it is therefore important to understand the spatial and temporal dynamics of neurotransmitters to understand how they achieve the transmission of information.

1.1 DOPAMINE IS A NEUROTRANSMITTER

One of the most extensively studied neurotransmitters is dopamine (DA). DA has several characteristics which have contributed to this. DA is critically important for brain functions ranging from the control of movement to reward and learning. It is the substantial societal costs associated with the breakdown of these functions, particularly in the context of drugs of abuse such as cocaine and methamphetamine, and diseases of old age such as Parkinsons, that have made the study of DA a key target of funding agencies. In addition, DA happens to be one of a few neurotransmitters which are amenable to rapid oxidation-reduction cycles. It is its facile oxidation which has made it possible to study DA's subsecond dynamics at microelectrodes with electrochemical methods such as amperometry and fast scan cyclic voltammetry. The available geometries of microelectrodes mean that it is possible to measure DA at or near the smallest spatial scales of functional relevance, while the relatively fast redox kinetics of DA mean that it is also possible to measure DA at the fastest temporal scales of functional relevance as well. DA also commonly reaches transient concentration changes in the brain microenviroment in the micromolar range; many other neurotransmitter transients are orders of magnitude smaller. The vast majority of neurotransmitters are currently not measurable on a subsecond timescale and to a high spatial resolution, because they lack one or more of the characteristics of dopamine which make it amenable to study.

1.2   HOW DOPAMINE IS MEASURED

Since the early 1980s, DA has been measured in brain tissue at carbon fiber microelectrodes with a technique known as fast scan cyclic voltammetry (FSCV).[1,2] To perform FSCV, the electrical potential at a microelectrode (versus an Ag/AgCl reference electrode) is scanned in some direction, and the direction of the scan is reversed at least once, in order to finish the scan at the potential at which it started. FSCV is commonly conducted at a scan rate of 400 V/s in order to measure DA. As the potential at the surface of the microelectrode changes, the thermodynamic favorability of redox reactions in the local environment also changes. As a redox reaction becomes thermodynamically favorable, it proceeds at a rate according to the rate law and kinetic constants of the reaction. This reaction is detected as a current flow to the instrumentation. The recorded flow of current is commonly charted against the applied potential to form what is called a cyclic voltammogram (CV). The redox reaction kinetics and thermodynamics are determined by the chemical identity of the redox couple, as well as the composition and dimensions of the electrode, as well as any other species present in the reaction solution which might influence the kinetics or thermodynamics of the reaction, or influence the adsorption of DA to the surface of the electrode. In addition to this, the simple act of rapidly scanning a potential at a microelectrode has the effect of psuedocapacitive charging and discharging. The pseudocapacitive current at a microelectrode is considerably larger than the faradaic current that typically results from measuring physiological concentrations of DA. It is therefore necessary to perform background subtraction of the CVs; that is to say, a CV can be recorded before some independent variable, such as an electrical stimulus of dopaminergic neurons. This CV can then be subtracted from CVs recorded after the electrical stimulus, which

yields the faradaic current that results from the independent variable.   This background-subtracted faradaic current can then be converted to a concentration of DA at each timepoint by means of a calibration curve.

Figure 1. Fast Scan Cyclic Voltammetry of Dopamine
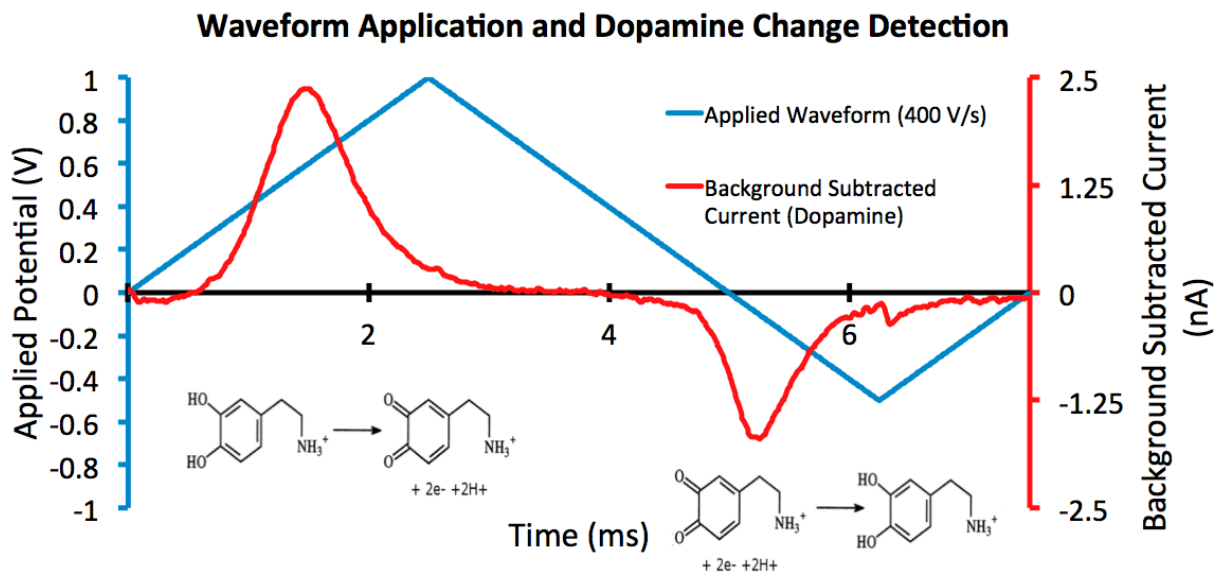
Figure 1: The detection of dopamine (DA) with fast scan cyclic voltammetry (FSCV). Faradaic current, shown in red, increases as the potential is ramped up, and then decreases to zero as all of the DA in the vicinity of the electrode is oxidized.   When applied potential becomes sufficiently low, the Faradaic current becomes negative as the newly formed quinone product undergoes a two electron reduction to regenerate DA. The non-Faradaic current has been removed from this data by background subtraction.   The concentration of DA present at the electrode during the approximately 8 millisecond scan can be determined by applying an experimentally-determined calibration factor to the peak oxidation current.

2.0   HISTORY OF DOPAMINE FSCV DATA ANALYSIS

This chapter presents a history of major developments of new ideas in the analysis of dopamine FSCV data, which attempt to parse additional information out of the response other than amplitude and duration of the evoked DA overflow. I will discuss only those analysis methods which make claims about the nature of the entire FSCV response and also present a new claim or insight.

2.1   THE ORIGINAL DOPAMINE KINETIC MODEL (1988)

The ability to measure evoked dopamine responses in the brain was developed in the very late 1970s and early 1980s. However, it was not until 1988 that a comprehensive whole curve analysis method for evoked DA responses as measured by FSCV was reported.[3] The math that decribes this original model is reproduced below:

Equation 1: The Original DA Model

$$\frac{d[DA]}{dt} = [DA]_p \cdot f - \frac{V_{max} \cdot [DA]}{[DA] + K_M}$$

The original model employs a scaling term, $[DA]_p$ specifying an increase in concentration of DA caused by each stimulus pulse within the extracellular volume that is sampled by the electrode. This increase is applied at the stimulus frequncy f. The other two parameters (V_{max} and K_M) describe uptake of DA from the extracellular space as the initial rate parameters of Michaelis-Menten kinetics. This gives the original DA model three adjustable parameters (since frequency f is defined by the experiment). However, while this model is able to approximate some evoked DA responses, it is unable by itself to generate responses which increase at an increasing rate over time, or responses which exhibit a signal overshoot. These deficiencies of the original model were remedied by the assumption of the existence of a physical gap between the DA terminals and the recording electrode.[3] It requires at least one additional adjustable parameter to specify the existence of a gap, so the more complex version of the original DA model requires 4 adjustable parameters. In practice, FSCV data were often deconvoluted[3–5] to account for the hypothesized diffusion gap, as opposed to being modeled with an extra parameter to account for the diffusion gap, but the mathematical complexity of the model is equivalent whichever way the calculation is carried out. In some cases, the deconvolution for a gap was intended to account for a layer of Nafion[6] coating the electrode, the purpose of which was to shield the electrode from interferents. However, in other cases, gap deconvolution was used with no Nafion layer[7] - being intended to represent the hypothesized instrinsic gap dimension present in the experiment. To date, there has been no experimental confirmation of the existence of physical diffusion gaps in the context of the FSCV experiment. The original DA model has seen heavy use in order to extract kinetic parameters describing brain activity from FSCV data.[7–10]

2.2   FIRST CONSIDERATION OF INSTRUMENTAL EFFECTS (2000)

The original evoked DA model does not account for the response time of the measurement system, in effect assuming that all responses are instantaneous. However, as a series of studies[11–13] quantifying the adsorption characteristics of the carbon fiber microelectrodes used in FSCV demonstrated, the response time resulting from adsorption is usually fast under most conditions, but not instantaneous. The potentially distorting effects of adsorption offer another possible explanation for responses which increase with time, as well as signal overshoots. The putative effects of adsorption on the kinetics of DA responses were not addressed[14] until after I had begun the work detailed in this document. Critically, this attempt at accounting for instrumental effects did not use data derived from the FSCV experiment, but from an entirely different kind of experiment called FSCAV. It was not confirmed that these FSCAV-derived parameters could be applied to FSCV to determine the extent to which adsorption distorted the dynamics of the evoked DA overflow. However, the body of work on DA adsorption to carbon fiber microelectrodes suggested that adsorption could be partially or wholly responsible for lag and overshoot distortions of the response features.

2.3   EXTENSION OF THE ORIGINAL MODEL (2003)

One case where the original DA model does not do an especially good job of accounting for the data is cases where the rate of uptake has been slowed, as with an inhibitor of the dopamine transporter (DAT). Since drugs which inhibit this transporter account for many

hundreds of billions of USD in legal and illegal trade annually, it is of paramount importance that the effects be well understood. In 2003, a modification[15] of the original DA model was published which was capable of fitting the large overshoot present in evoked DA responses collected from rats which had been dosed acutely with cocaine. This modification made the original model more complex, resulting in an extended model which contains at least 7 adjustable parameters in its simplest form. There is of course an ever present tradeoff for any model, whereby adding more parameters allows for the description of more unique processes, and typically causes the model to fit the data better, but also greatly increases the number of sets of parameter values which will fit any given response. This extended, more complex version of the model, did make good fits to post-cocaine evoked DA responses as recorded by FSCV. That so many parameters had to be invoked to fit the DA overshoot illustrate the difficulty that the field has historically experienced in quantitatively explaining this feature. The main idea behind the invocation of so many parameters was that there was more than one diffusion gap. It is relatively easy to imagine a biophysical rationale for this idea. If release is less near the electrode, perhaps due to the effects of the electrode implantation, and release increases with distance from the electrode, then it is easy to imagine a series of diffusion gaps or rather, a radial gradient of DA release extending from the electrode. However, there has been no experimental validation of these plausible ideas.

2.4　DYNAMIC GAIN CONTROL DOPAMINE MODEL (2004)

Shortly after the extension of the original DA model to explain post cocaine FSCV data, a

rather different model[16] was developed to explain complex patterns of plasticity of evoked DA reponses, as produced by complex stimulus trains. This model was the first to quantitatively apply the idea of short term plasticity to describe evoked DA reponses. The model focuses on drug-naïve data; it does not predict or account for DA signal overshoots.

2.5   PRINCIPAL COMPONENT ANALYSIS (2004)

By 2004, the original DA model had been substantially expanded[15], and additionally called into question the data due to the existence of adsorption which could potentially distort response kinetics. In 2004, the identity of the analyte measured by FSCV, as well as the kinetics, was also called into question with the idea that each cyclic voltammogram measured by FSCV was an additive composite of the voltammograms of the detected chemicals[17], with a residual containing noise and minor components. These principal components, then, represented those components of the signal which could be identified by the analysis. This technique has been very popular for accounting for interferents in naturally occuring DA transients[18–20], however, it has a fundamental issue[21,22] which can affect its accuracy. The issue is that any given cyclic voltammogram of a pure chemical generated in an FSCV experiment is a product of both reaction kinetics and thermodynamics. Because DA is so easily oxidized and reduced, the dominant factor that determines the voltammogram is the reaction kinetics. However, the DA redox mechanism is understood as a nine membered box, yielding a total of twenty reaction rate constants, and the geometry and surface chemistry of the electrode's surface can also affect the reaction kinetics. The reaction kinetics therefore can easily have variability over space and time,

which necessitates the careful development of a PCA training set for a very specific set of conditions, or else the analysis will be guaranteed to be incorrect.[21,22] PCA as a matter of course effectively requires more parameters to describe data than the original assumption that the data is created by just one chemical reaction, but it compensates for this by providing a additional data, using the entire cyclic voltammogram instead of just the peak current versus time to estimate concentration changes over time by means of a calibration curve. In many cases, particularly within the striatum, in isoflurane anaesthsized rats, and with the use of waveforms with a non-negative resting potential, it is uncontroversial that all or essentially all of the FSCV signal results from dopamine. Spontaneous DA transients in the awake animal as studied with the most commonly used waveform in the field (-0.4V to 1.3V to -0.4V vs. Ag/AgCl @ 400 V/s), tend to exhibit more interferents, which prompts the use of PCA.[18–20] It is important to note that this waveform enjoys a substantial benefit over the waveforms employed in this work, in that it is approximately three times more sensitive to DA. The original work in this document focuses on the study of dopamine kinetics in anaesthsized rats, with waveforms employing non-negative resting potentials, so PCA has not been employed.

2.6   POST-STIMULATION RELEASE DOPAMINE MODEL (2015)

Shortly after my work on this topic began to be published, a new model of evoked DA release appeared. While the Original Model and its refinements attributed overshoots primarily to the existence of a diffusion gap in space between the releasing sources, and the RD model that I conceived claimed that diffusion was kinetically slowed from reaching an equilibrium

concentration in space by diffusional barriers of some kind, this new model[23] made the claim that exocytotic release of dopamine continues well after the end of the stimulation. At this present time there have therefore been four explanations offered for the observation of overshoots in FSCV measurements of evoked DA in the brain.

3.0   A NOVEL, SIMPLE MODEL OF EVOKED DOPAMINE
Adapted from Walters et al. 2014 and Walters et al. 2015

3.1   INTRODUCTION

3.1.1   The Measurement Of Electrically Evoked Dopamine

Dopamine (DA), a neurotransmitter, is a significant contributor to normal brain function[24] and is implicated in multiple neurological and psychiatric disorders.[25–27] Although it is known that subsecond signals play a critical role in mediating DA activity in the brain, mechanistic undestanding of exactly how DA performs its functions is incomplete. A good mechanistic understanding of how this and other processes in the brain brain work is important to develop treatments to human diseases and develop future technologies. It is therefore imperative to understand the processes by which DA molecules convey information from DA terminals to pre- and post-synaptic DA receptors,[28] in order to build such a mechanistic understanding.   Those processes include DA release[29], reuptake[30], metabolism,[31] and mass transport.[32] It is not currently possible to directly measure most of these processes in living brains. Indeed, it has only been possible since the early 1980s to measure subsecond DA signaling in the brain at all.[1,2]   The technique which has enabled this measurement is in vivo fast-scan cyclic voltammetry (FSCV), using implantable, DA-sensitive, DA-selective carbon fiber microelectrodes.[2,33] Starting in the late 1980s, efforts were made to determine both the biophysical parameters and the values of those parameters that were responsible for the observed

extrasynaptic overflows of DA[3,29] that FSCV measures. These efforts yielded the Original

Dopamine Kinetic Model decribed in Chapter 2.1.

3.1.2   Simple Diffusion Gaps Cannot Explain All DA Overshoots

The Original DA Kinetic Model in its simplest 3 parameter form ([DA]$_p$, V$_{max}$, k$_M$) is

successful at making reasonable fits to many evoked DA responses. However, there are some

features of FSCV evoked DA data that the Original Model has no mechanism for explaining.

These features are 1. Lag, 2. Overshoot, and 3. Hangup. All three of these features are very

commonly observed in FSCV measurements of evoked DA in the brain.[34–40] The **Lag** feature

refers to the observation that, in many cases, the DA response does not immediately rise after the

stimulus begins, and that the rate of overflow increases as the stimulus goes on. The **Overshoot**

feature refers to the DA overflow continuing to increase after the stimulation has ended. Finally,

the **Hangup** feature refers to the failure of evoked DA responses to return to the baseline from

which they came, but rather to remain elevated. The Original Model describes DA overflows,

Equation 2: The Original DA Model

$$\frac{d[DA]}{dt} = [DA]_p \cdot f - \frac{V_{max} \cdot [DA]}{[DA] + K_M}$$

where $[DA]$ is the evoked extracellular DA concentration, $[DA]_p$ is the concentration of DA

released per electrical stimulus pulse, f is the stimulus frequency, and V_{max} and K_M are the

maximal rate and Michaelis constant, respectively, of DA uptake.[17] This model has the benefit

of being a simple model, as it is cast with just three adjustable parameters. This makes

extraction of unique parameter values from curve fitting feasible. However, a full mechanistic

understanding of DA signaling requires the ability to perfectly fit all of the features of the observed data, which the Original Model cannot do. The Original Model was made to incorporate the inferred influence of diffusion by means of a mathematical deconvolution step to explain lags and overshoots[3,41], and the complexity of the Original Model was increased[15] to explain the large DA overshoots that occur after treatment with uptake inhibiting drugs. The Hangup feature was attributed to be caused by non-dopaminergic components of the signal by means of PCA[17]. Thus, each of the three features that the Original Model failed to capture had been explained. It was suggested that Lag and Overshoot are experimental errors stemming from a poor choice of recording site.[41] Consequently, optimization of the placement of FSCV electrodes near putative DA 'hot spots' has been advocated as a procedure to minimize the perceived errors associated with diffusional distortion.[41] However, there was an issue with even the most complex physical gap based model. It makes the claim that the administration of nomifensine increases the width of the diffusion gap, due to the decreased rate of DA uptake permitting DA to diffuse farther before reuptake. However, an increased gap width is inconsistent with the observation that nomifensine dramatically decreases the **Lag** feature.[42] This paradox led to the re-evaluation of the nature of DA diffusion in the brain, and this re-evaluation led to the conclusion that the diffusion of DA in the brain must be restricted in some way.[36] It was initially thought that the diffusional restriction might occur for DA over bulk distance scales, being so powerful as to be able to help maintain the recently characterized Fast and Slow DA domains of the dorsal striatum (DS) and nucleus accumbens (NAc). However, I imagined a different kind of restricted diffusion, which could explain the overshoot phenomenon observed in our FSCV data, in lieu of a diffusional gap.[43] Significant work to characterize

14

mechanisms of restricted diffusion in and outside the brain has been done, including the trapping of molecules in dead space microdomains,[44] the obstruction of passageways by macromolecules,[45,46] and the presence of either specific[32] or non-specific[47] binding sites that impede the diffusing molecule. Because so many mechanisms are known which participate in the diffusional restriction of DA as it undergoes bulk diffusional transport from site to site in the brain, it seemed reasonable that restricted diffusion might also occur at a more local level. I thus imagined a new, local kind of restricted diffusion, only affecting DA as it moved from inside the DA terminals to the extracellular space immediately outside the terminals, at which point it was envisioned that standard Fickian diffusion, modified by the previously characterized tortuosity factor for DA, would describe the transport of DA. This new idea of a powerful local diffusional restriction of DA which could explain overshoots prompted me to develop the quantitative theory presented in this chapter.

3.1.3   Introduction Of The Restricted Diffusion Model of Dopamine

To understand how the restricted diffusion of DA could explain the signal overshoots which are so commonly observed in FSCV data[15,34,35,37,38,40], it is important to first consider how the earlier explanation[3] of a diffusion gap explains overshoots. In the Original Model of Evoked DA, DA ceases to be released into the extracellular space immediately as the stimulus ceases. Overshoots are then explained by the idea that there is a concentration gradient of DA, with DA being more concentrated farther away from the electrode, due to the presence of one[3] or more[15] diffusion gaps between the releasing source and the electrode. Indeed, provided that the release of DA ceases with the electrical stimulus, the presence of a concentration gradient is an absolute

requirement for the generation of an overshoot. However, a concentration gradient caused by a physical gap would also always create a lag in the response, and this does not always occur. *This dilemma can be solved by placing the DA releasing source immediately adjacent to the electrode, in an inner compartment (IC), with a partial barrier present between this volume and the outer compartment (OC) where the measurement takes place. This causes DA to be transiently retained by the IC, with the IC acting as a kinetic barrier to reaching concentration equilibrium.*

The exact nature of such a kinetic barrier is unknown, although there are many reasonable possibilities. Hypothetically, the synaptic cleft or the perisynaptic space, which is sometimes encased by a sheath of glial processes, might constitute a physical IC. Alternately, the IC might represent the dead spaces, blocked passages, or binding sites identified by Nicholson and coworkers,[32,44,47] or something else entirely.

The restricted diffusion (RD) model postulates that, within an arbitrary volume of brain tissue, DA 1) is released at an initial amount $\mathbf{R_p}$ into the IC, 2) is subsequently transported unidirectionally at a rate determined by rate constant $\mathbf{k_T}$ to the outer compartment, 3) is detected by FSCV in the outer compartment, and 4) is cleared from the outer compartment by DA uptake, which can be represented as another first order rate constant $\mathbf{k_U}$. (Fig. 2B).

The principal justification for these postulates is that the resulting RD model reproduces the lag, overshoot, and hang-up features of numerous evoked DA responses recorded under a broad range of conditions (vide infra). For relatively short stimulations, excellent fits to *in vivo* DA FSCV data over a wide variety of recording sites and drug states can be achieved with the use of only three adjustable parameters.. In addition, the parameter values appear to be

consistent for stimulations of varying length, provided that the stimulus is kept short. The fit

quality, parameter consistency, and model parsimony combine to suggest that restricted diffusion

is a powerful and plausible explanation for the observed data.

Figure 2. Features of Evoked DA Data and the RD Model Schematic

A.   **B.**
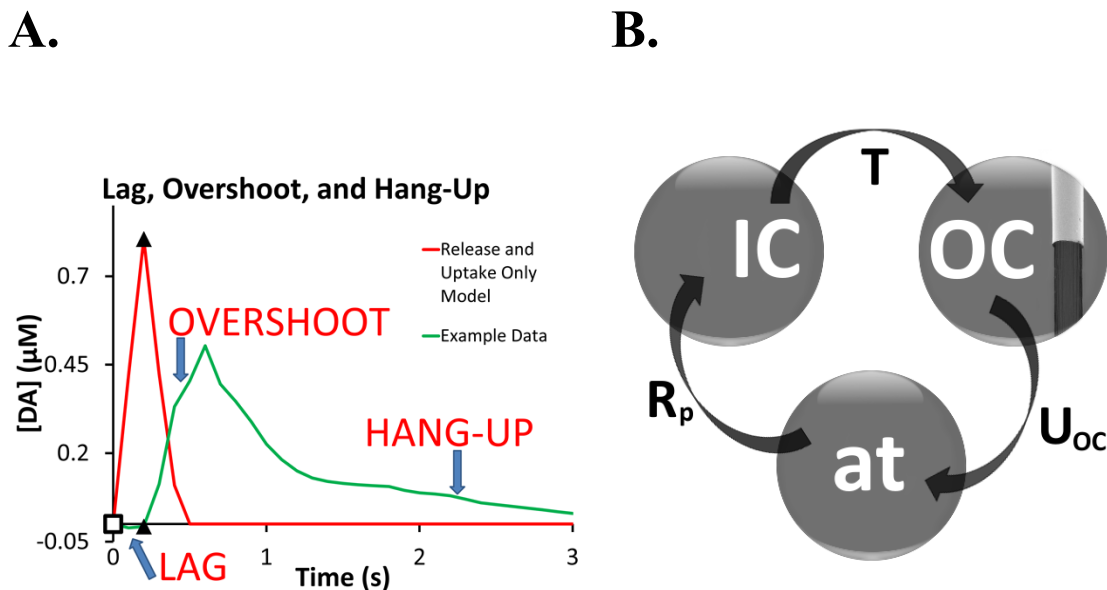
Figure 2. A: Evoked responses as predicted by the simplest Original Model (red line) rise during the

stimulus and decay to zero after the stimulus ends. However, observed responses (green line) exhibit varying

degrees of lag (an initial delay in the appearance of the signal), overshoot (the signal continues to rise after the

stimulus ends), and hang-up (the signal remains elevated for prolonged periods after the stimulus ends instead of

returning to baseline). The open square indicates the start of the stimulus and the closed triangles indicated the end

of the stimulus. **B:** A schematic representation of the RD Model. The extracellular space is divided into inner (IC)

and outer (OC) compartments. DA is released from axon terminals (at) to the IC, is subsequently transported to the

OC, and is removed from the OC by uptake. The model postulates that FSCV recording takes place in the OC. R_p

is release per pulse. **T** (represented as k_T throughout most of this document) is the first order unidirectional transport

parameter. $\mathbf{U_{OC}}$ (represented in this document both as first order uptake k_U and also by $V_{max} + k_M$) represents uptake of DA from the outer compartment.

3.2   METHODS

Methods

The Original Dopamine Model with a Diffusion Gap (DG)

Compactly stated, the original model with a diffusion gap can be represented as:

Equation 3: The Original DA Model with Diffusion Gap

$$\frac{d[DA]}{dt} = D\frac{\partial^2[DA]}{\partial x^2} + [DA]_p \cdot f - \frac{V_{max} \cdot [DA]}{[DA] + K_M}$$

where the first term on the right is the planar diffusion operator, x and t are the coordinates of space and time, respectively, and the other terms were explained above. From the initial condition of $[DA]_{x,t=0}=0$, $[DA]_{x,t}$ was determined by a finite element method (see Supplementary Information for additional details and example code), with the diffusion gap (width=w_g) interposed between the electrode and a region of active DA release and uptake.[15] The 5 adjustable parameters are the concentration of dopamine released per stimulus pulse ($[DA]_p$), the maximal rate and Michaelis constant of DA uptake (V_{max} and K_M, respectively), DA's diffusion coefficient (D), and the width of the gap, w_g.

To reduce the number of adjustable parameters to 4 we used a dimensionless gap parameter, $Gap = w_g/\sqrt{D/60}$ (where 60 Hz was chosen as convenient time base for the simulations of interest here). We used this dimensionless parameter as there is no value to retaining D and

w_g as independently adjustable parameters: this is because rapid diffusion across a wide gap is equivalent to slow diffusion across a narrow gap, and vice versa. With the D of DA in the striatum $(2.4 \cdot 10^{-6}\ cm^2/s)^{48}$, a *Gap* of 1 corresponds to a physical gap of 2 μm. With the D of DA in Nafion $(1 \cdot 10^{-9}\ cm^2/s)$,[6] a *Gap* of 5 corresponds to a film thickness of 200 nm. It is important to note that the number of adjustable parameters in this model could easily be reduced to 3 by replacing the V_{max} and k_M in the expression with a k_U. This is the same number of adjustable parameters the simplest version of the RD model contains.

The Restricted Diffusion (RD) Model

The RD model, in its simplest form, consists of two coupled differential equations:

Equation 4: Release and Diffusion from the Inner Compartment

$$\frac{dDA_{ic}}{dt} = R_p \cdot f - DA_{ic} \cdot k_T$$

Equation 5: First Order Uptake and Diffusion into the Outer Compartment

$$\frac{d[DA]_{oc}}{dt} = \frac{DA_{ic} \cdot k_T}{V_{oc}} - DA_{oc} \cdot k_U$$

where DA_{ic} is the amount of DA (moles) present in the inner compartment, V_{oc} is the volume of the outer compartment, and $[DA]_{oc}$ is the concentration of DA in the outer compartment (other terms are defined similarly to the DG model). The new model has 3 adjustable parameters: R_p is the amount of DA (moles) released per stimulus pulse; k_T is a first order reaction rate constant that describes the unidirectional transport of DA from the inner to the outer compartment; and k_U represents first order uptake from the OC. It is possible to formulate the RD model with additional parameters, but this is not necessary to fit short stimulations. However, some of the

19

fits in this chapter were generated with a 4 parameter version of the RD model which used V_{max} and k_M instead of k_U:

Equation 6: Release and Diffusion from the Inner Compartment

$$\frac{dDA_{ic}}{dt} = R_p \cdot f - DA_{ic} \cdot k_T$$

Equation 7: Michaelis-Menten Uptake and Diffusion into the Outer Compartment

$$\frac{d[DA]_{oc}}{dt} = \frac{DA_{ic} \cdot k_T}{V_{oc}} - \frac{V_{max} \cdot [DAoc]}{[DAoc] + K_M}$$

The RD model describes the transport of DA from the inner to the outer compartment as if it were a chemical reaction. This is the same strategy used throughout the DA modeling literature to describe DA uptake, the mass transport of DA through a transmembrane passageway formed by the DAT, as a chemical reaction exhibiting Michaelis-Menten kinetics. Both first order mass transport and first order uptake give excellent fits to FSCV data - for short stimuli, there is little or nothing to be gained in fit quality by using additional parameters, although it took some time to realize this.

The RD simulations were implemented with a finite element method, again starting with the initial condition that the extracellular space contains no evoked DA (see Supplementary Information for additional details and example code). Inspired by the ultrastructure of the striatum,[49] we fixed V_{oc} to 16 μm³: it turns out that any value could be used with a corresponding adjustment of R_P, so there is no purpose to treating V_{oc} as an adjustable parameter.

Curve fitting

We often encountered local minima in our attempts to use Simplex optimization[5] for curve fitting. So, instead, we used a brute-force algorithm that searched 80 points in the

parameter space, retained the one giving the best fit, and searched again until the sum of squared differentials was minimized.

In Vivo Recordings

In this report we compare simulated overflows to previously published overflows recorded in the DS and NAc. The detailed experimental procedures are also previously published.[35–38] Briefly, all the recordings were performed with microelectrodes formed with single carbon fibers (diameter = 7 μm, length = 200 μm, T650 fibers, Cytec Carbon Fibers, Piedmont, SC) sealed into pulled borosilicate capillaries with low-viscosity epoxy (Spurr, Polysciences, Warrington, PA). Fast scan cyclic voltammetry employed a triangular potential waveform (0 V to 1V to -.5 V to 0 V at 400 V/s) applied at a repetition rate of 10 Hz. The reference electrode was Ag/AgCl. The microelectrodes were calibrated after the in vivo experiments.

The University of Pittsburgh Institutional Animal Care and Use Committee approved all procedures involving animals. Male Sprague-Dawley rats (250-350g, Hilltop, Scottsdale, PA) were anesthetized with isoflurane (2.5% by volume in O_2), wrapped in a 37°C homeothermic blanket (Harvard Apparatus, Holliston, MA), and placed in a stereotaxic frame (Kopf, Tujunga, CA). A stainless steel, twisted bi-polar stimulating electrode (MS303/a, Plastics One, Roanoke, VA) was placed into the medial forebrain bundle and a carbon fiber microelectrode was placed either into the ipsilateral DS or NAc: detailed stereotaxic coordinates and procedures are published.[35–38] The MFB was stimulated with a biphasic, constant-current, square-wave delivered by a stimulus isolator (Neurolog 800, Digitimer, Letchworth Garden City, U.K.). The responses analyzed during this work were all obtained with a stimulus frequency of 60 Hz, a

current intensity of 250 µA, and pulse duration of 2 ms. The stimulus duration was variable and is specified in the Results and Discussion section.

The post-nomifensine evoked responses analyzed during this study were recorded 30 min after rats received a single dose of nomifensine (20 mg/kg i.p.).

3.3   RESULTS AND DISCUSSION

We first present the models and their fits to various data sets (simulated data points are reported at 100 ms intervals to match the FSCV recordings) and subsequently discuss the parameter values. The parameter values are tabulated in two formats in the Supplementary Information section.   In the first format, the parameters are indexed to the figures presented below.   In the second format, the parameters are listed according to brain region, domain, stimulus duration, and drug treatment.

Response features unique to the DS and NAc

Figure 3. RD & DG Model Fits to Short Stimuli
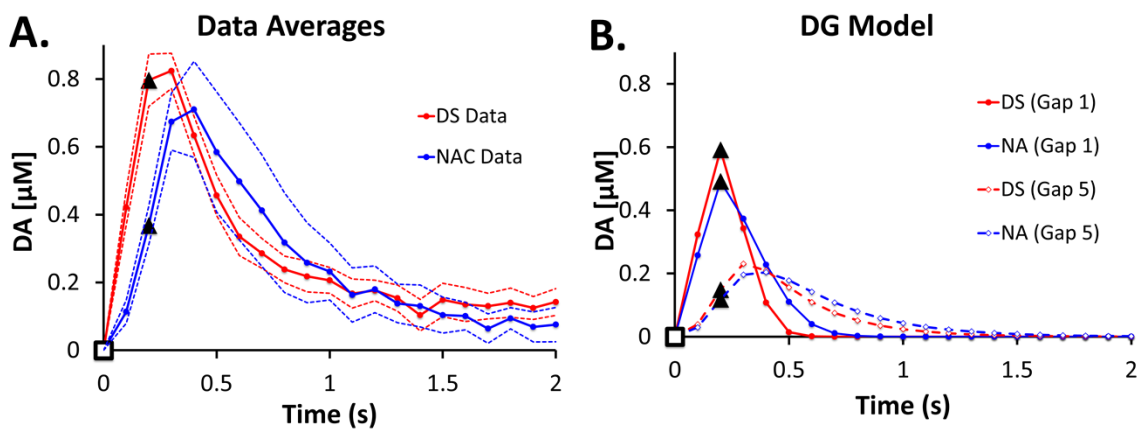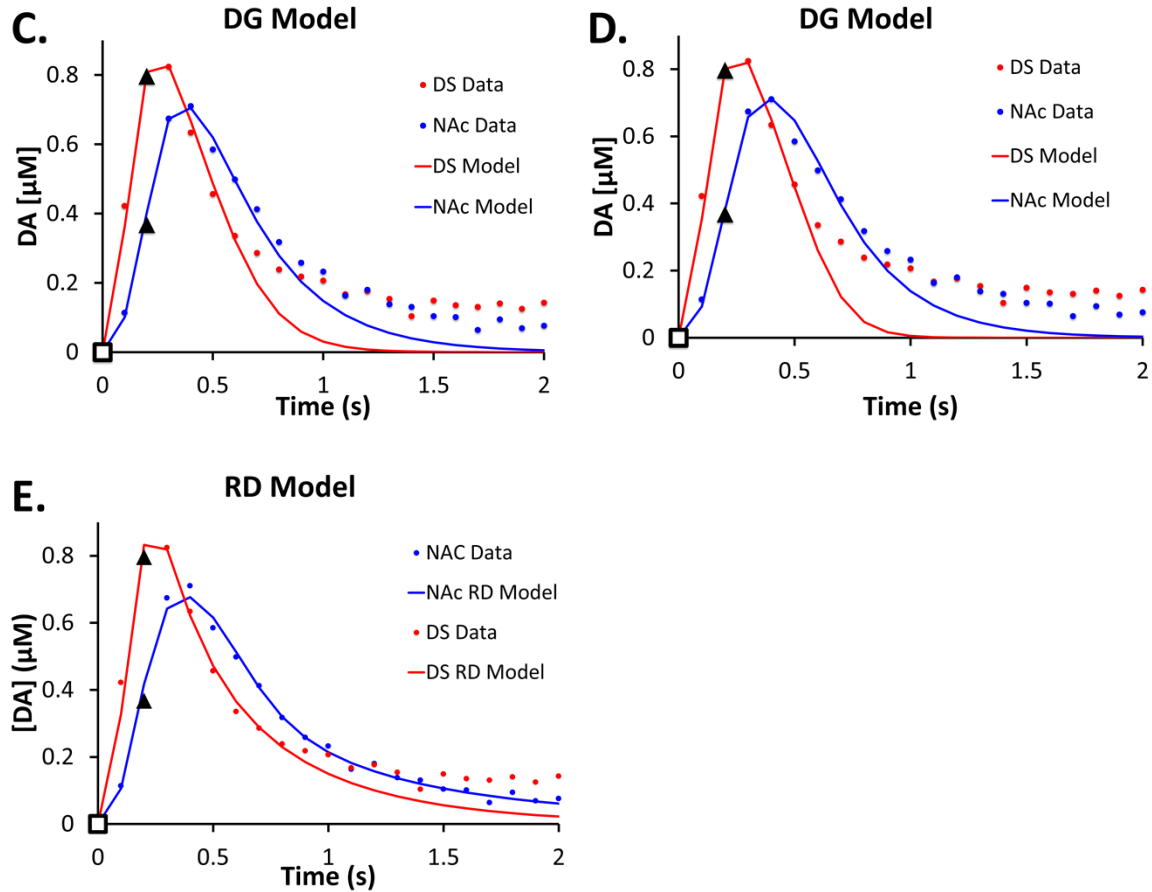
Figure 3. **A:** Evoked responses recorded in fast domains of the DS and NAc (stimulus = 200 ms, 60 Hz, 250 µA): the solid lines are the averaged responses and the dotted lines are the SEM intervals. **B:** DG simulations using the parameter values of (Wu et. Al 2001) and gap values of 1 and 5. **C:** DG simulations of the averaged DS and NAc data points (SEMs omitted for clarity). **D:** RD simulations of the averaged DS and NAc data points (SEMs omitted for clarity). The open square indicates when the stimulus begins and the closed triangle mark the data point at the end of the stimulus. The parameter values are reported in the Supplementary Information.

Evoked responses recorded in the fast domains of the DS and NAc exhibit marked distinctions in amplitude and profile (Fig 2A: the symbols and solid lines are the averaged evoked responses, the dotted lines show the SEM interval (n = 16 DS, n = 7 NAc); stimulus = 60

Hz, 200 ms, 250 µA; data from[36,37]). Lag and overshoot are far more pronounced in the NAc and the signal decay after the peak is slower in the NAc. Although these DS-NAc distinctions are well known in the literature,[37,50,51] we show next that they are not captured well by the Original DA Model with a diffusion gap, or DG model.

We performed DG simulations using the DS and NAc specific kinetic parameters reported by Wu et al,[5] who attributed the diffusion gap to a Nafion film. Since there is no known reason that the brain region should affect the dimension of a Nafion film, we ran the DS and NAc simulations using the same gap value (Fig 2B reports pairs of simulations with *Gap*=1 and with *Gap*=5: the *Gap* parameters is defined in the Methods section). However, the simulations fail to reproduce the distinct lag and overshoot features of the DS and NAc responses.

The only way to produce different lags and overshoots with the DG model is to use different *Gap* values (Fig 2c). This improves the fit but carries with it the surprising implication that the gap width is a property of the brain region rather the Nafion film, as previously assumed. The use of different gap values improves the fits, although the hang up feature is not captured.

The simulations in Fig. 2C suggest that the gap width is a property of the brain region. We find this highly confusing. The DG model interposes the gap between the electrode and the active tissue zone, but we know of no reason why it should be possible to position a microelectrode closer to DA terminals in the DS than in the NAc. Studies show a difference in the spacing between DA terminals of the DS and NAc,[50] which might affect DA_p and V_{max}. But, according to the DG model, DA_p and V_{max} do not affect lag and overshoot: only the gap does that. So, adjusting gap parameter produces better fits to the observed data, but the underlying logic of the adjustment is not obvious.

Surprisingly, the parameters from Fig. 2C indicate that DA release (DA_p) and DA clearance (V_{max}) are *faster* in the NAc than in the DS. This is surprising because it has been stated before that DA release and clearance are faster in the DS.[5] Even so, this outcome is logical: higher DA_p and V_{max} values are necessary to offset the NAc's apparently larger gap.

The RD simulations produce improved overall fits to the observed DS and NAc responses (Fig 2D). The parameters for curve fitting were identified objectively with the search algorithm. At the time of much of the work presented in this chapter, we were uncertain as to the source of the hang-up,[11,17] so here we only included data points between 0 and 1s in the parameter search as these data points are confirmed to be due to DA by their background subtracted voltammograms. Even so, the RD simulations provide good fits to the rising phase of the evoked responses and an improved fit to the hang-up, especially in the case of the NAc.

The effects of nomifensine, a competitive DAT inhibitor

Prior studies based on DG simulations have concluded that nomifensine acts solely by increasing the K_M of DA uptake.[52] However, in fast domains, nomifensine dramatically increases the duration and amplitude of overshoot even though the responses exhibit no lag (Fig 4A, the symbols at the averaged responses, SEMs omitted for clarity, stimulus = 60 Hz, 200 ms, 250 µA). DG simulations fail to reproduce this feature (Fig. 4A, lines) even when K_M is increased to 20 µM, which produces a maximum effect.

In animals treated with nomifensine, evoked responses with prominent overshoot and no lag are absolutely commonplace.[35–38] As we explained above and have documented before,[34] DG simulations do not reproduce overshoot without lag, so we conclude that the DG model does

not capture the key features of responses recorded in animals treated with nomifensine. Wightman and co-workers also encountered difficulty fitting the original DG model to post-nomifensine responses, and introduced a revised model.[15] However, the premise of the revised, more complex model, that nomifensine increases the apparent gap width, is inconsistent with nomifensine's ability to decrease lag (i.e. decrease the gap) in slow domains of the DS and NAc.[35–38] Thus, the revised model does not offer a comprehensive explanation of nomifensine's actions.

Figure 4. RD & DG Model Fits to Short Stimuli After Nomifensine
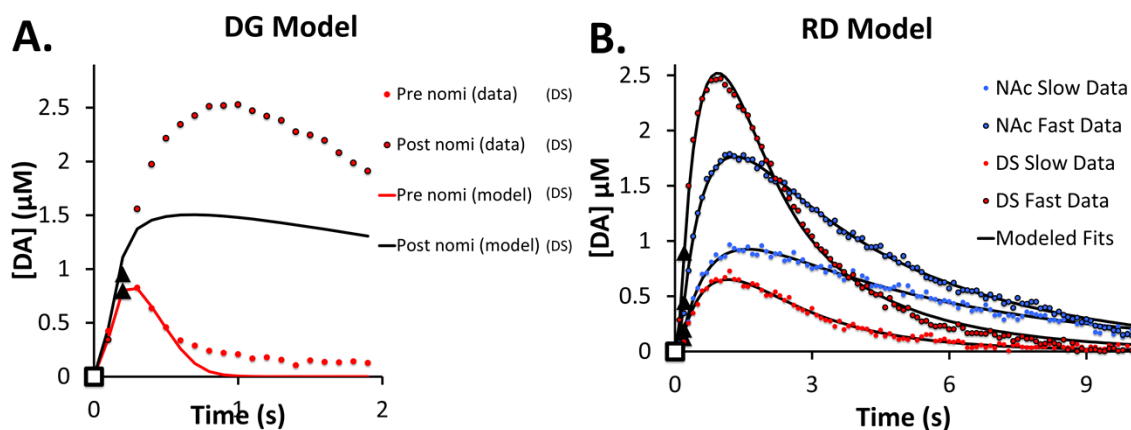
Figure 4. Fits of the DG (A) and RD (B) models to averaged responses from the dorsal striatum (A, B) and nucleus accumbens (B). In 4A, "pre nomi" refers to the stimulus as collected at a recording site in a drug naive rat, whereas "post nomi" refers to data collected at the same site after i.p. administration of the competitive uptake inhibitor nomifensine. The parameter values are reported in the Supplementary Information.

The RD model produces excellent fits to post-nomifensine responses from the fast and slow domains of the DS and NAc (Fig 4B, symbols are average responses, SEMs omitted for clarity, stimulus = 60 Hz, 200 ms, 250 μA). Thus, the RD model captures evoked responses with

26

prominent overshoot but no lag. The RD model produces excellent fits to these post-nomifensine responses out to 10 s, and all these data points are identifiable as DA from their background subtracted cyclic voltammograms. The fit quality was actually slightly higher when the 3 parameter RD model was used (Figure 5) intead of the 4 parameter RD model using V_{max} and k_M (Figure 4B). Because of this, it appears that it is not possible to obtain information about V_{max} and k_M from FSCV data.

Figure 5. Simplest RD Model Fits to Short Stimuli After Nomifensine
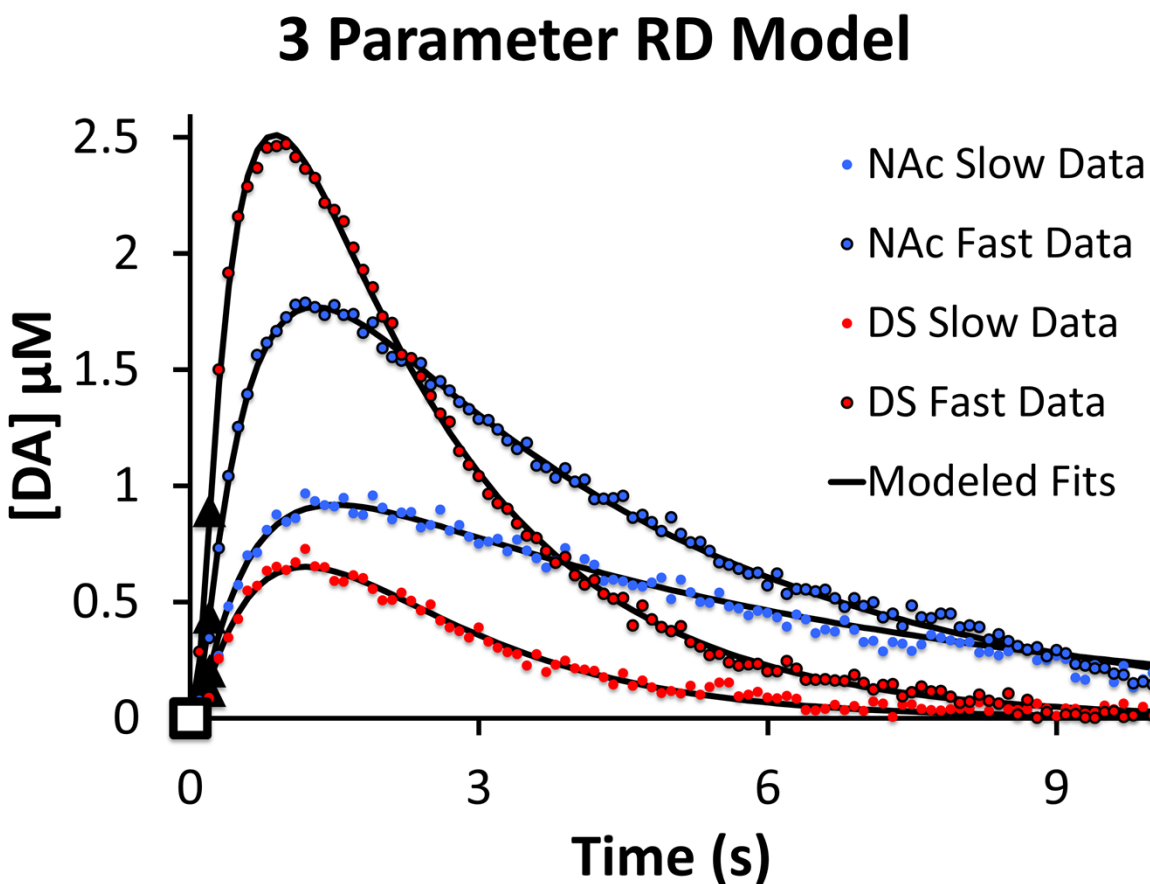
Figure 5. 3-parameter RD simulations of post-nomifensine averaged responses to 0.2s 60Hz stimuli recorded in the dorsal striatum and the nucleus accumbens. Parameter values are reported in Table 2.

27

I considered it extraordinarily promising that such a complex set of DA responses as appears in Figure 5 could be fit so easily by a biophysically-inspired model with just three parameters. However, I thought it was quite important to confirm whether or not the parameter values for this simple model could be consistent for stimulations of different lengths. For longer stimulations (of 180 pulses at 60 Hz stimulation frequency, for example), the model would always make fits (with 4 parameters - R_p, V_{max}, k_M, k_T used, at least), but the parameter values were often nonsensically large, and they changed as a function of stimulus time. It therefore became important to determine if there was a window of stimulus time in which the simplest, 3 parameter RD model parameters showed consistency regardless of the number of stimulus pulses applied.. While the previous data had been collected by Mitch Taylor and Zhan Shu, originally for other purposes, the next set of data would be collected by Elaine Robbins with the very deliberate experimental design aim of testing the model's consistency.

Validation of the Simplest, 3 Parameter RD Model.

We identified fast DS sites in n=10 rats. Then, we administered nomifensine and recorded responses evoked by 1 to 6 stimulus pulses (Fig. 9). The responses underwent a hang-up correction (see Chapter 4 for an explanation of the hang-up correction, but in this case the effect of the correction was miniscule, and the raw responses are reported in Supplementary Information Figure S4). We modeled each response individually (Fig. 9a: these fits are excellent but the Pearson correlation coefficients are ~0.96 due to the residual noise). The fits in Fig 9a were obtained with the 3-parameter RD model). Thus, Fig. 9a shows that the individual responses can each be fit with 3 adjustable parameters. We then modeled all six responses simultaneously (Fig. 8b: the fit is excellent but the correlation coefficient is also ~0.96 due to

residual noise). Fig. 9b shows that the entire data set can be modeled with a single set of 4 adjustable parameters (see Chapter 5 for a full explanation of this 4 parameter RD model). However, it is really not necessary to use a 4 parameter model for this - the parameter values obtained from the 3 parameter model are essentially identical, and, as is explained in Chapter 7, much of the small amount of variability in the parameter values that is present can be explained by noise present in the signal. Thus, this experiment is evidence of the basic correctness of the simplest, 3 parameter RD model as it is applied to short stimuli - the simplest imaginable theoretical model, in terms of number of parameters, fits the data, and it does so in a way that produces parameter values that are consistent regardless of the number of stimulus pulses (as long as this number is kept relatively small). This builds confidence that the 3 parameter RD model is a basic theoretical-mathematical foundation upon which a further understanding can be built, and solidifies the importance of accounting for effects of the k_T parameter, which we have cast as representing restricted diffusion.

Figure 6. Simplest RD Model Fits to Stimuli of 1 to 6 pulses After Nomifensine

A.   **B.**
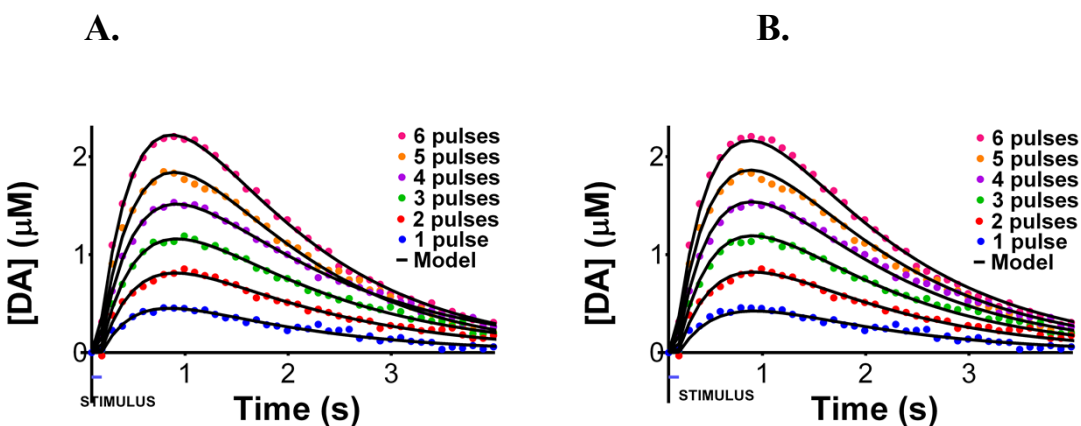
Figure 6: Symbols: Responses evoked by 1-6 stimulus pulses in rats (mean of n=10, SEMs omitted for clarity) treated with nomifensine (20 mg/kg i.p.). Lines: Best-fit models. (a) Best-fit models to each evoked

response. (b) The single best-fit model to all six evoked responses. The parameters are reported in the Supplementary Information Table S4.

The Effect of Uptake on Overshoot

The RD Model is fundamentally focused on explaining overshoots. It is therefore necessary to consider cases with minimal or no overshoots, and to consider what causes those cases, as a good theory should explain all of the data. What we find from modeling is that the overshoot is always an inherent feature of the brain, but it can be truncated by a high rate of uptake. An obvious example of this is found in the transition from a short pre-drug stimulus to a short post-drug stimulus. While it appears that more parameters than just uptake change upon administration of nomifensine, one thing that can be observed by comparing these responses is that the high rate of uptake found in the pre-drug recording site truncates or eliminates the overshoot, and the low rate of uptake in a nomifensine treated site allows the overshoot to be very prominent (Fig 7) Evoked responses exhibit overshoot, i.e. a continued increase in the DA signal after the stimulus ends. The amplitude and duration of overshoot are sensitive to DAT inhibitors including nomifensine.[53,42,36,38] In the past, overshoot has been attributed to diffusion gaps.[54] However, our data and our restricted diffusion model speak against the presence of diffusion gaps. Next, we show that the restricted diffusion model reproduces the effect of nomifensine on overshoot.

Figure 7 shows the 6-pulse stimulus response from animals treated with nomifensine and the best-fit restricted diffusion model (black dots and line, respectively, re-plotted from Fig. 6a). Fig. 7 also plots responses calculated with the model using the same best-fit parameters except for k_U, which was increased to 2 s^{-1} (blue line) and 4 s^{-1} (purple line). Qualitatively, adjusting

30

only the value of k_U reproduces the observed effect of uptake inhibition on the amplitude and duration of overshoot (see also Fig. 4 of Ref. 25).

Figure 7. The Effect of Modulating k_U On DA Overshoots For Short Stimuli
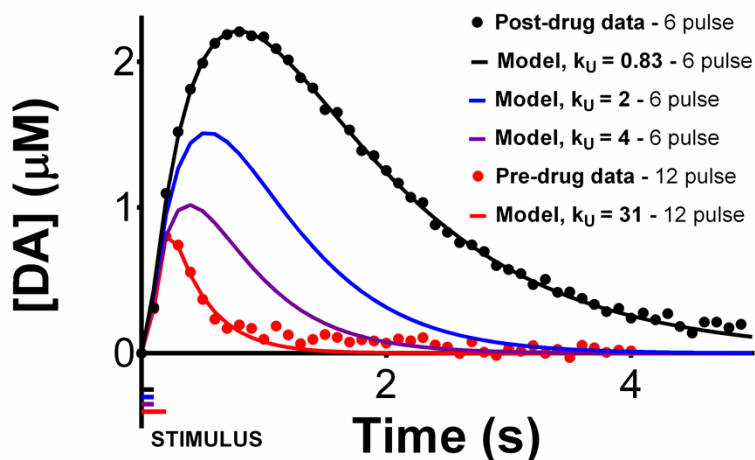
Figure 7: The effect of k_U on overshoot. The 6-pulse evoked response from animals treated with nomifensine (black symbols) and its best-fit (black line). Additional responses were modeled by changing only k_U to 2 s^{-1} (blue line) and 4 s^{-1} (purple line). The pre-nomifensine response (red symbols) and best-fit (red line) are included for comparison.

Equivalent Solutions to Models

Although it was not immediately obvious to us, it was eventually discovered that each curve has two sets of parameters which produce the exact same curve, whereby the k_T and the k_U are flipped. A table illustrating this can be seen in the supplementary information to this chapter. We are able to report one of these sets of parameters, because one of the parameters, k_T, is insensitive to uptake inhibitors, while the k_U is of course extremely sensitive to uptake. This issue of two parameter sets generating the same fit applies equally to both 3 and 4 parameter

formulations of the RD Model. Such issues of nonunique sets of parameters producing fits become worse as the number of parameters in any given model increases, particularly with real data that contains noise.

3.4   CONCLUSION

The RD simulations successfully reproduce the lag, overshoot, and hang-up features of numerous evoked responses recorded in the fast and slow domains of the DS and NAc when stimulus conditions are kept short, both in drug-naïve and uptake inhibited animals. Therefore, the model mathematically supports the hypothesis that DA undergoes restricted diffusion in the extracellular space. The parameter values for the simplest, 3 parameter version of the RD model are stable for stimulations ranging from 1 to 6 pulses, which is an encouraging sign as to the model's correctness. Alternative explanations, such as a physical diffusion gap of some sort of very specific gradient, or a hybrid mechanism, cannot be ruled out solely on the basis of modeling, but they are more mathematically complicated and therefore less compelling. Subsequent chapters of this work rule out some other alternative explanations, but ultimately, an experiment designed to test for the existence of restricted diffusion of DA will be necessary to conclude with certainty that this is the sole operating principle behind the plain mathematical validity of the new k_T parameter.

3.5   SUPPLEMENTARY INFORMATION

Table 1. Simplest RD Model Parameters for Brief, Post-Nomifensine Stimuli

	R_p (mols $\times 10^{-21}$)	k (s^{-1})	T (s^{-1})
DS fast, 0.2 s + nomi	25	2.54	0.51
DS slow, 0.2 s + nomi	3.7	1.30	0.59
NAc fast, 0.2 s + nomi	24	1.93	0.26
NAc slow, 0.2 s + nomi	17	1.84	0.17

Table 1 - The set of parameter values initially reported for the fits in Figure 5. Together with table 2, this is one illustration of the k_U and k_T "flipping" effect. Here, k_U is printed as 'k', and k_T is printed as 'T'.

Table 2. Simplest RD Model Parameters for Brief, Post-Nomifensine Stimuli, k_T ~2

	$R_{p\,(zmol)}$	k_U (s^{-1})	k_T (s^{-1})
DS fast	5	0.51	2.54
DS slow	1.7	0.59	1.30
Nac fast	3.2	0.26	1.93
Nac slow	1.6	0.17	1.84

Table 2 - The set of parameter values reported for the fits in Figure 5 after it was realized that the k_T term hovered around a value of 2 and, unlike k_U, was not affected by nomifensine or other uptake inhibitors.

Table 3. RD Model Parameters for Brief, Post-Nomifensine Stimuli of 1-6 Pulses

Figure 9	$R_{p\ (zmol)}$	$k_U\ (s^{-1})$	$k_T\ (s^{-1})$	$k_R\ (s^{-1})$
9A - 1 pulse	12	0.71	2.8	0
9A - 2 pulses	11	0.67	2.5	0
9A - 3 pulses	10	0.67	2.3	0
9A - 4 pulses	10	0.64	2.4	0
9A - 5 pulses	11	0.82	2.1	0
9A - 6 pulses	10	0.77	2.3	0
9B	12	0.73	2.3	4.1

Table 3 - The parameter values obtained by objectively fitting the 3-parameter ($k_R = 0$) restricted diffusion model to the 1-6 pulse stimulus responses (Fig. 6a). As before, in these nomifensine-treated animals k_U is consistently smaller than k_T. The parameters are essentially independent of the number of stimulus pulses. The 4-parameter model that invokes short term plasticity (see Chapter 5, $k_R \neq 0$) also provides excellent agreement (Fig. 6b) with all six responses with a single fit.

Figure 8. Raw FSCV Responses to Stimuli of 1 to 6 pulses After Nomifensine
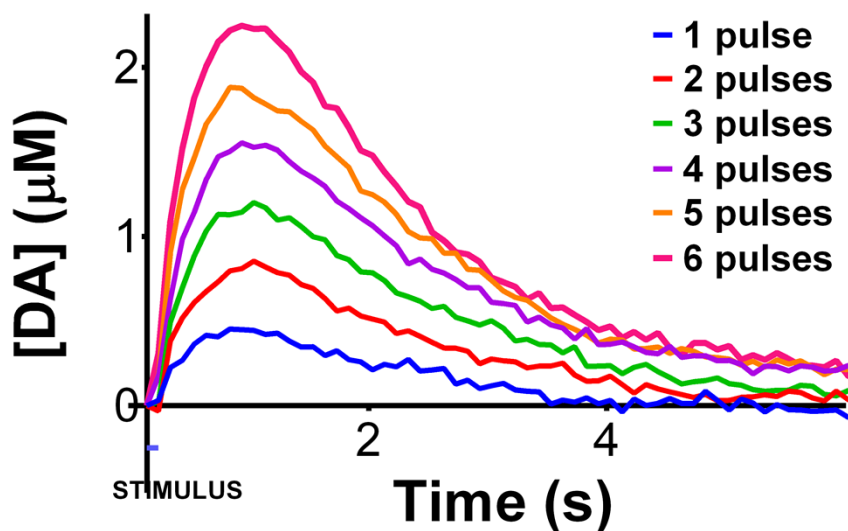
Figure 8 – These are the raw (uncorrected) responses evoked by 1-6 pulse stimuli in rats treated with nomifensine. Corrected versions of these responses are analyzed in Fig. 9 of the main text. Each line is the average of responses recorded at fast sites in n=10 animals. In some cases, a small correction was applied for downward drift in the response. Due to the relatively short exposure time (<1 s) and to the relatively low DA concentrations (<2 μM), the hang-up corrections were minor.

Table 4. Equivalent, Inverted RD Model Parameters

$R_{p \, (zmol)}$	$k_U \, (s^{-1})$	$k_T \, (s^{-1})$	$k_R \, (s^{-1})$
5.9	2.02	0.96	0.01
2.8	0.95	2.06	0.00

Table 4 - Two sample sets of parameters that produce equivalent best fits to an evoked DA overflow in the brain. The k_R parameter (see Chapter 5) is negligible here, but the issue of k_T and k_U "flipping" is present with or without a k_R. The only way to know which is which is to see which one does not change over a large set of data when an uptake inhibitor is administered. This has told us that, under all known conditions, the k_T parameter has a value of approximately 2, plus or minus 1. The parameter values in this table should be taken to have no more than 2 significant digits (see section 7.4 for sources of error).

Table 5. Summary Tables of RD and DG Model Parameters, Figs 3 and 4

DG Model Parameters

	[DA]$_p$ (µM)	V$_{max}$ (µM/s)	Gap	K$_M$ (µM)	k (s^{-1})
Fig 2B, DS Gap 1	0.12	5.18	1.0	0.2	25.9
Fig 2B, DS Gap 5	0.12	5.18	5.0	0.2	25.9
Fig 2B, NAc Gap 1	0.08	2.85	1.0	0.2	14.3
Fig 2B, NAc Gap 5	0.08	2.85	5.0	0.2	14.3
Fig 2C, DS	0.16	5.40	2.0	0.5	10.8
Fig 2C, NAc	0.27	9.00	5.0	0.5	18.0
Fig 2D, DS	0.17	4.40	2.0	0.2	22.0
Fig 2D, NAc	0.25	6.20	5.0	0.2	31.0
Fig 3A, predrug	0.17	4.40	2.0	0.2	22.0
Fig 3A, + nomi	0.17	4.40	2.0	20.0	0.22

RD Model Parameters

	R$_p$ (mol)	V$_{max}$ (µM/s)	T (s^{-1})	K$_M$ (µM)	k (s^{-1})
Fig 2E, NAc Fast 0.2 s	4.5E-20	23.1	0.62	0.25	92.4
Fig 2E, DS Fast 0.2 s	3.9E-20	106	1.77	1.88	56.4
Fig 3B, NAc Fast 0.2 s + nomi	2.9E-20	29.6	0.23	12.3	2.4
Fig 3B, NAc Slow 0.2 s + nomi	1.6E-20	16.5	0.18	8.60	1.9
Fig 3B, DS Fast 0.2 s + nomi	4.7E-20	20.2	0.34	3.36	6.0
Fig 3B, DS Slow 0.2 s + nomi	5.6E-21	7.7	0.45	3.67	2.1

Table 5 – DG and RD model parameters for Figures 3 and 4. There are errata in the table: Fig 2X should read Fig 3X, and Fig 3X should read Fig 4X. It is very important to note that, for these short stimuli, the use of this or any other 4 parameter RD model is not required to achieve excellent fits to RD simulations fitting DA overflows evoked by short stimuli, rather, the simpler 3 parameter RD model will produce fits of equivalent quality to DA oversflows provided that the stimulus is kept short (12 pulses or fewer at 60 Hz). The 4 parameter (V$_{max}$, k$_M$) RD model fits and parameter values are reported here simply because the material was adapted from published manuscripts that took that approach. The parameter values in this table should be taken to have no more than 2 significant digits (see section 7.4 for sources of error).

4.0   CORRECTING FOR DA ADSORPTION IN KINETIC MODELING
Adapted from Walters et al. 2015 and Walters et al. 2016

4.1   INTRODUCTION

Electrically evoked DA responses are suitable targets for mathematical kinetic modeling,[3,43] in part because the timing of the stimulus pulses is known. A simple, 3 parameter kinetic model based on the concepts of restricted diffusion reproduces pre and post nomifensine DA responses observed in the DS and NAc, so long as the stimulus is kept relatively short.[43] However, when the duration of the stimulus is extended, the RD model is not able to account for a feature of the responses known as 'hangup' - even if an additional parameter is added. This 'hangup' is a ubiquitously observed tendency for DA responses as measured by FSCV to remain elevated above their baseline long after the stimulus ends, and DA would be expected to have been cleared by uptake. The hangup feature is minimized in the case of short stimuli, as seen in Chapter 3. However, when longer stimuli are conducted, it becomes a more prominent feature. Thus, to extend the usefulness of the RD model to the description of longer stimuli, as well as to understand the relevance of the hangup feature to chemical neurotransmission, it is necessary to understand the cause of this feature.

Herein we show that hang-up is caused by adsorption of DA to the surface of FSCV electrodes. This new hangup mode of adsorption is kinetically slower than the mode of adsorption described by the work[11] mentioned in Chapter 2. We also introduce a simple means of correction that can be used to subtract the hangup from both in vitro and in vivo DA

responses. The hangup correction dramatically improves the fit of the restricted diffusion model to longer stimuli, permitting a full explanation for the kinetic diversity of evoked DA responses from the DS.

In addition, It has also recently been claimed[14] that the previously characterized[11] fast DA adsorption mode distorts the shape of the signal. Indeed, with the appropriate rate constant values assumed for normal mode adsorption, the k_T parameter of restricted diffusion can be disregarded, and adsorption can generate overshoots entirely on its own, without the need to invoke a restricted diffusion mechanism[43]. It therefore became imperative to fully and quantitatively understand the effects on the DA overflow of both modes of DA adsorption - normal and hangup, and to learn how to correct for each as proved necessary.

If adsorption is distorting the measured FSCV signals in any way, then it is imperative to understand and correct for this, so that instrumental errors do not prompt erroneous assumptions about DA neurobiology which could mislead the community. Previous work from our laboratory shows that DA responses as recorded by FSCV can be objectively classified as belonging to several fast and slow kinetic types,[42,36,38,34,55,39,37] which reveals a substantial diversity of dopamine kinetics in the dorsal[42,36,34,55,39] and ventral[38,37] striatum. If this observed kinetic diversity is an instrumental error caused by adsorption[14], then it is critical to understand this so that we are all not led astray, especially in light of the history of in vivo electrochemical techniques being called into question for issues of kinetic fidelity.[13,14,56–62]

Thus, in addition to demonstrating that the hangup is a kinetically slow adsorptive feature, and providing a mathematical correction for it, this Chapter also evaluates adsorptive distortion in a direct manner by recording DA with an FSCV protocol that eliminates DA

adsorption. This enables us both to account for any distortions caused by "normal mode" adsorption, and to validate our hangup correction procedure. Our results confirm that the slow-type evoked response features are not a product of DA adsorption, and indeed, that adsorption plays no role in explaining kinetic diversity observed in the brain, as adsorption does not appreciably distort the shape of any recorded signal. We emphasize that DA adsorption is highly beneficial in FSCV[60,63,64]: it increases the signal-to-noise ratio, sensitivity, and selectivity of FSCV with only minor, and easily managed[65], effects on the temporal response. This work substantiates that DA's kinetic diversity with the striatum is not an FSCV artifact, and that adsorption plays essentially no role in the creation of overshoot features in FSCV data. This offers additional support to the assumptions behind the restricted diffusion model.

4.2   METHODS

The *in vivo* methods employed for this study are similar to those used in prior recent work from our laboratory[42,36,34,39,37] with the exception of the new FSCV waveform, Waveform B.

FSCV

Carbon fiber electrodes (7 μm in diameter and 200 μm in length) were prepared with T650 fibers (Cytec LLC, Piedmont, SC, USA). The electrodes used in the experiments with Waveforms A&B received a mild electrochemical pretreatment *in vivo*, consisting of 5 minutes of scanning at 60Hz waveform application frequency a 400 V/s waveform beginning at 0.1V, rising to 1.3V, falling to -0.5V, and rising again to the 0.1V resting potential. The electrodes were then allowed to stabilize for 30 minutes under the application of Waveform A prior to any

reported measurements. Waveform A scans the potential from 0 to 1V to -0.5V to 0V. Waveform B scans the potential from 0.333V to 1V to to 0V to 0.333V. The voltage sweep rate for both waveforms was 400 V/s and both waveforms were applied at 10 Hz. The Waveform B measurements were repeated up to 3 times at each recording site to partially alleviate the low signal to noise ratio by signal averaging; this was especially helpful for reducing noise in the 12 pulse, 60 Hz stimulus recordings. Where multiple recordings were taken, they were averaged together and treated as a single measurement for the purposes of model fitting and statistical analysis. The in vitro experiments to characterize the hangup feature were performed with waveform A without electrode pretreatment. The in vivo experiments from which the hangup feature was removed were previous data from Taylor et. al 2015. FSCV was performed with a fast-scan potentiostat (EI-400, out of production) and CVTarHeels software (courtesy Prof. Michael Heien, University of Arizona). FSCV calibration was performed in a homemade flow cell using DA (Sigma, St Louis, MO, USA) dissolved in N_2purged artificial cerebrospinal fluid (142 mM NaCl, 1.2 mM $CaCl_2$, 2.7 mM KCl, 1.0 mM $MgCl_2$, 2.0 mM NaH_2PO_4, pH 7.4).

Subjects and In Vivo Procedures

All procedures involving animals were approved by the University of Pittsburgh Animal Care and Use Committee. Rats (male, Sprague-Dawley, 250-450g, Charles River Inc., Wilmington, MA) were anesthetized with isoflurane (2.5% by volume O_2), placed in a stereotaxic frame (David Kopf, Tujunga, CA), and connected to an isothermal blanket (Harvard Apparatus, Holliston, MA). Carbon fiber electrodes and stimulating electrodes (MS303/a, Plastics One, Roanoke, VA) were implanted in the dorsal striatum and ipsilateral medial forebrain bundle. The stimulus waveform was a biphasic constant current square wave (2 ms

pulses, 60 Hz, 250 μA, 200 ms or 3 s in duration) delivered with a stimulus isolation unit (Neurolog 800, Digitimer, Letchworth Garden City, UK). Alternating between Waveform A and Waveform B, evoked responses were recorded before and after i.p. administration of a cocktail containing 2 mg/kg raclopride and 20 mg/kg nomifensine.

Hang-up Correction

The hang-up correction was explained in detail[65] by Walters et al, 2015. Briefly, the algorithm assumes that DA undergoes first order adsorption and desorption at the surface of the FSCV electrode according to the following rate expression:

Equation 8: The Rate of Hang-up

$$\frac{dH}{dt} = k_{on}C - k_{off}\Gamma_{DA}$$

which is used to construct a hang-up signal component, $H(t)$, by curve fitting to the hang-up segment of the measured response. The correction is performed by subtracting the calculated signal component from the measured response.

In performing the hang-up correction, it is important to avoid distorting DA's apparent kinetics. This could occur, for example, by curve-fitting $H(t)$ to the measured response before the time where the measured response is caused solely by hang-up. To avoid this outcome, we fit $H(t)$ to later and later segments of the reponse until $H(t)$ stops changing.

The DA Kinetic Model

The DA kinetic model has been explained and used in prior recent reports[43,65,39] from our laboratory. It is intended to provide a generic description of restricted diffusion in the brain extracellular space. To do so, it treats the extracellular space as if it were divided into an inner and outer compartment. The model postulates that DA is released into the inner compartment

41

and undergoes restricted diffusion to the outer compartment where it is detected by the FSCV electrode. Uptake then removes DA from the outer compartment. The model is composed of two equations:

Equation 9: Release and Diffusion from the Inner Compartment

$$\frac{dDA_{ic}}{dt} = R_p \cdot f \cdot e^{-k_R t} - DA_{ic} \cdot k_T$$

Equation 10: First Order Uptake and Diffusion Into the Outer Compartment

$$\frac{d[DA]_{oc}}{dt} = \frac{DA_{ic} \cdot k_T}{V_{oc}} - [DA]_{oc} \cdot k_U$$

which describe changes in amount of DA in the inner and outer compartments, DA_{ic} (in moles) and $[DA]_{oc}$ (in concentration), respectively. This version of the RD model, more thoroughly explained in Chapter 5, contains four adjustable parameters; R_p represents the moles of DA released per stimulus pulse, k_R is a first order rate constant that modifies DA release, k_T is a first-order rate constant for transport between the compartments, and k_U is a first-order rate constant for DA uptake. There are two fixed parameters; V_{oc} is the volume of the outer compartment (16 μm^3, see Walters et al)[43] and f is the stimulus frequency.

Statistics

Statistical analysis was performed in Microsoft Excel (t-test) and SPSS (ANOVA). All t-tests performed were two-tailed, independent sample t-tests with an assumption of equal variance. For the two way ANOVA with repeated measures tests performed for Figure 3, the first 99 data points of the stimuli were tested (9.9 seconds of comparison). For the two way ANOVA with repeated measures done for Figure 6, the first 40 data points of the stimuli were tested (4.0 seconds of comparison).

4.3   RESULTS AND DISCUSSION

The In Vitro Hang-Up

As we recently reported,[39] the DS produces 5 statistically distinct evoked DA responses, 4 fast types and 1 slow type. All these responses, however, exhibit a feature called hang-up, which refers to the tendency of the DA signal to remain above the pre-stimulus baseline after the stimulus ends.[13] The hang-up confounds kinetic modeling of the responses.[39] We show here that the hang-up is caused by the tendency of DA to adsorb to FSCV electrodes.

FSCV calibration is routinely performed in a flow system that uses a loop injector to deliver a bolus of DA solution to the FSCV electrode. Neither the sensitivity nor the response time of the FSCV electrode is affected by the fluid flow.[13] When the DA bolus arrives the FSCV signal rapidly rises to a quasi-steady state with a continued but gentle upward slope (Fig 1, blue line). When the DA bolus ends the FSCV signal rapidly falls but not to the baseline: instead, it hangs-up above the baseline and gently slopes downward. The persistence of the signal after the bolus ends shows that DA remains adsorbed to the electrode surface, as has been documented before.[32,33] The hang-up amplitude is small and may not always be readily distinguished from noise. However, the blue line in Fig 1 is the average of responses from n=7 individual electrodes in a relatively large DA concentration (20 μM), so the hang-up is clearly detected.

Figure 9. In Vitro DA Hangup and Its Correction
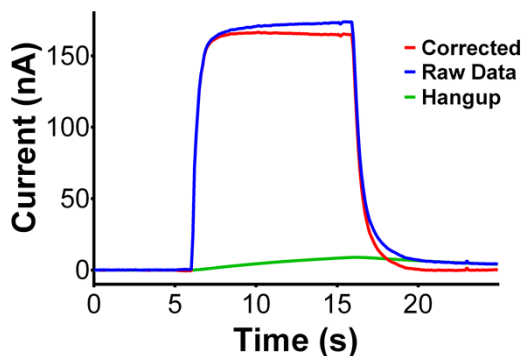
Figure 9: Blue line: The in vitro FSCV calibration response to a bolus of 20-µM DA (mean of n=7 electrodes, SEMs omitted for clarity).   Green line: The hang-up component calculated with Equation 3 of the Methods section.   Red line: The corrected calibration response obtained by subtracting the green line from the blue line.

To further characterize the in vitro hang-up, we exposed n=7 electrodes to 5 consecutive 20-µM DA boluses (Fig. 10a). The hang-up produces a step-wise increase of the signal in the intervals between each bolus.   However, the responses to the individual boluses are superimposable (Fig. 10b: the responses are re-zeroed to the signal just before the start of each bolus).   Additional in vitro hang-ups are reported in the Supplementary Information of this Chapter.

Figure 10. Hangup is an Slow Adsorptive DA Mode

A.

B.
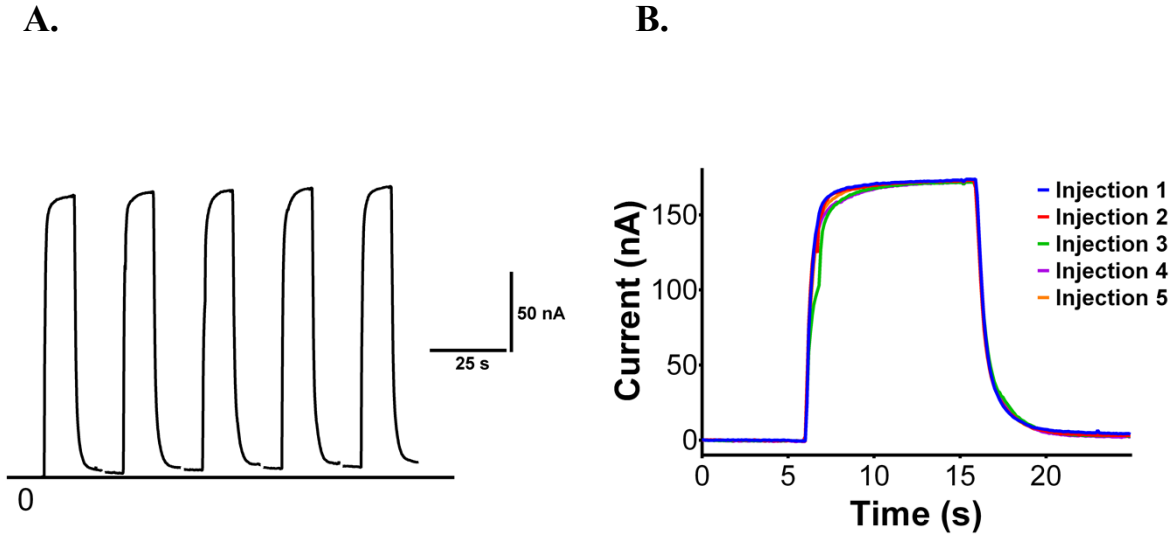
Figure 10: (a) The in vitro response to 5 consecutive DA boluses (20 µM) (average response, n=7, SEMs omitted for clarity). (b) The 5 consecutive responses from panel (a) re-zeroed and superimposed.

The Hang-Up Correction

We modeled the hangup (see Methods) using the data measured between t=20s and t=25s for optimization (Fig. 9, green line). We then subtracted the modeled hang-up from the measured response (Fig. 9, red line). The hang-up correction 'squares-up' the response by removing the gentle upward slope of the quasi-steady state DA signal during the bolus and 'pulls' the response back to baseline after the DA bolus ends.

We applied the same hang-up correction to evoked DA responses measured in vivo (Fig. 11). Fig. 11 shows the type 1 fast response from the DS (blue dots, from Taylor et al 2015[39]), the modeled hang-up (green line, obtained by fitting Equation 3 using the data between t=8s and t=10s for optimization), and the corrected evoked response (red dots, obtained by subtracting the

green line from the blue dots). The correction slightly alters the ascending phase of the response

and pulls the descending phase back to the baseline after the stimulus.

Figure 11. In Vivo DA Hangup and Its Correction
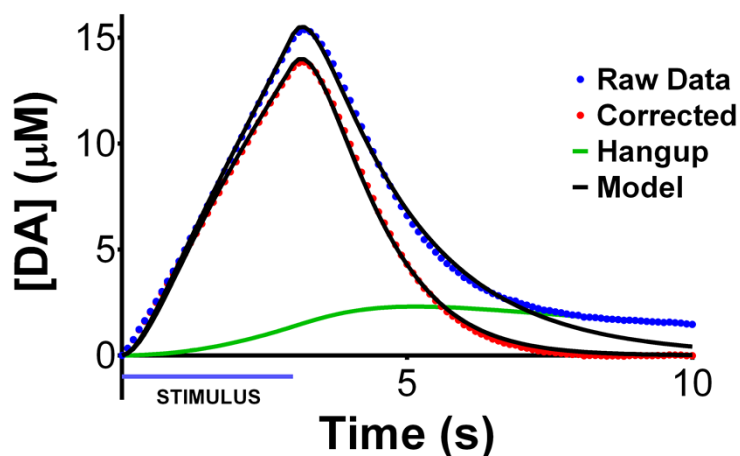
Figure 11: (a) The average type 1 fast DS response (blue dots, from Taylor et. al 2015), the modeled hang-up (green line), and the corrected response (red dots). The solid black lines are the best-fit RD models of the in vivo responses, before and after the hang-up correction. The Pearson's correlation coefficient for fit to the corrected response is 0.9990. Note that the RD model used here has 4 parameters, and is explained further in Chapter 5.

The solid black lines in Fig. 11 are the best-fit restricted diffusion models (see Equations 1 and 2) of the raw and corrected responses. The best fits were obtained by curve fitting using the data between t=0s and t=8s for optimization. As we previously reported, the model does not reproduce the hang-up. However, the fit to the corrected response is nearly perfect (Pearson's correlation coefficient = 0.9990).

The effect of the hang-up correction is similar to that reported in Fig. 7 of Bath et al[11] who compared FSCV responses recorded at 10 Hz to 240 Hz: at 240 Hz there is very little time

available for adsorption to occur. Increasing the frequency to 240 Hz had minimal effect on the ascending phase of responses recorded in brain slices and in vivo but 'pulled' the descending phase back to the baseline, in similar fashion to the hang-up correction introduced here (Fig. 11).

Figure 12. Normal Mode DA Adsorption Greatly Enhances Sensitivity
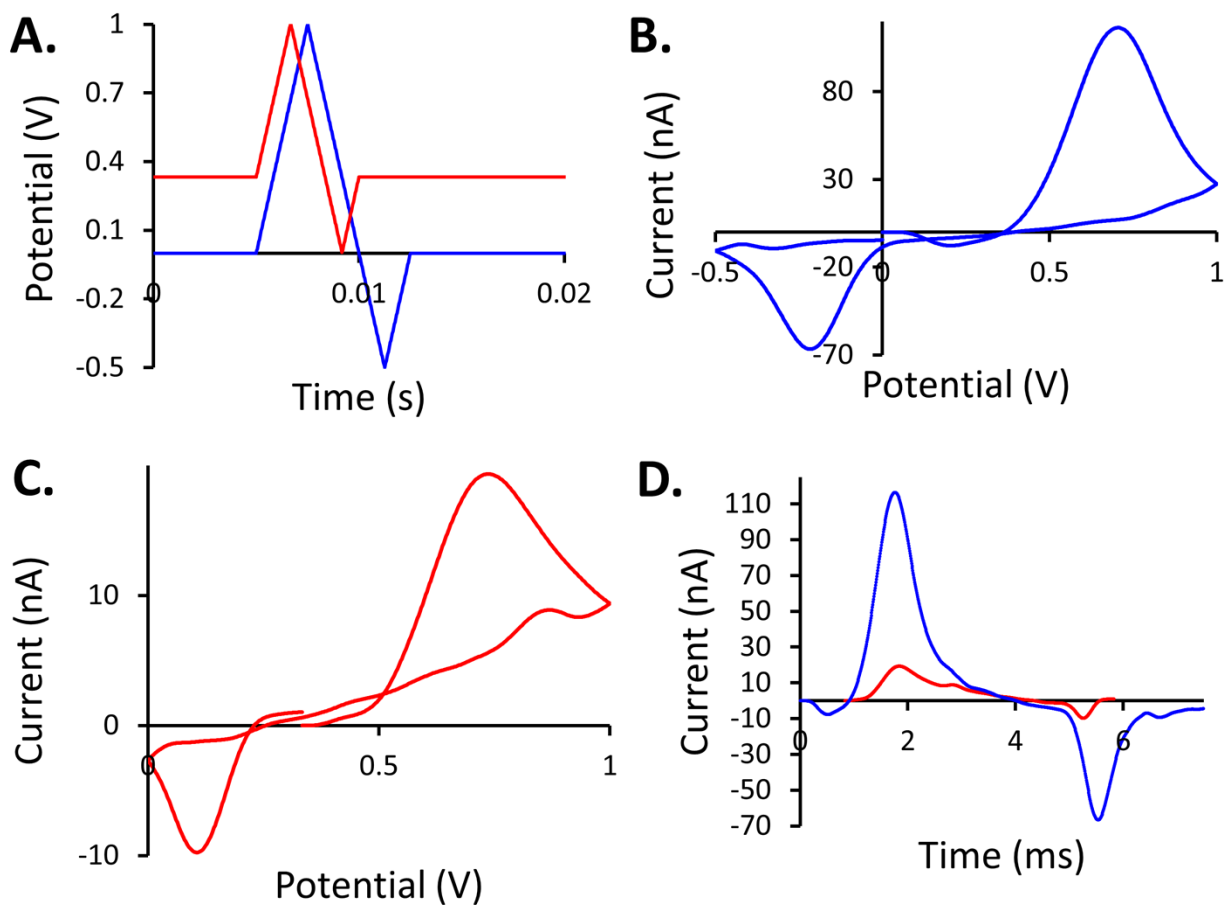
Figure 12: **A)** Waveforms A (blue) and B (red). **B)** Cyclic voltammogram of DA produced by Waveform A. **C)** Cyclic voltammogram of DA produced with the same electrode by Waveform B. **D)** The same voltammograms plotted versus time instead of potential.

Two FSCV Protocols: Waveforms A and B

Waveform A holds the potential at 0.0 V (voltages vs. Ag/AgCl) and sweeps first in the positive direction to +1.0 V, then in the negative direction to -0.5 V, and then back to 0.0 V (Fig. 12A). DA is not oxidized at 0.0 V so, as usual[11,13,56], it adsorbs to the electrode between the FSCV scans. The oxidation of adsorbed DA leads to a large and nearly symmetric voltammetric peak near +0.7 V (Fig 1B): the peak symmetry is indicative of adsorption.[66] Oxidation of DA produces dopamine-o-quinone (DoQ), which reduces back to DA near -0.2 V.

Waveform B holds the potential at +0.33 V and sweeps to +1.0 V, 0.0 V, and +0.33 V (Fig. 12A). Oxidation of DA at +0.33 V prevents it from adsorbing to the electrode. For this reason, Waveform B produces a smaller and more asymmetrical DA oxidation peak (Fig 12C): the peak asymmetry is indicative of diffusion.[66] Waveform B's DoQ peak appears at a different potential but this is a kinetic effect. The DoQ peaks line up with each other when the voltammograms are plotted against time rather than voltage (Fig. 12D).

Figure 13. In Vitro DA Detection With Adsorptive and Non-Adsorptive FSCV
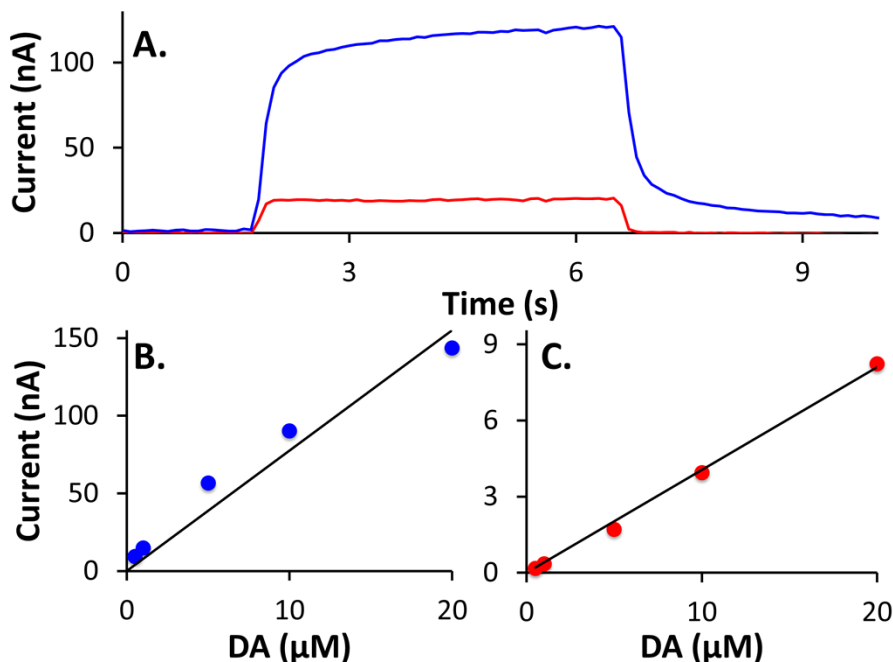
Figure 13: **A)** Temporal profiles obtained during electrode post-calibration (DA= 20 μM) with Waveforms A (blue) and B (red). **B)** DA calibration curve produced by Waveform A. **C)** DA calibration curve produced by Waveform B. In B and C, each data point is the average from post-calibration of n=6 different electrodes.

FSCV post-calibration in a flow cell with Waveforms A and B produces different response profiles (Fig. 13A). Due to DA adsorption, Waveform A produces a larger response that is delayed in reaching its maximum and in returning to its baseline when the DA bolus arrives and departs. Due to the absence of DA adsorption, Waveform B produces a smaller response that rapidly rises and falls. Thus, eliminating DA adsorption increases FSCV's temporal response but at the expense of ~15-fold loss in sensitivity. Waveform A produces a non-linear calibration curve (Fig 13B), which confirms DA adsorption. The non-linearity, however, is sufficiently slight that calibration of in vivo responses with the linear and non-linear

49

regression lines makes no noticeable difference (data not shown). Waveform B produces a linear

calibration curve (Fig. 13C), confirming the absence of adsorption.

Figure 14. In Vivo DA Detection with Adsorptive and Non-Adsorptive FSCV
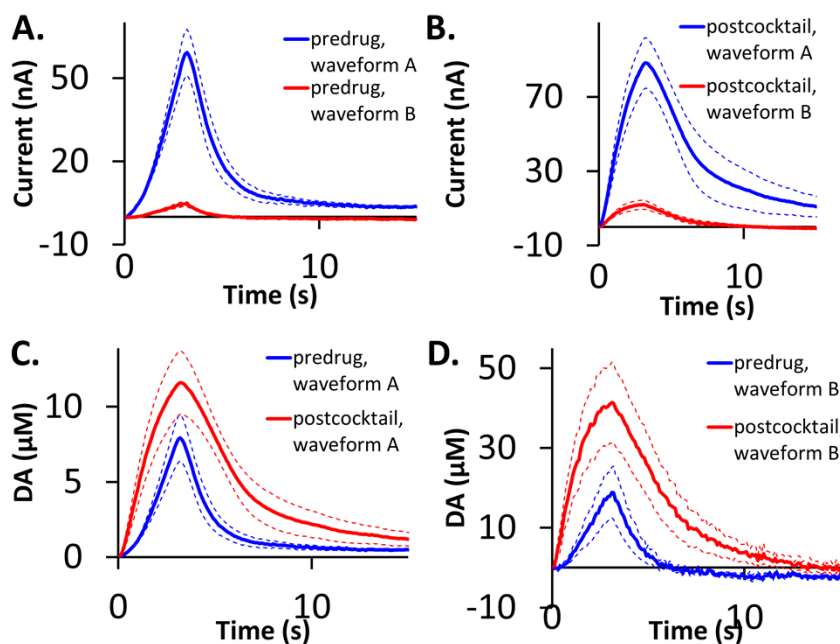
Figure 14: **A)** Pre-drug responses (current) obtained with Waveforms A (blue) and B (red). **B)** Post-drug

responses (current) obtained with Waveforms A (blue) and B (red). **C)** Pre- and post-drug responses (concentration)

obtained with Waveform A. **D)** Pre- and post-drug responses (concentration) obtained with Waveform B. The solid

lines are the average of n=6 responses obtained with n=6 electrodes in n=6 rats. The dashed lines are the standard

errors. The stimulus was delivered for 3 s (beginning at t=0) at 60 Hz. The drug cocktail contained nomifensine (20

mg/mg) and raclopride (2 mg/kg) and was delivered i.p. As determined by two way ANOVA with repeated

measures, the drug cocktail significantly affected the evoked responses (**C** & **D**) obtained with both Waveforms A

(p = 0.003) and B (p = 0.016).

Recording of Evoked DA Responses with Waveforms A and B

Waveforms A and B produce different FSCV responses during recordings of evoked DA release in the striatum (Fig 14A and 14B). Waveform B produces ~15-fold less voltammetric current, consistent with its lower sensitivity for DA (Fig. 13). Post calibration of the responses obtained with Waveforms A (Fig. 14C) and B (Fig. 14D) leads to three notable differences. First, there is a systematic difference between the DA amplitudes obtained with Waveforms A and B. Second, Waveform A produces responses that hang up[65], i.e. that do not return to baseline after the stimulus. Third, Waveform B produces a lower signal-to-noise ratio and more baseline drift.

There are two likely contributing factors to the different DA amplitudes obtained with Waveforms A and B. One is Waveform B's low signal-to-noise ratio. Standard approaches in analytical chemistry define the detection limit as the signal that is 3x the noise and the limit of quantitation as 10x the noise.[67] The signal amplitudes produced by Waveform B do not exceed 10x the noise, so DA quantitation by this waveform is unreliable. A second contributing factor could be the presence in brain tissue of high concentrations of ascorbic acid (AA), which is well known to reduce DoQ to DA.[13,61,68] This reaction affects the DA concentration in the vicinity of the electrode while it is at the hold potential (+0.33 V) of Waveform B. Thus, the elimination of adsorption also decreases FSCV's selectivity for DA. We did not investigate this matter further because Waveform A provides higher signal-to-noise ratio and measures DA without interference by AA.[13,61,68,69]

Figure 15. DA Adsorption Minimally Impacts Kinetic Profiles
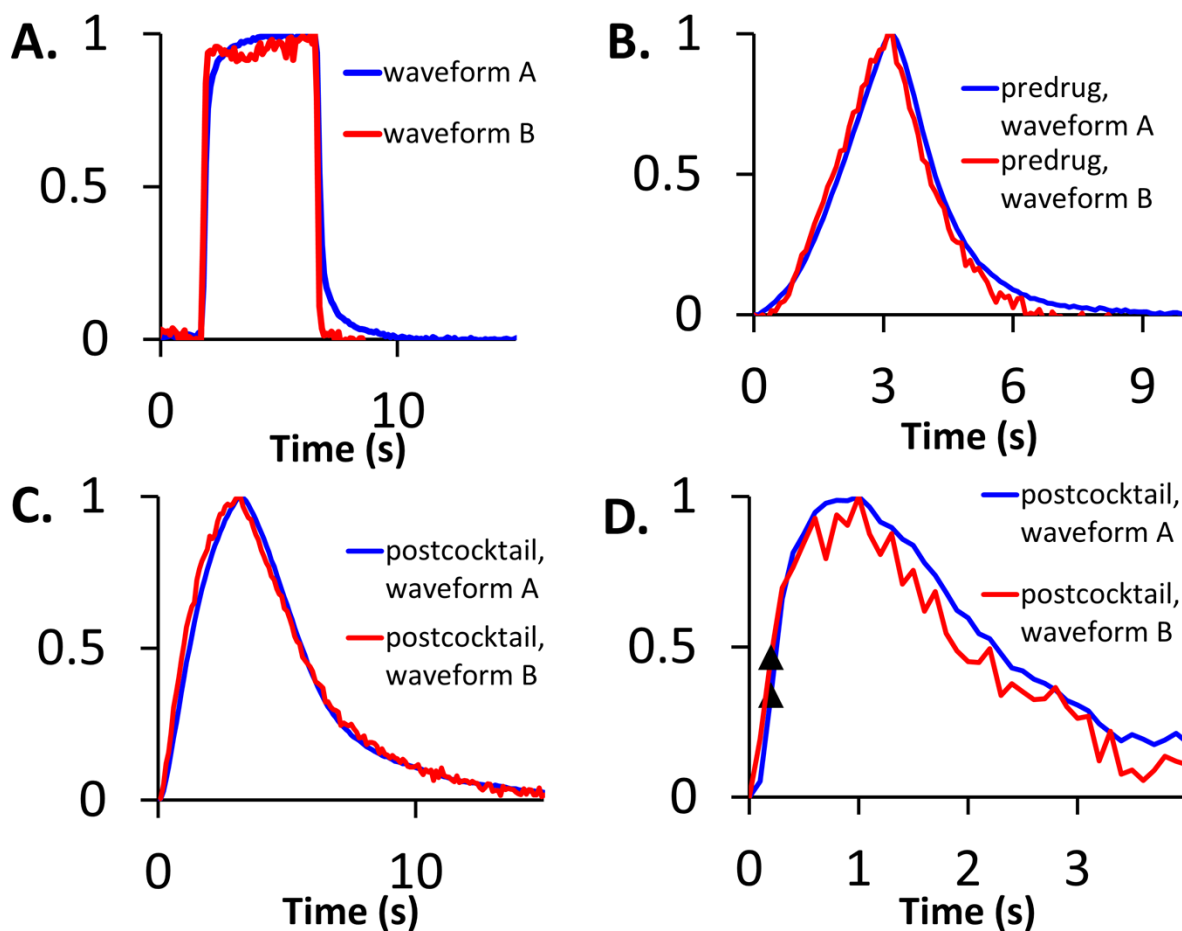
Figure 15: Comparisons of the temporal profiles of responses obtained with Waveforms A (blue) and B (red). Responses obtained with Waveform A were corrected for hang-up. Responses obtained with Waveform B were corrected, as needed, for baseline drift. All responses normalized to their maximum amplitude. **A)** Calibration (representative example from one electrode). **B)** Predrug 3-s stimulus responses. **C)** Postdrug 3-s stimulus responses. The raw data for B and C are shown in Fig 3. **D)** Postdrug 200-ms stimulus responses (average of n=6 responses obtained with the same electrodes and animals as C and D). SEMs omitted from B, C, and D for clarity.

The Temporal Profiles of Responses with Waveforms A and B

Figure 15 compares the temporal profiles of calibration and *in vivo* evoked responses produced by Waveforms A and B. To facilitate the comparison, three manipulations of the data were performed. First, in the case of Waveform B, where necessary, a correction was applied for baseline drift (see in Fig. 14D where the blue trace drifts below the baseline). Second, in the case of Waveform A the responses were corrected for hang-up by the procedure explained in Walters et al[65] (see Methods). Third, the responses were normalized with respect to their maximum amplitude.

Figure 15 validates the hang-up correction procedure presented in Figures 9 and 11 and substantiates that slow-type response features (Fig. 15B) are not a product of adsorptive distortion. After the corrections for baseline drift and hang-up, only the in vitro calibration responses exhibit a noticeable temporal difference (Fig. 15A). It must be emphasized, however, that the flow system used for calibration causes very rapid changes in the DA concentration, much faster than those observed during *in vivo* FSCV.

The pre-cocktail responses exhibit slow-type features, including an initial lag in the signal when the stimulus begins and a "concave-upwards" profile of the ascending phase of the response (Fig. 15B). The ability of the drug cocktail to eliminate the slow response features (Fig. 15C), even with the same electrodes in the same recording locations, confirms that the slow features are not due to inherent temporal limitations of the recording technique.

Figure 15D reports post-cocktail responses to a 200-ms (12-pulse) stimulus. These responses exhibit the feature called overshoot,[42,36,38,43] where the evoked response continues to rise after the end of the stimulus. The results show that the temporal features of the overshoot

are likewise unaffected by DA adsorption, and offer additional support to the restricted diffusion mechanism[43].

Figure 15 confirms that adsorptive distortion does not explain the difference between the DA concentrations obtained with Waveforms A and B (Figs. 14C and 14D). Theoretically, adsorption would decrease the apparent DA concentration by dampening the FSCV response but no such dampening is evident in Fig. 15.

Kinetic Analysis with the Restricted Diffusion Model

Figure 15 substantiates that the slow-type responses features of lag and overshoot are not produced by adsorptive distortion. This is point is important because explaining DA lag and overshoot in FSCV data has been a historical challenge. Recently, we introduced a restricted diffusion model[43,65] (see Methods) that explains lag and overshoot. The restricted diffusion model (here using 4 parameters) provides excellent fits (Pearson's $r^2 > 0.995$ for each case where the average of the modeled fits is compared to the average of the data) to the pre-and post-cocktail responses obtained with Waveforms A (hang-up corrected) and B (Fig. 16).

Figure 16. DA Adsorption Is Not Required to Detect Drug Effects

Table 6. Waveform A & Waveform B parameters I
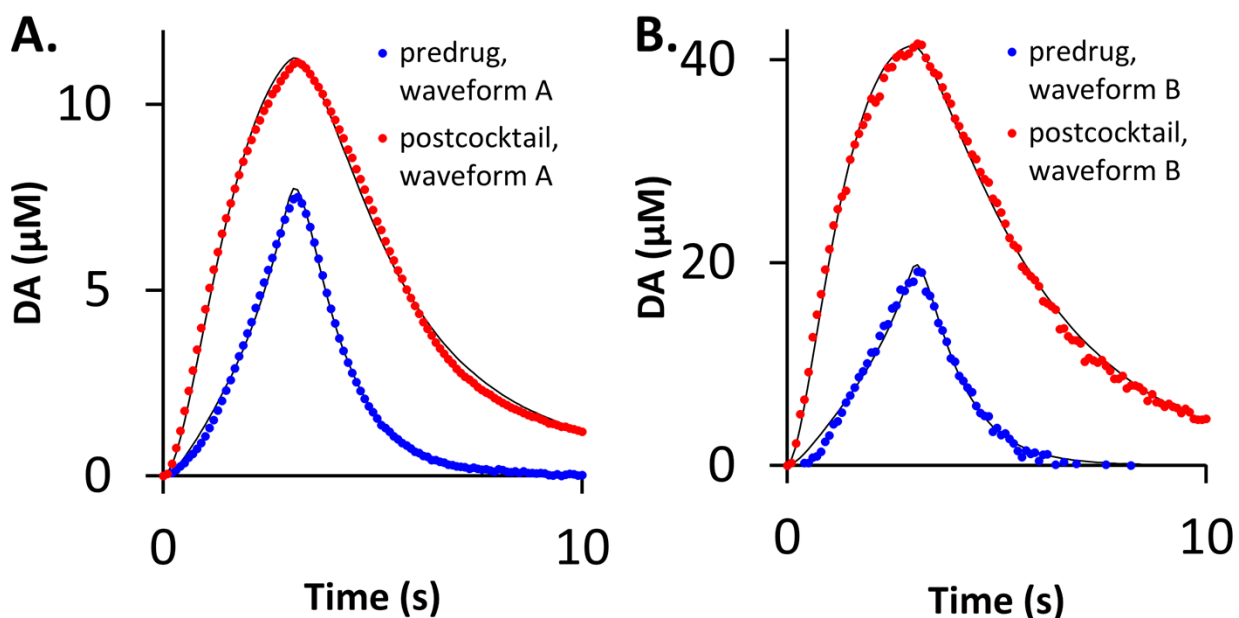
	R_p (zmols)	k_U (s^{-1})	k_T (s^{-1})	k_R (s^{-1})
Waveform A predrug	1.0 ± 0.1 *	2.0 ± 0.6 *	1.6 ± 0.3 *	-0.6 ± 0.1 *
Waveform A postcocktail	5.6 ± 1.1 *	0.7 ± 0.1 *	0.7 ± 0.1 *	0.4 ± 0.2 *
Waveform B predrug	7.9 ± 5.0 *	7.9 ± 5.6	2.1 ± 0.4	-0.7 ± 0.1 *
Waveform B postcocktail	42.0 ± 13.5 *	2.0 ± 1.4	1.1 ± 0.5	0.7 ± 0.3 *

Figure 16: Best fits of the restricted diffusion model (black lines) to pre- and post-drug evoked responses (3 s, 60 Hz) obtained with (A) Waveform A (corrected for hang-up) and (B) Waveform B (corrected for baseline drift). The table reports the corresponding parameter values. With waveform A, all parameter values were significantly different after the administration of the drug cocktail: R_p (p = 0.0022), k_R (p = 0.00028) k_U (p = 0.046) and k_T (p = 0.0083). With waveform B, only R_p (p = 0.039) and k_R (p = 0.00049) were significantly different after the administration of the drug cocktail, while k_U (p = 0.34) and k_T (p = 0.12) were not significantly different.

The parameter values obtained with the model (Table 6) show generally good agreement between Waveform A and B. However, Waveform B produced parameters with larger standard deviations that diminish their statistical significance. But, some general observations are useful. First, Waveforms A and B produced different values of R_p because of the concentration differences explained above. Even so, the magnitude of the change in R_p induced by the cocktail is similar, ~7-fold in each case. Second, there are no significant differences between the values of k_U, k_T, or k_R obtained with Waveforms A and B (statistical details in the figure legend). This is because these parameters are first order rate constants determined by the temporal profile, rather than amplitude, of the responses. Both waveforms show that the cocktail, which includes nomifensine, decreases the rate constant for DA uptake, k_U. The decrease in k_U reported by Waveform A was significant.

Figure 17. Adsorption Impacts Apparent Measured DA Concentrations

Table 7. Waveform A & Waveform B parameters II
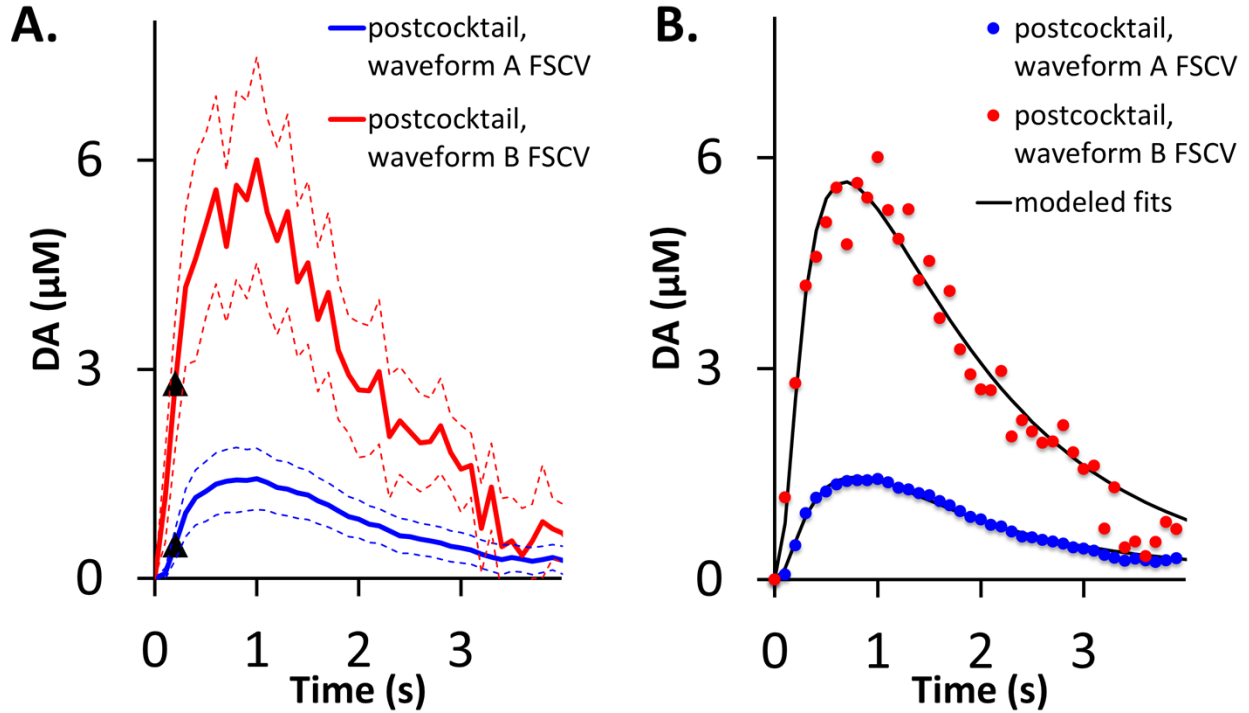
	R_p (zmols)	k_U (s^{-1})	k_T (s^{-1})
Waveform A	4.6 ± 1.2 *	1.1 ± 0.3	1.6 ± 0.3
Waveform B	18.2 ± 3.4 *	1.6 ± 0.4	2.6 ± 0.8

Figure 17: **A)** Post-drug responses to a 200-ms stimulus obtained with Waveforms A (blue) and B (red). Solid line is the average of n=6 responses each obtained with a different electrode in a different animal. Dashed lines are the SEMs. **B)** Best fits of the restricted diffusion model (black lines) to the data points from A. The table gives the corresponding parameter values. The R_p, k_U, and k_T parameter values as measured with the two waveforms were also tested for significant differences by an independent sample two tailed t-test. The k_U (p = 0.48) and k_T (p = 0.28) parameter values are not significantly different when measured with either waveform, although the R_p is significantly (p = 0.0034) different when measured with the different waveforms. As determined by two way ANOVA with repeated measures, the waveform used significantly affected the evoked response (p = 0.017).

We also modeled post-cocktail 200-ms stimulus responses (Fig. 17: as reported before[36,34] slow sites do not respond to a pre-drug 200-ms stimulus). Again, Waveform B produced a larger concentration estimate and a lower signal-to-noise ratio. As we have explained before[43], these brief stimulus responses can be fit with a simplified, 3-parameter version of the restricted diffusion model that omits the plasticity factor, k_R (this 4 parameter model will be explained in detail in Chapter 5). Waveform B produces a larger value of R_p to account for the larger apparent concentration whereas the two waveforms produce similar values of the rate constants, k_U and k_T (statistical details in the figure legend).

4.4 CONCLUSION

Efforts to understand the influence that adsorption has on DA signals have had three important consequences. The first consquence is as additional validation of the simple RD model, as it confirms that adsorption is not responsible for the existence of DA overshoots. The second consequence is that the hangup, which has been previously not well understood, is established as a feature of a second, slower adsorption mode than previously characterized adsorption. Because the hangup is amenable to being corrected for with a simple mathematical procedure, this instrumental influence can be removed from the data, which ought to improve the accuracy of the data and the values of modeled parameters extracted from the data, if the method for correcting the hangup in vivo is reasonable. The observation that hangup corrected waveform A (hangup adsorption removed) is identical in shape to waveform B (no adsorption), strongly suggests that the hangup correction procedure as used improves the accuracy of the data

at determining the DA concentration at the electrode surface over time. The fact that this makes the RD model fit longer stimuli better is also comforting, although a 4 parameter RD model is still required to fit most DA responses to longer stimuli. This is the subject of Chapter 5. Finally, this work substantiates that DA's apparent kinetic diversity is not an artifact of adsorptive distortion. The same FSCV electrodes in the same recording locations produce both fast-type (post-cocktail) and slow-type (pre-drug) responses, which would be impossible if the temporal response of FSCV were adsorption limited.

Waveforms A and B produced different estimates of *in vivo* DA concentration. This is likely due to the low signal-to-noise ratio (see Figure 6) and selectivity of Waveform B during *in vivo* measurements. Although Waveform B is useful in some respects, we do not advocate it for routine use as a substitute for Waveform A. Waveform A produces higher sensitivity, signal-to-noise ratio, and selectivity over ascorbate.

4.5   SUPPLEMENTARY INFORMATION

Figure 18. The Hangup is An Adsorptive Feature
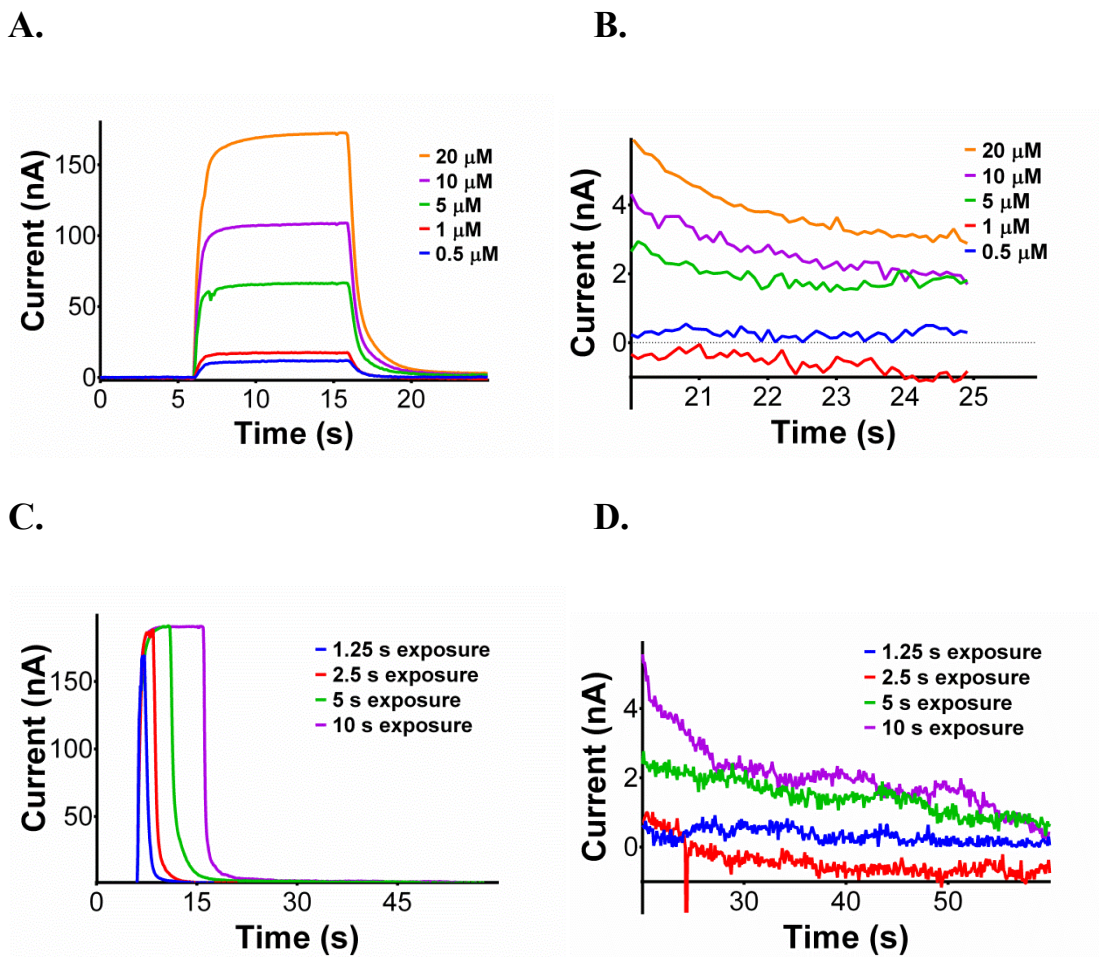
Figure 18 – Hang-ups observed during in vitro FSCV calibration in a flow system. Panels A and B show the dependence of hang-up on DA concentration at a fixed bolus duration of 10s (Panel B reports the same data as Panel A on an expanded scale). Panels C and D show the dependence of hang-up on the bolus duration at a fixed DA concentration of 20 μM (Panel D reports the same data as Panel C on an expanded scale). Each line reports the average of responses recorded from n=7 FSCV electrodes (SEMs omitted for clarity). These data show that hang-up is minimal if either the DA concentration is low (<1 μM) or the exposure time is kept brief (<2.5 s). However, at

higher concentrations or longer durations the hang-up increases in both amplitude and duration, which is consistent with the behavior expected for a process involving adsorption.

Figure 19. Hangup Adsorption Does Not Affect Kinetic DA Diversity
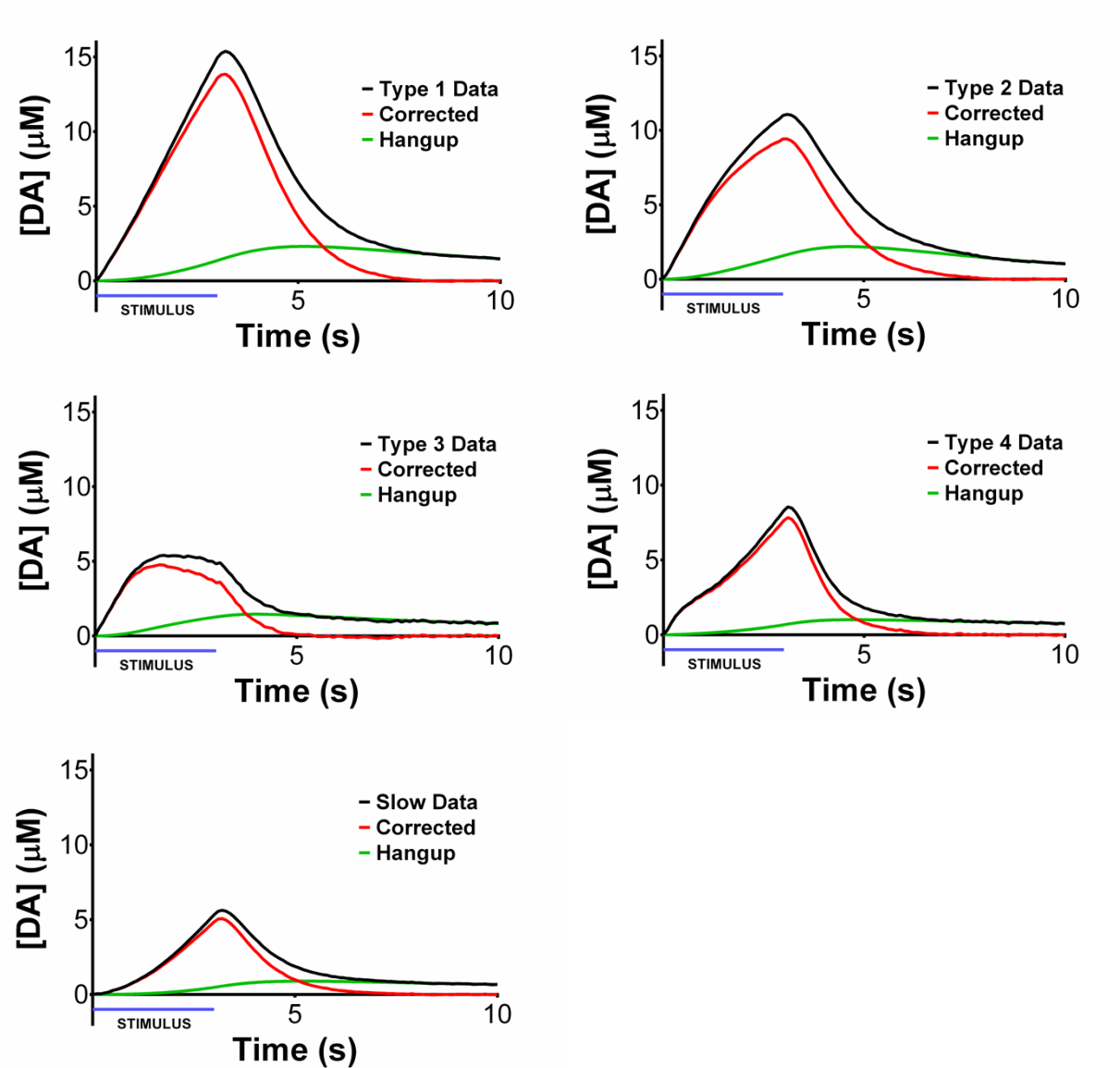
Figure 19 - The hang-up corrections applied to the five evoked responses produced in the DS, four fast types and one slow. The raw (uncorrected) responses are in black, the modeled hang-ups are in green, and the corrected responses are in red. The raw responses are from our recent paper Taylor et al 2015.

5.0   EXTENSION OF THE RD MODEL TO DESCRIBE LONGER STIMULI
Adapted from Walters et al. 2014 and Walters et al. 2015

5.1   INTRODUCTION

Dopamine (DA) is an important neurotransmitter in the central nervous system.[28]   It

contributes to many aspects of healthy brain function[70–72] and plays a central role in multiple

neurological[73–76] and psychiatric[77–79] disorders. Fast-scan cyclic voltammetry (FSCV), a popular

and powerful method[80–84] for monitoring DA in terminal fields such as the dorsal striatum (DS)

and nucleus accumbens (NAc), is often paired with electrical stimulation of DA axons in the

medial forebrain bundle. Electrical stimulation produces evoked DA responses that are

heterogeneous[85–87] in amplitude and temporal profile. Although sometimes attributed to

distortions of the FSCV signal,[4,7,54] recent evidence suggests instead that the heterogeneity

derives from an inherent diversity of DA kinetics.[42,36,38,43,34,39,37] Such kinetic diversity could be

a contributing factor in DA's functional diversity. As such, it is very important to understand the

mechanistic causes of this kinetic diversity. In Chapter 3, we presented a simple and novel

model which explains many important features of DA overflows with the use of only three

adjustable parameters. However, much of the kinetic diversity of DA signaling in the brain is

only apparent upon the application of longer stimulations, commonly 180 stimulus pulses

applied at 60 Hz. While in some cases the simplest 3 parameter RD model can describe the

evoked DA overflows resulting from these longer stimulations, in many cases, even after hangup

correction (Chapter 4), it provides poor fits. Thus, some additional parameter is required to explain the kinetic diversity that occurs with longer stimulations in anaesthesized rats.

5.2   METHODS

The RD Model with Plasticity

The RD Model with plasticity is a slight modification of the one introduced by Walters et al[43] and used by Taylor et al.[39] It is set up to be a generic model of restricted diffusion. It divides the extracellular space into an inner and outer compartment: DA is released into the inner compartment and subsequently transported to the outer compartment, where it is detected by FSCV. The inner and outer compartments are just constructs in the model: they do not necessarily correspond to actual physical compartments in the extracellular space. However, the transport step between the inner and outer compartment effectively captures the concept of restricted diffusion, and is mathematically sound (see Chapter 3). The model can be stated as follows:

Equation 11: Dynamic Release and Diffusion from the Inner Compartment

$$\frac{dDA_{ic}}{dt} = R_p \cdot f \cdot e^{-k_R t} - DA_{ic} \cdot k_T$$

Equation 12: First Order Uptake and Diffusion into the Outer Compartment

$$\frac{d[DA]_{oc}}{dt} = \frac{DA_{ic} \cdot k_T}{V_{oc}} - [DA]_{oc} \cdot k_U$$

The first equation describes the amount (in moles) of DA in the inner compartment, DA_{ic}, and the second equation describes the concentration of DA in the outer compartment, $[DA]_{oc}$. There are four adjustable parameters; R_p is the moles of DA released per stimulus pulse, k_R is a first order rate constant that modifies DA release, k_T is a first-order rate constant for transport between the compartments, and k_U is a first-order rate constant for DA uptake. There are two fixed parameters; V_{oc} is the volume of the outer compartment, which is set to 16 μm^3 (see Walters et al),[43] and f is the stimulus frequency, which is set according to the experimental conditions.

Other Models

The details of how the other models are simulated are reproduced in the methods sections of Chapters 3 and 4.

FSCV Procedures

Procedures for FSCV are identical to those described in recent reports from our laboratory.[29] Briefly, carbon fiber electrodes (T650 fibers, Cytec LLC, Piedmont, SC, USA) were 200 μm in length and 7 μm in diameter. The FSCV waveform had a rest potential of 0 V, a positive limit of 1 V, a negative limit of -0.5 V (all vs. Ag/AgCl), a sweep rate of 400 V/s, and a repetition frequency of 10 Hz. All of the data presented in this Chapter were collected by Mitch Taylor and Zhan Shu.

In Vitro FSCV Calibration

In vitro FSCV calibration was performed in a homemade flow cell attached to a Rheodyne loop-style low-pressure sample injector valve. Flow was generated by hydrostatic

pressure from an elevated reservoir containing N_2-purged artificial cerebrospinal fluid (142 mM NaCl, 1.2 mM $CaCl_2$, 2.7 mM KCl, 1.0 mM $MgCl_2$, 2.0 mM NaH_2PO_4, pH 7.4).

In Vivo Procedures

All procedures involving animals were carried out with the approval of the University of Pittsburgh Animal Care and Use Committee. Several evoked DA responses used herein for modeling are taken from previous publications, which contain the full experimental details.[36,39]

5.3   RESULTS AND DISCUSSION

Different 4 parameter models

When we were first trying to fit our FSCV data, we used at first a 4 RD parameter model as previously explained in Chapter 3:

Equation 13: Release and Diffusion from the Inner Compartment

$$\frac{dDA_{ic}}{dt} = R_p \cdot f - DA_{ic} \cdot k_T$$

Equation 14: Michaelis-Menten Uptake and Diffusion into the Outer Compartment

$$\frac{d[DA]_{oc}}{dt} = \frac{DA_{ic} \cdot k_T}{V_{oc}} - \frac{V_{max} \cdot [DAoc]}{[DAoc] + K_M}$$

However, we learned that while this 4 parameter model was able to fit some DA responses resulting from stimulus conditions which the 3 parameter version of the RD model did

not fit well (namely, many 180 pulse stimuli at 60 Hz), the parameter values that this produced were highly nonsensical. In other words, the additional mathematical flexibility provided by the 4th parameter can be helpful even if the result is meaningless. Since we were able to determine that V_{max} and k_M information are not extractable from FSCV data anyway from the short stimulus experiments presented in Chapter 3, we decided to leave uptake as a first order term, and focus on making one of the parameters dynamic. The parameter we chose to make dynamic was the release parameter, although in principle any parameter could be made dynamic. It is simple to make the release parameter dynamic, because there is an stimulus-defined period of release. A simple exponential can be considered to approximate changing release, and is prevented from bringing the parameter it modifies either to zero or an absurdly large number by the limited stimulus duration. This 4 parameter RD model with dynamic release, as explained in the methods section of this Chapter, makes excellent fits to a wide variety of FSCV signals. However, it is important to note that any or all of the RD model parameters may change with time, and the fact that a 4 parameter RD model with dynamic release makes excellent fits to the data does not mean that the concept of dynamic release is correct per se, only that allowing the release parameter of the simplest, 3 parameter RD model to be modified by an exponential is adequate to make fits to many DA responses arising from extended duration stimuli which are not amenable to being fit with the simplest model. Some factor in the RD model is changing on a subsecond timescale, but the modeling results here merely demonstrate that it is plausible that it is the release that is changing - they do not, by themselves, constitute a proof.

DS fast and slow domains with the DG model and 4 parameter V_{max}/k_M model

We ran 4 parameter DG simulations of fast and slow DS responses (Fig. 20a: symbols are averages, SEMs omitted for clarity, stimulus = 60 Hz, 1 s, 250 µA). We fixed K_M at 0.2 µM, a value cited many times in the literature.[44] A *Gap* of 2 reproduces the minimal lag and overshoot of the fast response (Fig 20a, red) but, overall, the simulation does not fit the data. A *Gap* of 10 reproduces the prominent lag in the slow response (Fig 20a, blue) but, overall, the simulation does not fit the data. For the reasons we explained above, the DG model cannot produce responses with a prominent lag but no overshoot even though such responses are commonplace in slow domains.[20,21] The 4 parameter V_{max}/k_M RD model reproduces all the features of the fast and slow DS responses (Fig 3B). The parameter values obtained from these fits are undoubtedly distorted, but the ability of this 4 parameter model to fit the data illustrates that it is the inclusion of an extra parameter into the RD model that allows it to fit the data. So, not all 4 parameter models can fit this data, but the 4 parameter V_{max}/k_M RD model can.

Figure 20. The RD Model Improves Description of Longer Stimuli
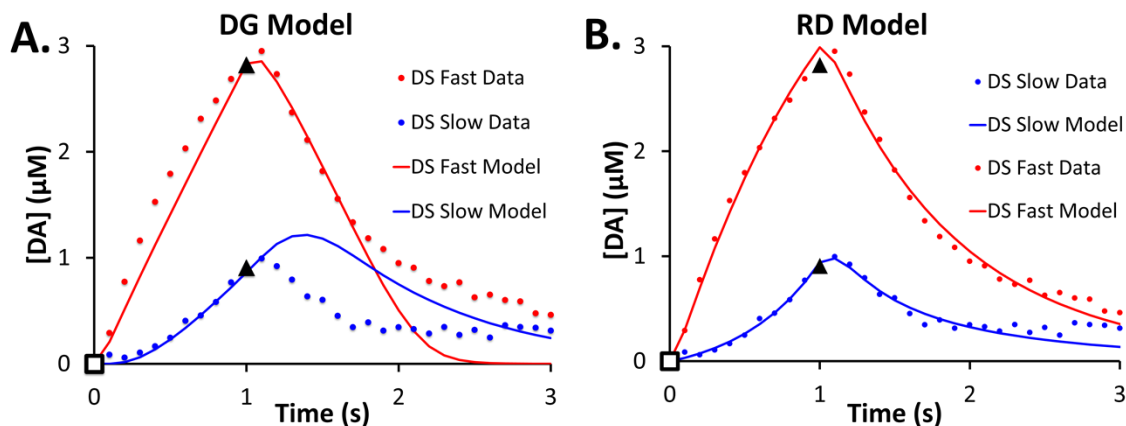
Figure 20. Fits of the DG (A) and RD (B) models to averaged responses from fast and slow domains of the dorsal striatum. The parameter values for these fits are reported in the Supplementary Information.

We ran RD simulations of pre- (Fig. 5, blue) and post-nomifensine (Fig. 5 green) responses from the fast and slow domains of the DS and NAc (Fig 5, the simulations are shown as lines, the averaged data points are shown as symbols, SEMs are omitted for clarity, stimulus = 60 Hz for .2, 1, and 3 s, 250 µA). We used the search algorithm to identify all the parameters. The 4 parameter V_{max}/k_M RD model provides excellent fits to the data but with a few exceptions: so, we conclude that this RD model captures most, but not quite all, the features of these evoked responses.

Figure 21. RD Model Fits DA Responses to Longer Stimuli Throughout the Striatum
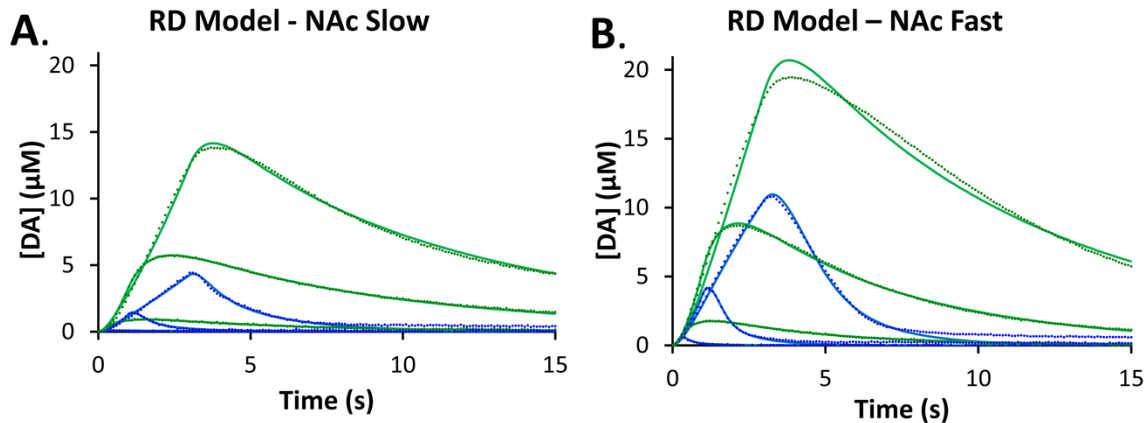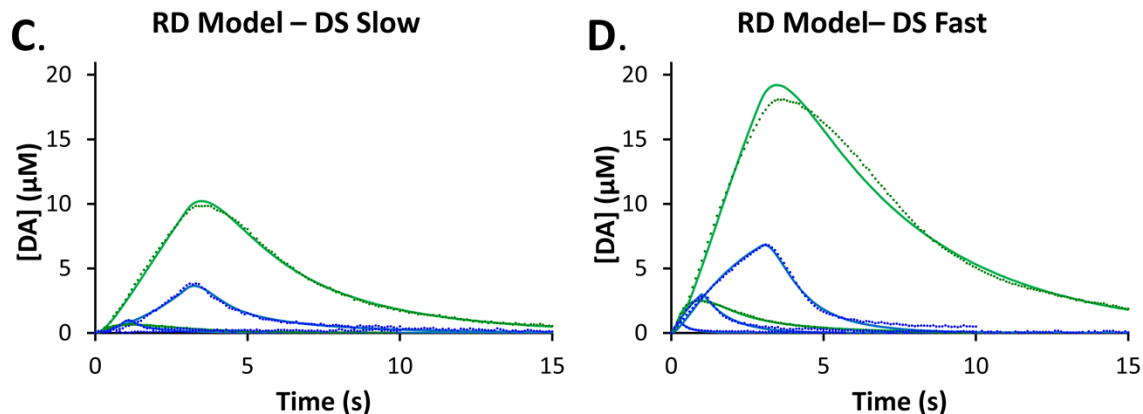
Figure 21. Fits of the 4 parameter V_{max}/k_M RD model to averaged responses from the dorsal striatum and nucleus accumbens both before (blue) and after (green) animals were treated with nomifensine.

Parameter values

We used the search algorithm to identify all the parameter values for the RD simulations in all Figures in this document. We have imposed no constraints on any of the values and we have only simulated "raw" data that have not been modified through deconvolution or principal components methods. We believe this to be a completely unbiased, objective approach to evaluating the parameters.

Our unbiased approach, however, produced some extreme parameter values here. The V_{max} values reach as high as 910 and 3200 μM/s in some cases of Fig 21. However, these extreme V_{max} values are paired with equally extreme K_M values of 41.4 μM and 1600 μM, respectively: such extreme K_M values are impossible because they far exceed any DA concentration measured in any of our experiments. These extreme values appear when the data exhibit first order character, which causes the model to optimize the pseudo-first order rate constants ($k=V_{max}/K_M$), which turn out to have perfectly reasonable values of 22 s^{-1} (from an animal not treated with nomifensine) and 2 s^{-1} (from an animal treated with nomifensine).

69

It is important to emphasize that in instances where the actual data are kinetically pseudo-first order, the evoked profiles contain no intrinsic information about V_{max} or K_M. For this reason, we have included the pseudo first order rate constants in the parameter tables in the Supplementary Information.

The parameter values obtained with the 4 parameter V_{max}/k_M RD model vary consistently with duration of the stimulus (Supplementary Information). For reasons we do not understand, the DA release (R_p), clearance (k_U), and transport (k_T) parameters decreased (with one or two exceptions) as the stimulus duration increased. We speculate that time-dependent factors such as depletion of the readily releasable pool, depletion of the DA terminals' energy reserves, or changes in the occupation of DA autoreceptors are contributing factors. This prompted us to move on from the 4 parameter V_{max}/k_M RD model to a 4 parameter RD model with dynamic release.

Dynamic release 4 parameter RD Model

Figure 22 shows corrected versions of the five evoked responses produced in the DS (data from Taylor et. al 2015, see the Chapter 4 Supplementary Information for the individual hang-up corrections). The solid lines are the best-fit restricted diffusion models of each response type. Overall, the fits are excellent (Pearson's correlation coefficients >0.99) although, as discussed below, there are noticeable differences just after the stimulus begins.

Figure 22. 4 Parameter Dynamic Release RD Model Fits DA Kinetic Diversity
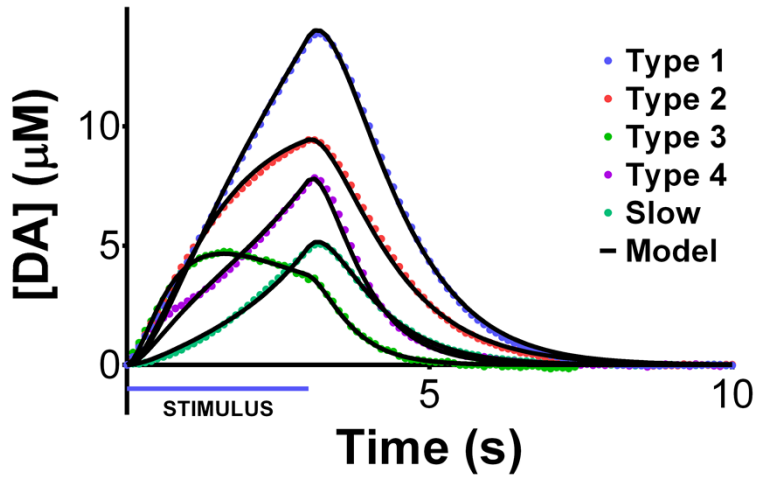
Figure 22: Dots: Hangup corrected versions of the five DS evoked responses (raw data from Taylor et al 2015). Lines: Best fits of the restricted diffusion model (Pearson's correlation coefficients all exceed 0.99.

Table 8. 4 Parameter RD Model Parameter Values for 5 Kinetic DA Types

Table 1: Parameters from Fig. 4				
	R_p (zmol)	k_U (s^{-1})	k_T (s^{-1})	k_R (s^{-1})
Type 1	3.45	1.29	1.29	-0.24
Type 2	5.87	2.02	0.96	0.01
Type 3	6.75	3.79	1.86	0.24
Type 4	2.96	3.33	1.45	-0.42
Slow	0.895	2.52	1.22	-0.67

Table 8 (mislabeled in the Table as Table 1) lists the values of the 4 adjustable parameters obtained from Fig. 22. The parameters Rp and kU represent the kinetics of DA release and uptake, respectively. In contrast to the more conventional use of Michaelis-Menten kinetics,3 we use first-order kinetics for uptake because the descending phase of the evoked responses exhibit purely first order behavior.[39] The parameter k_T accounts for the mass transport of DA to the electrode.[43] The parameter k_R modifies the rate of DA release. It behaves as a 'short term plasticity factor': positive values reproduce the short-term depression of fast responses and negative values reproduce the short-term facilitation of hybrid and slow responses. The conventional model[3] does not contain any plasticity factor, so this is a novel feature of our modeling. The parameter values in this table should be taken to have no more than 2 significant digits (see section 7.4 for sources of error).

Figure 23. Nomifensine Alters Short Term Plasticity of Release

A.   **B.**
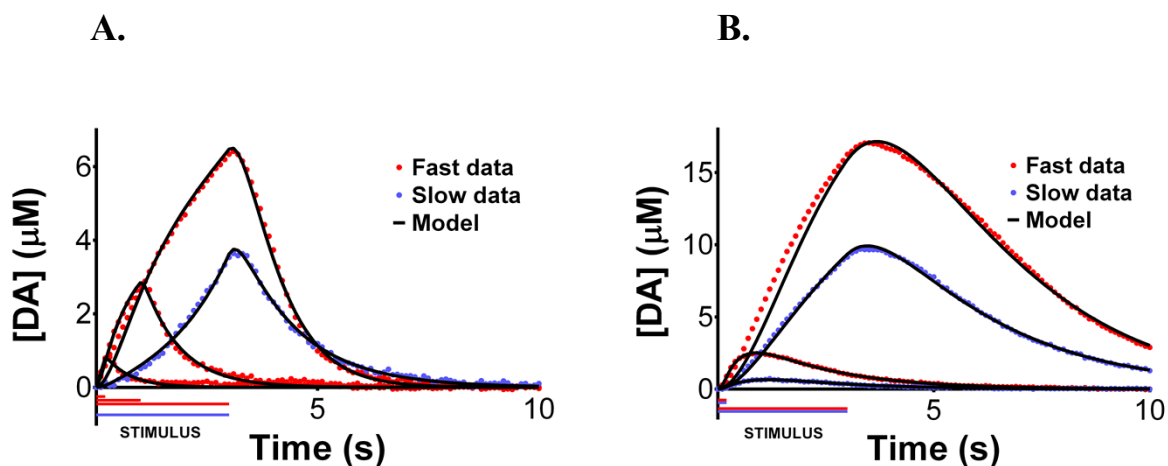
Figure 23: Evoked responses corrected for hang up (symbols) from the fast (red) and slow (blue) domains of the DS from rats before (a) and after (b) treatment with nomifensine (20 mg/kg i.p.). The lines show the best-fit models: the parameters are reported in the Supplementary Information Table S3. The raw as-measured responses are reported in Figs. 5c and 5d of Ref. 28.

This work shows that the descending phase of the response reflects the rate of transport or uptake, whichever is slower. This is because the model postulates that transport and uptake occur in serial fashion, i.e. that transport is a preliminary step in the mechanism of uptake.

72

We believe this has profound implications because prior models have postulated that transport and uptake occur in parallel fashion,[3] i.e. that diffusion distorts the intrinsic DA response. But, if transport and uptake occur in serial fashion, as we now suggest, then FSCV measures DA as it diffuses from release sites to uptake sites. This implies that FSCV provides a direct measurement of intrinsic DA.

Table 9. 4 Parameter RD Model Fits Before Nomifensine, k_T ~2

Figure 7A	$R_{p\,(zmol)}$	$k_U\,(s^{-1})$	$k_T\,(s^{-1})$	$k_R\,(s^{-1})$
Fast 12 pulse	47	46	1.8	0
Fast 60 pulse	19	14	1.2	0.09
Fast 180 pulse	2.7	2.1	1.3	-0.19
Slow 180 pulse	1.3	5.0	0.72	-0.72

Table 10. 4 Parameter RD Model Fits After Nomifensine, k_T ~2

Figure 7B	$R_{p\,(zmol)}$	$k_U\,(s^{-1})$	$k_T\,(s^{-1})$	$k_R\,(s^{-1})$
Fast 12 pulse	5.2	0.52	2.5	0
Fast 180 pulse	6.4	0.5	0.50	0.24
Slow 12 pulse	1.6	0.37	1.4	0
Slow 180 pulse	1.7	0.55	1.2	0

Tables 9&10: The parameter values obtained from objective curve fitting of hang-up corrected fast and slow responses from the DS before (see Fig. 23a) and after (see Fig. 23b) administration of nomifensine (20 mg/kg i.p.). The pre-nomifensine uptake rate constant, k_U, is consistently faster than the transport rate constant, k_T, so the transport step determines the overall rate of descent of the response after the stimulus. The post-nomifensine uptake rate constant is consistently slower than the transport rate constant, so the uptake step determines the overall rate of the descent of the response after the stimulus. Both pre- and post-nomifensine the transport rate constant is in the range 1-2 s^{-1}. The parameter values in these tables exhibit two other trends worth noting. First, the post-

nomifensine k_R is slow sites is zero: this seems to imply that nomifensine, in addition to changing the rate of uptake, also affects the plasticity of evoked DA release. Second, in both fast and slow domains the post-nomifensine parameters show relatively little dependence on the stimulus duration. This could also indicate that nomifensine impacts the plasticity of evoked release.

5.4   CONCLUSION

While DA overflows resulting from short stimuli, after DA uptake inhibition are fit easily in both fast and slow DA recording sites by the 3 parameter RD model, extending the stimulus duration to 180 pulses at 60 Hz causes both of the 4 parameter RD models that I have constructed to fail to fit the resulting responses in fast DA domains, but not in slow DA domains. This failure occurs only after nomifensine, the before nomifensine responses are fit well in both fast and slow domains. I hypothesize that this is due to the inherently larger release in the fast domains depleting vesicular dopamine to an extent that k_R is no longer treatable as a simple exponential when the stimulation is carried out for such a large stimulus train as 180 pulses. While the 4 parameter RD model with subsecond plasticity of release (k_R) does a good job of fitting many additional stimuli, and is a reasonable explanation for the kinetic diversity of DA overflows that is observed in the striatum upon application of extended stimulus trains, it is not the whole story of evoked DA dynamics. In particular, it remains a challenge to make parameter sets have the same values for very different lengths of stimulus (such as 12 pulses

and 180 pulses). This is an important step for validation of any model. It is important to note that this is more or less the case in slow domains after nomifensine, as the parameter values are quite similiar for these two stimulus durations. Future improvements to the model are desirable, but ideally such improvements will be made by experiments orthogonal to FSCV that give additional information. As the parameterization of the RD model is increased, it is critical that each step be validated, or else the parameter values will become more and more meaningless.

6.0   USING THE RD MODEL TO ANALYZE DRUG EFFECTS ON DA DYNAMICS
Material comprising this chapter is drawn from a manuscript in prepraration

6.1   INTRODUCTION

After I had created the RD model, seen that it was validated with experiments, extended it to describe plasticity (and thereby the DA overflows that result from longer stimulations), and learned how to properly correct for the influences of DA adsorption on the reponses, I was ready to begin using the model to try to learn new things about the brain, and in turn, receive additional feedback from the data which might inform me how to further refine the model. I had been training an undergraduate, Brendan Sestokas, for some time, and he collected data presented in this chapter under my supervision.

The experimental design that I created with Brendan was a timecourse study of a pharmaceutically-relevant DA uptake inhibiting drug, buproprion, to understand how the parameters would change over time, in the previously characterized fast and slow domains of the striatum. Previous studies from our lab had only ever measured drug naïve responses and compared them with responses recorded at a single timepoint well after the drug had been administered. I reasoned that watching a continous evolution of the parameters might give some insight as to what was happening in the brain.

6.2 METHODS

The *in vivo* methods employed for this study are similar to those used in prior recent work from our laboratory.[40] The FSCV protocols, animal protocols, hangup correction, and mathematical modeling approaches are all identical to the methods presented in Chapters 4 and 5 and used in Walters et al 2016, with the exception that Waveform B was not used here.

6.3 RESULTS AND DISCUSSION

Figure 24. 4 Parameter RD Model Fits to Post-Buproprion DA Responses Over Time
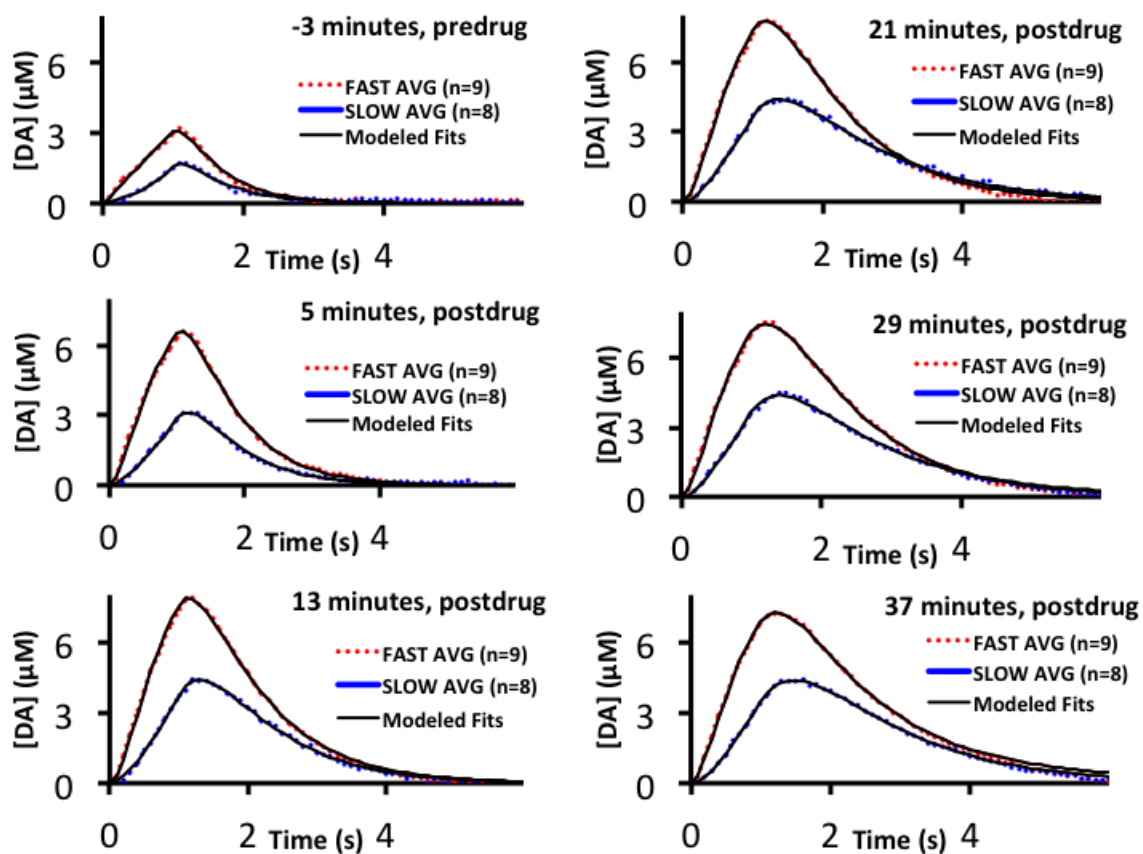
Figure 24. The response of evoked DA in fast and slow dopamine domains to buproprion over time. The fast domain n=9, slow domain n=10. The administration of buproprion increases the size of, and prolongs the duration of the evoked DA overflow. The fast and slow curves are averages of the data; the modeled fits are averages of the modeled fits. All modeled fits had an $R^2 > 0.99$. The stimulus was set at 60 pulses and 60 Hz, 250 uA stimulus current. The dose of buproprion was 80 mg/kg.

Figure 24 displays averages and averages of modeled fits of buproprion, an atypical antidepressant which blocks the dopamine transporter. Figure 24 shows the RD model being used to fit the subsecond kinetics of evoked dopamine responses as they are affected by a major drug in human medicine. The fits themselves demonstrate that the model fits the data; the parameter values obtained from these fits (Fig 6) offer a mechanistic explanation of the actions of this drug on the subsecond signaling kinetics of the dopamine system.

Figure 25. RD Model Parameters For Post-Buproprion DA Responses Over Time
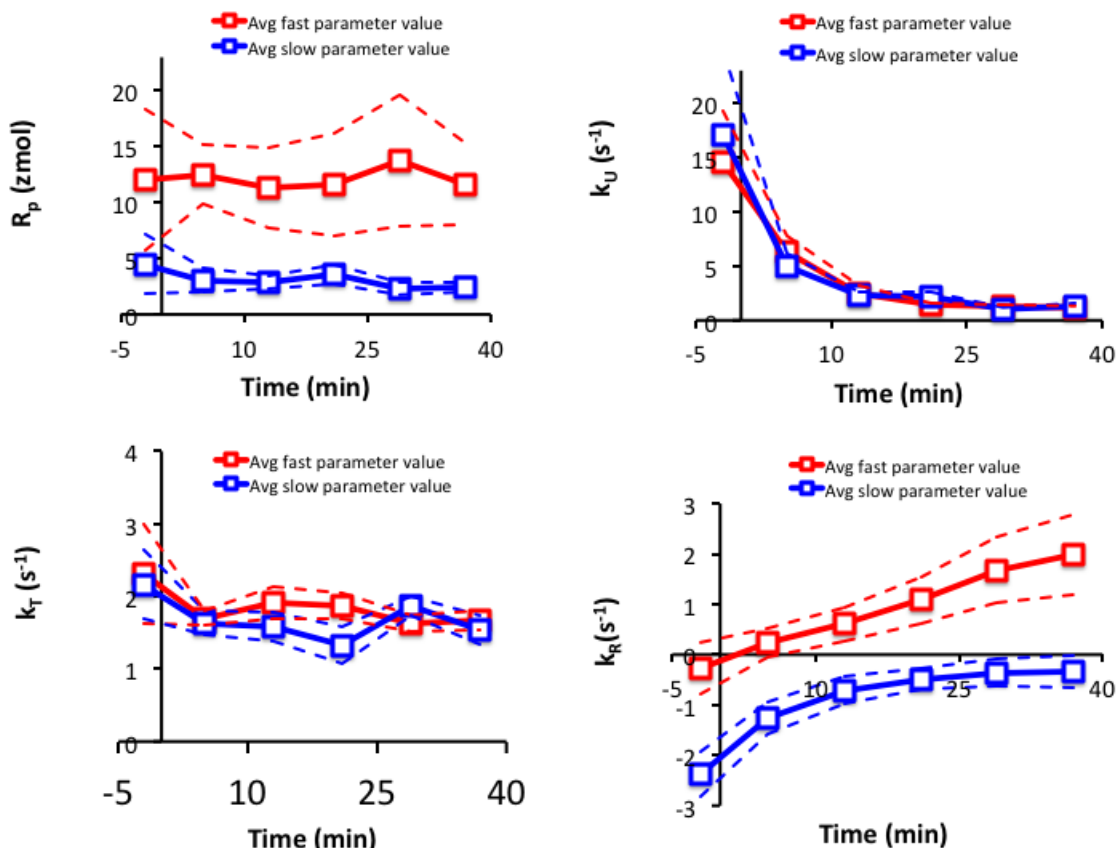
Figure 25. Changes of the modeled parameter values over time in response to buproprion. The fast domain contains n=9, slow domain n=8). The initial evoked release per stimulus pulse (R_p) is significantly greater in the fast domain than the slow domain, and is unaffected by buproprion. b) the uptake (k_U) is highly responsive to buproprion, and not significantly different in fast and slow domains. c) the mass transport parameter k_T is not sensitive to buproprion, and not significantly different in fast and slow domains. d) the exponential plasticity factor k_R is significantly different in fast and slow domains, and responds differently to buproprion. In the fast domains, k_R changes linearly with time after drug administration from a small average short term facilitation (negative k_R) to a steadily increasing short term depression of release (positive k_R). In the slow domains, the value of kR also rises, but appears to form an asymptote at zero, meaning that the short term facilitation of release is lessened, but the slow sites do not experience short term depression of release.

Figure 25 shows how the four parameter values which create the modeled fits in Fig 24 change over time. It is plain that there is a substantial visual contrast between what happens to the parameter values of release, uptake, mass transport, and plasticity in response to buproprion as compared to examining the evoked overflows alone. This illustrates the utility of the RD model – it is capable of revealing interesting kinetic information about dopamine, in response to drugs of human interest, that the data themselves do not make apparent upon casual examination.

6.4   CONCLUSION

The timecourse of the parameter values of fast and slow DA domains with the 4 parameter RD model with subsecond plasticity of release, in response to an uptake inhibitor is quite compelling. First, it may be noted that, in contrast to the longer stimulations in fast domains after the uptake blocker nomifensine, these 60 pulse stimulus results are all fit extremely well by the 4 parameter RD model - in both fast and slow domains.

It is compelling that the initial release parameter, and the k_T parameter remain unchanged over the timecourse of the experiment. Given the large changes to the curves which are being modeled, it is reasonable to expect that many models would register changes to all of the parameters. This model registers change only to the uptake, and to the kR parameter. If as has been previously supposed, DA vesicles operate by a kiss-and-run mechanism, the changes to the kR parameter make very good sense. Since an uptake inhibitor slows the rate of DA uptake by the DAT, it also slows the rate of DA uptake by the VMAT into the vesicles, as DA must enter the cell before it can be repackaged. If reuptake of extracellular DA is required to maintain a

given rate of release, it is logical that blocking that reuptake would result in a slowing of the rate of release over time. This is exactly what is observed in the context of this modeling.

Many uptake inhibitors have been suggested to increase the amount of DA released by a stimulus pulse. Our modeling indicates that, for buproprion, the amount of initial release is quite constant over time in both fast and slow DA domains, but that the total amount of release is actually decreased, as kR is increased. Many uptake inhibiting drugs of abuse have been found to show increased DA release by multiple modeling approaches - including the RD model, by another group that has begun to use it.   It is possible that buproprion is different than many other uptake inhibitors in this regard, and it is possible that this is why it is not an abused drug, although further study will be required to confirm this.

7.0   USING THE RD MODEL TO STUDY ANATOMICAL DIFFERENCES IN DA
Material comprising this chapter is drawn from a manuscript in prepraration

7.1   INTRODUCTION

Dopamine is a neurotransmitter which is involved in many brain functions and dysfunctions. Dopamine signaling in the brain possesses kinetic diversity, and can be described in exacting detail by a simple model based on restricted diffusion. In this work, we localize both prevalence and identity of dopamine kinetic signaling patterns to substriatal regions: dorsolateral, dorsomedial, ventrolateral, and ventromedial. We report the observation of silent dopamine sites, which we expect are related to the silent dopamine terminals recently reported by the Sulzer lab. We find that the average rate of dopamine uptake within a striatal subregion is inversely related to the proportion of silent dopamine sites that subregion contains, and we explain the purpose of higher rates of dopamine uptake, such as are found in the dorsolateral striatum, as being to spatially constrain dopamine signaling in cases where the density of actively signaling varicosities is higher. We determine via modeling that the silent dopamine terminals do not engage in dopamine uptake, and that restricted diffusion makes it impossible for dopaminergic neuron firing to code information in frequency at a rate greater than about 1 Hz. This then prescribes a role for phasic burst firing of dopamine neurons to simply produce a larger concentration of dopamine at its receptors.

Dopamine (DA) is a neurotransmitter which plays a key role in many functions[88–91] and dysfunctions[92,18,93,94] of the brain. Since the early 1980s, it has been possible to study DA

signaling with micrometer spatial and subsecond temporal resolution by means of fast scan cyclic voltammetry (FSCV)[2]. Such signaling can either be artificially induced, as by electrical[2], optogenetic[95], or magnetic[96] stimulation, or be observed in response to normal brain activity[97].

The high resolution of FSCV has permitted observation of diversity of subsecond DA signaling[8,10,42,36,38,34,39,37,98,99]. Some of this diversity arises from differences in the local biological regulation[42,34,100,101] of DA releasing structures, rather than their simple prescence or absence. Recent advances in mathematical modeling of evoked DA responses[43,65,40,102] illustrate that these differences can be quantitatively explained by variation in the values of just four biologically meaningful parameters. The four parameters describe local DA release per stimulus pulse, uptake, mass transport, and change in release over time. When the number of stimulus pulses is kept low, the change-in-release parameter is unneccessary and can be omitted while still achieving excellent fits to FSCV data[43,65,40,102].

The present study uses spatial mapping to characterize kinetic DA diversity throughout the rat striatum. Functional specializations of multiple regions within the striatum are well characterized[89,91,18,103,104], and we hypothesized that local differences in DA kinetics are involved in creating some of these specializations. This is presumably enabled by the distinct DA circuit pathways[105] innervating these areas. In this study, we connect differences in DA kinetics among striatal subregions to these previously characterized functional specializations, with the aim of offering mechanistic insight into DA's function. We additionally demonstrate that high signal to noise ratio is necessary for the accurate extraction of kinetic parameter values from voltammetric data, and offer strategies to analyze data sets in cases where DA responses cannot be optimized.

7.2 METHODS

FSCV

Carbon fiber electrodes (7 μm in diameter and 200 μm in length) were prepared with T650 fibers (Cytec LLC, Piedmont, SC, USA). The electrodes detected DA via a 400 V/s waveform beginning at 0.1V, rising to 1.3V, falling to -0.5V, and rising again to the 0.1V resting potential. This waveform was applied at 10 Hz. We have previously used this waveform to electrochemically pretreat electrodes, and it was used in this study to obtain good sensitivity from the 1.3V oxidation limit. FSCV was performed with a fast-scan potentiostat (EI-400, out of production) and CVTarHeels software (courtesy Prof. Michael Heien, University of Arizona). FSCV calibration was performed in a homemade flow cell using DA (Sigma, St Louis, MO, USA) dissolved in N_2purged artificial cerebrospinal fluid (142 mM NaCl, 1.2 mM $CaCl_2$, 2.7 mM KCl, 1.0 mM $MgCl_2$, 2.0 mM NaH_2PO_4, pH 7.4).

Subjects and In Vivo Procedures

All procedures involving animals were approved by the University of Pittsburgh Animal Care and Use Committee. Rats (male, Sprague-Dawley, 250-450g, Charles River Inc., Wilmington, MA) were anesthetized with isoflurane (2.5% by volume O_2), placed in a stereotaxic frame (David Kopf, Tujunga, CA), and connected to an isothermal blanket (Harvard Apparatus, Holliston, MA). Carbon fiber electrodes and stimulating electrodes (MS303/a, Plastics One, Roanoke, VA) were implanted in the dorsal striatum and ipsilateral medial forebrain bundle. The stimulus waveform was a biphasic constant current square wave (2 ms

pulses, 60 Hz, 250 µA, 1 s or 3 s in duration) delivered with a stimulus isolation unit (Neurolog 800, Digitimer, Letchworth Garden City, UK).

Hang-up Correction

The hang-up correction was explained in detail by Walters et al, 2015. Briefly, the algorithm assumes that DA undergoes first order adsorption and desorption at the surface of the FSCV electrode according to the following rate expression:

Equation 15: Rate of Hang-Up

$$\frac{dH}{dt} = k_{on}C - k_{off}\Gamma_{DA}$$

which is used to construct a hang-up signal component, $H(t)$, by curve fitting to the hang-up segment of the measured response. The correction is performed by subtracting the calculated signal component from the measured response.

In performing the hang-up correction, it is important to avoid distorting DA's apparent kinetics. This could occur, for example, by curve-fitting $H(t)$ to the measured response before the time where the measured response is caused solely by hang-up. To avoid this outcome, we fit $H(t)$ to later and later segments of the reponse until $H(t)$ stops changing.

The Restricted Diffusion Model

The DA kinetic model has been explained and used in prior recent reports from our laboratory. It is intended to provide a generic description of restricted diffusion in the brain extracellular space. To do so, it treats the extracellular space as if it were divided into an inner and outer compartment. The model postulates that DA is released into the inner compartment

and undergoes restricted diffusion to the outer compartment where it is detected by the FSCV electrode. Uptake then removes DA from the outer compartment. The model is composed of two equations:

Equation 16: Dynamic Release and Diffusion from the Inner Compartment

$$\frac{dDA_{ic}}{dt} = R_p \cdot f \cdot e^{-k_R t} - DA_{ic} \cdot k_T$$

Equation 17: First Order Uptake and Diffusion Into the Outer Compartment

$$\frac{d[DA]_{oc}}{dt} = \frac{DA_{ic} \cdot k_T}{V_{oc}} - [DA]_{oc} \cdot k_U$$

for the amount of DA in the inner and outer compartments, DA_{ic} (in moles) and $[DA]_{oc}$ (in concentration), respectively. There are four adjustable parameters; R_p represents the moles of DA released per stimulus pulse, k_R is a first order rate constant that modifies DA release, k_T is a first-order rate constant for transport between the compartments, and k_U is a first-order rate constant for DA uptake. There are two fixed parameters; V_{oc} is the volume of the outer compartment (16 μm^3, see Walters et al) and f is the stimulus frequency.

Statistics

Statistical analysis was performed in Microsoft Excel (t-test) and SPSS (ANOVA). All t-tests performed were two-tailed, independent sample t-tests with an assumption of equal variance. For the two way ANOVA with repeated measures tests performed for Figure 3, the first 99 data points of the stimuli were tested (9.9 seconds of comparison). For the two way ANOVA with repeated measures done for Figure 6, the first 40 data points of the stimuli were tested (4.0 seconds of comparison).

Voltammetry Data Analysis

Objective Classification of Kinetic DA Types

Fast DA sites are those which produce an identifiable dopamine response to 12 pulses of 250 uA electrical stimulus of the medial forebrain bundle.[34] If they do not do this, but eventually respond to electrical stimulus if more pulses than 12 are administered, they are deemed to have slow DA overflow kinetics.

Statistics for Voltammetry Data Analysis

Statistical analysis was performed in Microsoft Excel (t-test) and SPSS (ANOVA). All t-tests performed were two-tailed, independent sample t-tests with an assumption of equal variance. For the two way ANOVA with repeated measures tests performed for Figure 3, the first 99 data points of the stimuli were tested (9.9 seconds of comparison). For the two way ANOVA with repeated measures done for Figure 6, the first 40 data points of the stimuli were tested (4.0 seconds of comparison).

Statistics for Mathematical Modeling

Statistical analysis was performed in Microsoft Excel (t-test) and SPSS (ANOVA). All t-tests performed were two-tailed, independent sample t-tests with an assumption of equal variance. For the two way ANOVA with repeated measures tests performed for Figure 3, the first 99 data points of the stimuli were tested (9.9 seconds of comparison). For the two way ANOVA with repeated measures done for Figure 6, the first 40 data points of the stimuli were

tested (4.0 seconds of comparison).

7.3   RESULTS AND DISCUSSION

Figure 26. Fast, Slow, and Silent DA Responses in Four Striatal Sampling Tracks
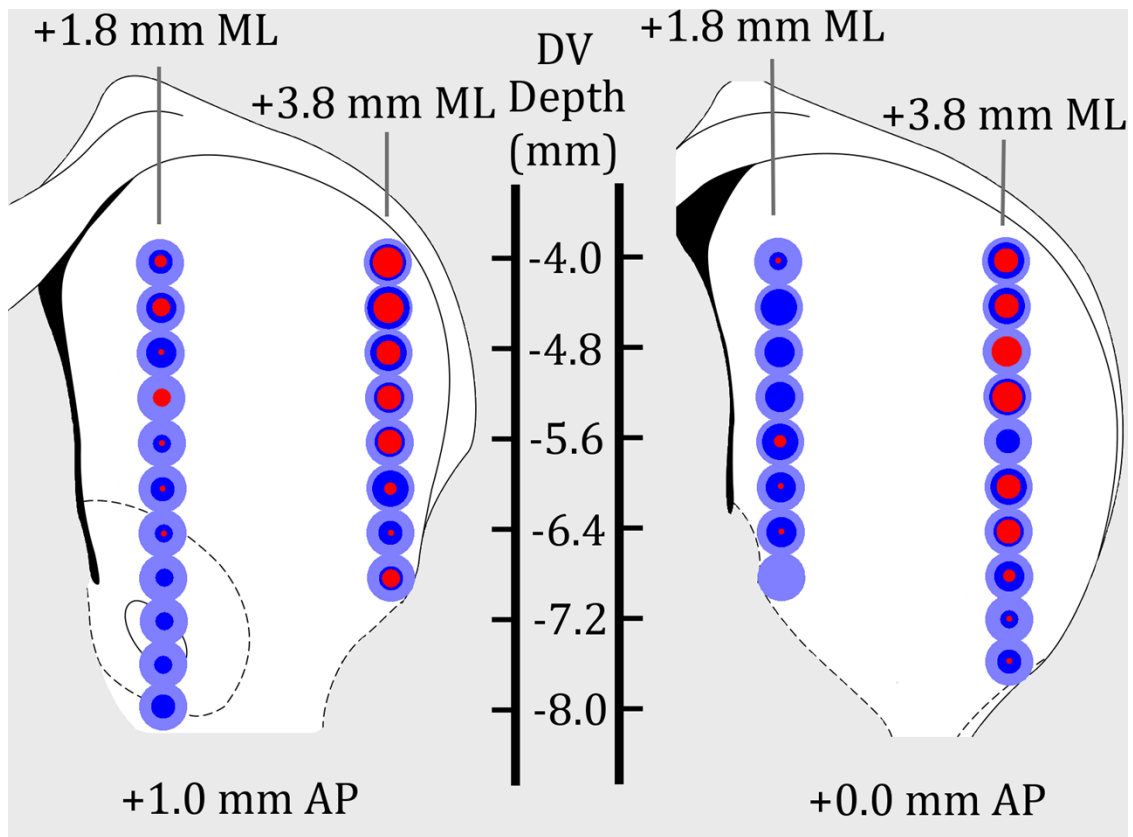
Figure 26: Distribution of fast and slow responses within 4 striatal recording tracks. All measurements were taken with a carbon fiber working electrode of 200 um length and 7 um diameter. Each concentric circle represents a recording site. Recording sites were separated sequentially by 400 um. The outer light blue circle represents the total number of measurements taken at each recording site, which was 8, across 8 animals. The inner dark blue circle represents the total number of times that dopmaine was observed above its limit of detection (~100 nM) in response to a 60 Hz, 60 pulse, 250 uA stimulus at each recording site. The inner red circle represents the

number of times that fast DA kinetics (defined as the DA signal exceeding the limit of detection at 200 ms after the start of stimulation) were observed. In each case, the visible diameter of the circle is exactly proportional to the number of times each observation was made at that recording site (between 0 and 8). A measurement made in the dorsolateral striatum (depth between -4.0 and -6.0 mm inclusive) was observed to have a higher incidence of having fast kinetics than a measurement made in the dorsomedial striatum (depth between -4.0 and -6.0 mm inclusive).   A measurement made in the ventrolateral striatum (depth between -6.4 and -7.6 mm inclusive) was observed to have a higher incidence of having fast kinetics than a measurement made in the ventromedial striatum (depth between -6.4 and -8.0 mm inclusive).

Distribution of Fast and Slow DA Domains within the Striatum

We have previously categorized kinetically diverse dopaminergic recording sites in the striatum according to whether or not they give an immediate response to an electrical stimulus[34]. FSCV recording sites are dimensionally defined by diffusion of DA to the active surface of a recording electrode, which is a cylinder of 200 microns height and 7 microns diameter. Those DA sites which immediately respond to electrical MFB stimulus have been classified as "fast sites", while those that do not have been classified as "slow sites"[34]. Fast sites have been further subdivided into four different types according to their kinetic profile upon extended stimulation[39]. In this study, we exclusively employ a relatively short stimulation of 60 pulses over 1 second, and so recording sites have been grouped according to fast and slow classifications, but fast sites have not sorted by type. However, this study found that 41% of all sampled recording sites within the striatum did not exhibit a detectable DA response in response to 60 pulse MFB stimulation. We have termed these DA sites "silent", after the phenomenon recently reported at dopaminergic synapses by Sulzer and coworkers[101].

Because our data were collected in a 4-track grid pattern, it was feasible to make comparisons by dividing the data in half or as nearly in half as the anatomy permitted along each of the three axes: anterioposterior, mediolateral, and dorsoventral. Combining two of these axes then divides the striatum into four regions, and combining all three would yield eight regions. Examining the probability of sampling a given type of site in each region was then used to test for significant differences in prevalence of different kinds of sites across each axis and then within each region. Testing along the anterioposterior axis (Fig 27) revealed no significant difference in prevalence of fast, slow, or silent DA sites. The anterioposterior axis was therefore not used to further subdivide the sampled striatal sites. However, both the dorsoventral axis and mediolateral axis showed significant differences in prevalence of fast sites, while the ventral striatum had significantly more silent sites than the dorsal striatum, and the medial striatum had significantly more slow and silent sites than the lateral striatum. Therefore, the striatal sites of both fast and slow types were divided into four groups for further analysis: dorsolateral striatum (DLS), dorsomedial striatum (DMS), ventrolateral striatum (VLS), and ventromedial striatum (VMS).

Figure 27. Distribution of DA Site Types Among Striatal Subregions
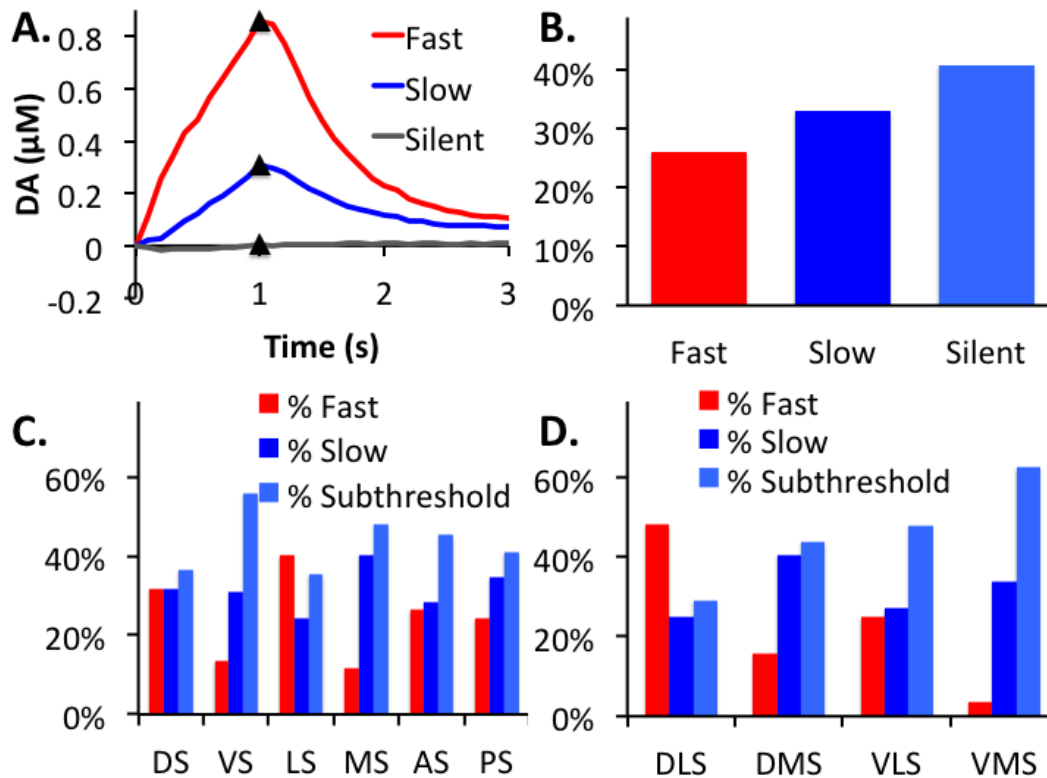
Figure 27: **A.** Percentage of fast, slow, and subthreshold DA sites in various subdivisions of the striatum. DS=dorsal striatum (all measurements taken at -4.0 to -6.0 mm DV); VS= ventral striatum (all measurements taken at -6.4 to 8.0 mm DV); LS= lateral striatum (all measurements taken at +3.8 mm ML); MS = medial striatum (all measurements taken at +1.8 mm ML); AS = anterior striatum (all measurements taken at +1.0 mm AP); PS = posterior striatum. (all measurements taken at +0.0 mm AP). **B.** DLS = Dorsolateral striatum (all measurements -4.0 to -6.0 mm DV and +3.8 mm ML); DMS = Dorsomedial striatum (all measurements -4.0 to -6.0 mm DV and +1.8 mm ML); VLS = Ventrolateral striatum (all measurements -6.0 to -7.6 mm DV and +3.8 ML); VMS=Ventromedial striatum (all measurements -6.4 to -8.0 mm DV and +1.8 ML). C. Average fast and slow responses collected from the striatum; fast N=75, slow N=95. The stimulus begins at time=0. D. Average subthreshold responses collected from the striatum; silent N=118.

Figure 28. DA Kinetic Differences of Striatal Subregions
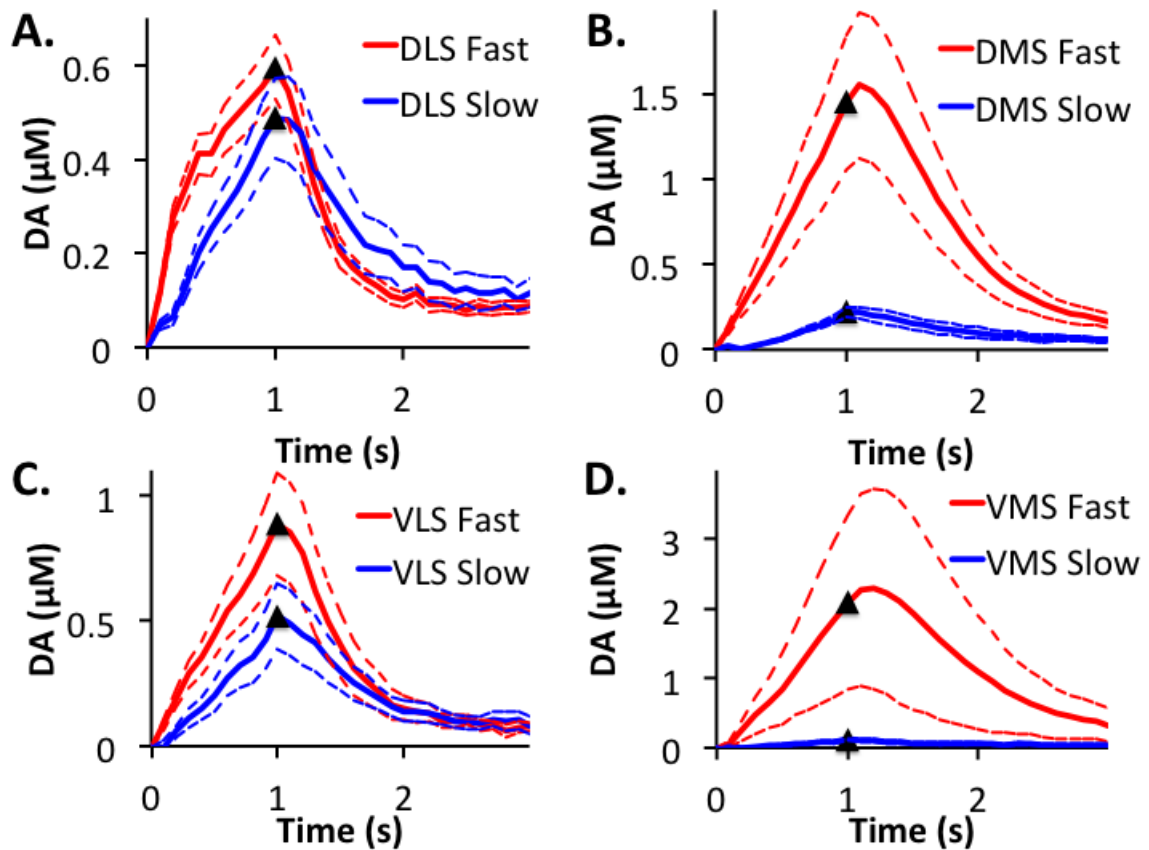
Figure 28: Average kinetics of fast and slow responses within anatomical subregions of the striatum. **A.** Fast and slow dorsolateral measurements (-4.0 mm to -6.0 mm depth, +3.8mm ML). N=44 fast sites and N=24 slow sites. **B.** Fast and slow dorsomedial measurements (-4.0 mm to -6.0 mm depth, +1.8mm ML). N=15 fast sites and N=39 slow sites. **C.** Fast and slow ventrolateral measurements (-6.4 mm to -7.6 mm depth, +3.8mm ML). N=12 fast sites and N=13 slow sites. **D.** Fast and slow ventromedial measurements (-6.4 mm to -8.0 mm depth, +1.8mm ML). N=2 fast sites and N=19 slow sites.

Grouping the data in this way (Fig 28) makes it apparent that there are various differences in both fast and slow DA responses among the brain regions in question.

Kinetic Analysis of Fast and Slow DA Domains In Striatal Subregions

Our recently developed model of DA signaling[43,65] quantitatively reproduces all of this data whether considered as individual responses or as an average. (Fig 29)

Figure 29. RD Model Explains DA Kinetic Differences of Striatal Subregions
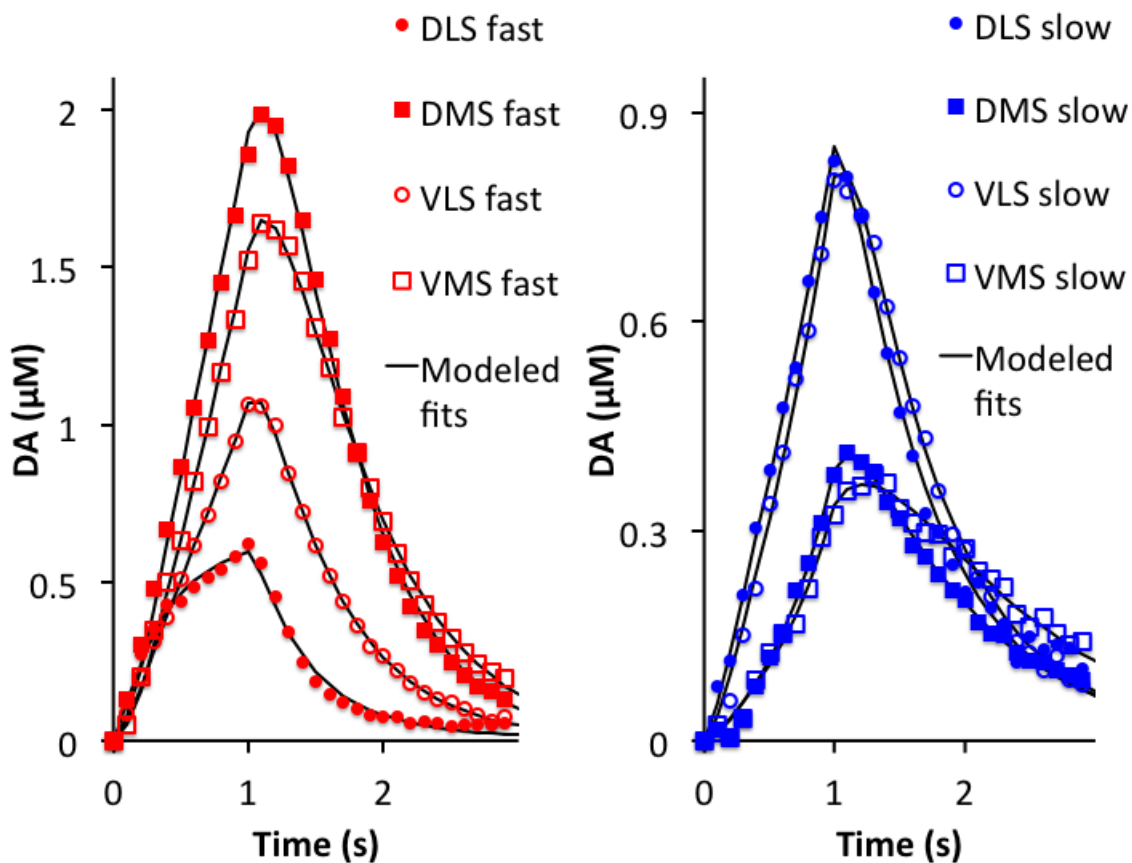
Figure 29 The average of modeled fits to the average of hangup-corrected data from the studied striatal subregions. In contrast to Figure 3, only data with S/N > 10 has been included here, as only data with S/N > 10 was hangup corrected and fit with the RD model.

However, we discovered that there is a problem with attempting to extract kinetic parameter values via objective fitting from DA responses with signal to noise ratios of less than about 25. Fits to these responses experienced systematic errors of the extracted parameter values (this is discussed extensively in the Supplementary Information). Due to the nature of the experimental design, many responses with relatively small signal to noise ratios were collected for analysis (both because of differences in the DA signal and noise arising from the brain). We found that averaging the signals of a particular type obtained from each studied striatal subregion and fitting that average produced broadly the same parameter values as averaging the individual fits to responses of S/N ratio > 25 (Fig 30)

and fitting that average produced broadly the same parameter values as averaging the individual

fits to responses of S/N ratio > 25 (Fig 30)

Figure 30. RD Model Parameters of Striatal Subregions
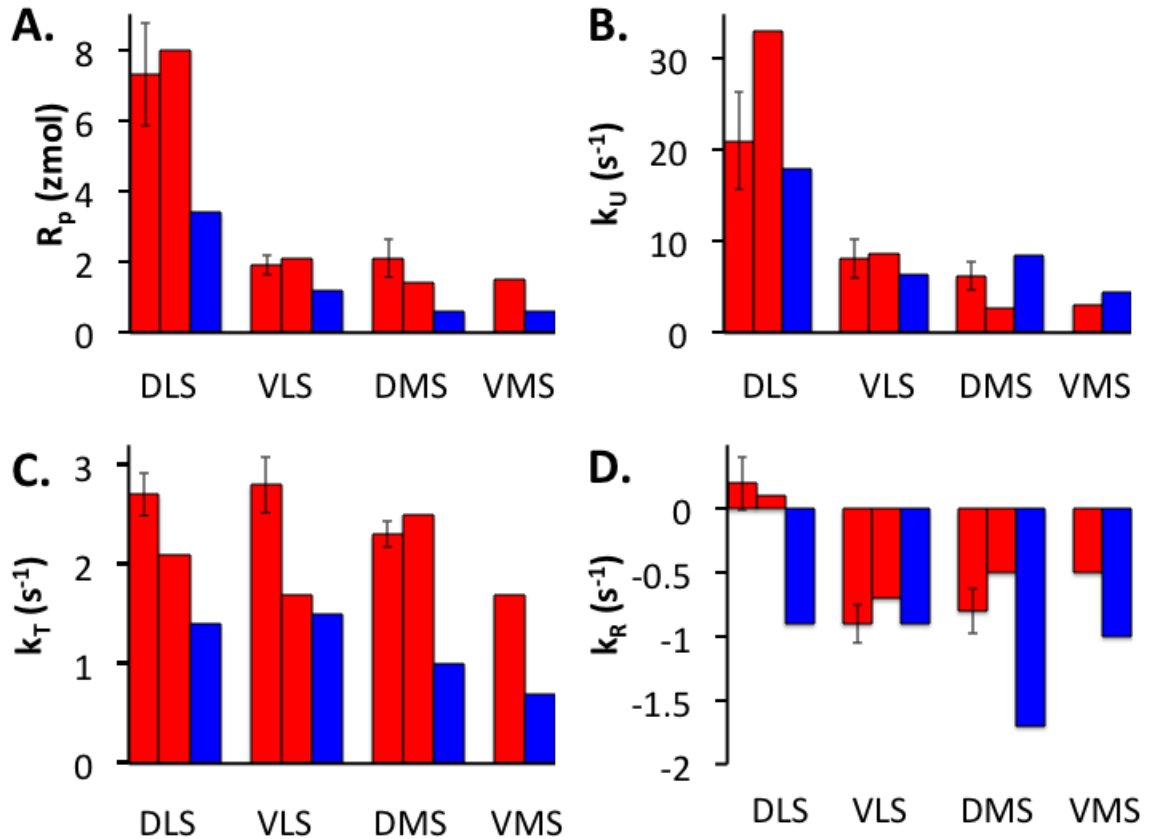
Figure 30 Reported average parameter values for each domain type within each brain region. Where error bars are shown, only signals of S/N > 25 have been included in the average. Where error bars are not shown, the value presented is the fit to the average data in that category (including all signals of S/N>10). For S/N > 25; DLS fast n=10, VLS fast n=8, DMS fast n=10, VMS Fast n=2, DLS slow n=1, VLS slow n=2, DMS slow n=2, VMS slow n=0. For S/N > 10; DLS fast = 36, VLS fast = 13, DMS fast = 12, VMS fast = 2, DLS slow = 13, VLS slow = 6, DMS slow = 15, VMS slow = 3. The R_p, k_U, and k_R are all significantly different in the DLS than in the VLS or DMS. None of these parameter values is significantly different from one another between the VLS and DMS fast sites.

Table 11. RD Model Parameter Values for Fast and Slow Domains with S/N ratio > 25

Type	n	R_p	k_U	k_T	k_R
Fast (S/N > 25)	30	3.8±0.7	11.5±2.2	2.5±0.1	-0.5±0.1
Slow (S/N > 25)	5	1.2±0.3	9.5±3.9	2.0±0.3	-1.4±0.2

Table 11 reports the average ± SEM of all striatal fast and slow sites which had an S/N ratio of > 25. R_p and k_R are significantly different between fast and slow sites.

DA Release

The restricted diffusion (RD) model[43,65,102] (Fig 4) is useful for determining spatially resolved parameter values (Fig 5) for DA release (R_p), change in release (k_R), uptake (k_U), and mass transport (k_T). The dimensions of the working electrode determine the degree of spatial resolution obtained. In the RD model, DA release is defined in terms of a molar amount of DA release which diffuses into the outer compartment volume (OCV), an arbitrary volume of extracellular space[43]. DA release, as cast in the RD model, represents the net effect of several biophysical processes which occur proximate to this space. These processes comprise a causal chain which results in the net effect observed with R_p: DA is contained in vesicles, electrical impulses cause some vesicles to fuse with the cell membrane, and some of the contents of the vesicles which fuse are released with each fusion event. Because numerical values for these processes have been previously determined[106–109], this allows us to make an independent test of some predictions of the RD model. We can therefore define DA release as:

Equation 18: Biophysical Subdivision of Release per Pulse

96

$$R_p = DApV \cdot TVP \cdot fFV \cdot fVE$$

where *DApV* is the average dopamine content of a vesicle that feeds into the OCV, *TVP* is the total vesicle pool within the OCV, *fFV* is the fraction of vesicles in the pool which undergo fusion in response to a stimulus, and *fVE* is the fraction of vesicle emptying upon fusion. Previous literature in the field[106–109] supports the following values for these parameters: *fVE* = 0.40, *fFV* ≤ 0.16. By definition of the OCV volume, combined with the number of DA terminals present within the OCV[49], combined with the number of vesicles per terminal, *TVP* = 8. *DApV* = 33,000. This places an upper bound on the value of R_p at 28 zmol, which is in good agreement with all of the values we report in Fig 5, and in agreement with the largest single observed release value in this study (17 zmol). It is possible that some of these values may be underestimates for the striatal DA system; the *fVE* value is for example derived from PC12 vesicles. It is also possible that some conditions exist which might be able to violate the condition that *fFV* ≤ 0.16. In any case, at most *fFV*=1 and *fVE*=1. Thus, there is an ultimate physical upper bound that R_p ≤ 440 zmol. Detailed calculations supporting this can be found in the Supplementary Information.

With R_p defined as the product of a set of parameters, the change in R_p over time (k_R) can be defined as the net effect of changes of those parameters. In this study, essentially all observed k_R values were less than or equal to zero, meaning that, under these experimental conditions, R_p was either time invariant or increased with time. Since *DApV* and *TVP* are factors which would only decrease during a series of stimulus pulses, changes in *DApV* or *TVP* cannot explain the present data set. Therefore, changes in *fFV* and/or *fVE* must underlie the values of kR that we have observed.

The ratio of $R_p * e^{-k_R t}/28$ zmol is therefore an indication of the fraction of DA vesicles which are actively engaged in signaling within the volume that the electrode samples. An *fFV* value of 0.16 (the maximum), coupled with distributing these fusing vesicles as widely as possible throughout the sampled volume, implies at 4 DA vesicles per terminal that at most 16-64% of DA terminals within any sampling volume release DA in response to any given stimulus pulse. This is in good agreement with the recent observation of Pereira et al that ~83% of DA terminals in the striatum are silent[101]. This also means that DA terminals which are engaged in release do so to the maximum extent – i.e. if 16% of all vesicles are engaged at the upper bound of release in response to a stimulus, and 17% of all terminals are engaged in response to a stimulus, then the active terminals must have all of their vesicles actively engaged. It is important to note that this observation puts an even greater demand on the DA terminals that are operational to uptake and continue releasing DA. The silent DA terminals cannot be engaged in uptake over time, or else the active DA terminals would rapidly be completely depleted of DA, and the silent terminals would become crowded with DA. This necessitates that the DA uptake be "turned off" at these silent terminals.

DA Uptake

We continue to observe in this work, as previously[43,65,39,40,102], that DA uptake is well described by a first order rate parameter, k_U.

DA Mass Transport

We continue to observe in this work, as previously[43,65], that DA mass transport is well described by a first order unidirectional rate constant, k_T with a value of ~ 2 s^{-1} (Fig 5, Table 1).

The k_T value arises essentially entirely from restricted diffusion of DA in the brain[36,43], with adsorption kinetics having a negligible effect.[40]

DA Kinetic Diversity: Cause and Effect

Kinetic analysis of evoked DA responses with the RD model yields several interesting conclusions. First is that, slow sites have a much lower initial DA release (R_p) than fast sites. Table 1 indicates that R_p is more than threefold greater in slow sites than in fast sites, and Figure 5 indicates similar conclusions within each striatal subregion. In contrast, DA uptake (k_U) is not significantly different between fast and slow sites on average, according to Table 1, and Figure 5 also supports that this conclusion is true within each studied striatal subregion. The model indicates that mass transport (k_T) is slightly slower in slow sites as compared to fast sites in Table 1 and Figure 5 as well. The difference in change in release (k_R) between the average fast and slow site is greater, but, as can be seen from Figure 5, most of this is due to the extreme difference in fast and slow k_R in the DLS, while the other three brain regions show more similarity in k_R among fast and slow sites.

Understanding R_p as a composite of neurobiological factors, as shown above, and its change k_R as a change in those factors, is very helpful for understanding the mechanistic differences between fast and slow sites. The lower R_p in slow sites is due at least in part to a lower percentage of initial vesicle fusion (some combination of *fFV* and *fVE*). We know this because the release accelerates over time via k_R (and accelerates much faster in slow sites on average than fast sites). The initial electrical impulses do not cause as much exocytotic release in the slow sites as in the fast sites, but release on average (Table 1) becomes more comparable

over time, due to the more negative value of k_R observed in slow sites.

The most strikingly distinct striatal subregion is the DLS. The DLS possesses a significantly greater proportion of fast sites and a significantly lesser proportion of silent sites than the rest of the striatum. In addition, the fast sites the DLS possesses are on average significantly greater in initial release (R_p) and uptake (k_U) than the fast sites in every other subregion of the striatum. The change in release rate (k_R) is also significantly different than all other fast sites; the DLS fast sites are unchanging or slightly attenuated with time, while all other fast sites increase their release rate with time. The DLS fast sites, apart from the entire rest of the striatum, are thus set from the start for maximal DA release without being under any suppression to be overcome. However, this large DA release is also attenuated both spatially[15] and temporally by the largest average uptake value found in the striatum, in this study. DLS uptake has previously been characterized (by means of an older model) as greater in rat[110], mouse[110], and primate[110–112] but not guinea pig brain slices[112] as compared to the VMS. The restricted diffusion model describes a substantially larger difference in uptake between these regions than did previous reports. Rapid uptake in the DLS is mediated by the large quantities of DAT found there[113]. This very fast uptake is however not useful for enabling phasic frequency DA communication in the extracellular space (see Supplementary Figure S7). This is because continued mass transport from the IC, enabled by k_T, countervails against the effects of both even very fast uptake and diffusion away from release sites. This means that phasic DA firing cannot encode information with firing frequencies above ~1 Hz, and that the purpose of phasic DA burst firing is simply to generate a larger DA concentration at that site. Indeed, a recent direct test of the postsynaptic effects of DA on IPSCs in medium spiny neurons perfectly

confirms this timescale[114] (see Fig 2A, 3C, and 6B in reference 34).   Just as in the simulations

shown in Fig S7B, It takes ~1 second for real single pulse DA to be cleared, both in vivo[115], and

in vitro[116]. The RD model, using the parameters determined in this work for the average of 60

pulse, 60 Hz VMS data, also exactly predicts the previously observed peak height (25 nM) and

peak time (0.3 s) for the VMS data[115] in Ref 42, when extrapolated backwards to a single pulse

(Fig S7B).

Therefore, the purpose of the rapid DA uptake in the DLS cannot be to increase the

information bandwidth. Since this is the case, the only function that the high DA uptake of the

DLS can serve is to restrict signaling crosstalk by truncating volume transmission. We find

(Figure 2, Figure 5) that the average rate of DA uptake within a region is inversely related to the

proportion of silent sites within that region. This is quite logical, for two reasons. First, there is

less silence and more release in the DLS, which means that more terminals are actively engaged

in signaling at any one time. This creates a need for additional shielding from signaling

crosstalk, and explains the higher rate of uptake in the DLS. And secondly, the presence of a

higher number of active varicosities implies that there will be a greater amount of uptake, as

uptake is needed (and found)[113] on each terminal to satisfy the needs of mass balance over time

with signaling. DA uptake cannot be active on silent terminals[101], to satisfy mass balance.   That

is to say, the DA concentrations that receptors would be predicted by the RD model to

experience from normal DA signaling are no higher in the the DLS than in the rest of the

striatum, but the adjustments to release and uptake in the DLS enable a higher density of

equivalent DA signaling without crosstalk as compared to the VLS, VMS, and DMS.

7.4 SUPPLEMENTARY INFORMATION

The Effect of Signal to Noise Ratio on Kinetic Modeling

We report as a matter of general interest for those interested in kinetic modeling on the level of signal quality required to extract biophysically relevant information from DA curves. Work being conducted with the goal of extracting kinetic brain parameters from neurotransmitter responses should put emphasis on the generation of high S/N data, whether by optimizing for robust responses, increasing sensitivity, lowering noise, or some combination thereof. However, we observed that the level of noise is significantly different in the lateral striatum as compared to the medial striatum, meaning that it is impossible to rigorously control noise in *in vivo* brain experiments, as some noise (and difference in noise) is simply a product of natural brain function.

We discovered that noise was capable of confounding kinetic parameter values when objectively fitting the curves from our *in vivo* data set. Many responses with small amplitudes were claimed to result from a paired combination of implausibly large release and uptake, along with greatly expanded variability in the rate of mass transport and the rate of change in release. When arranged according to S/N ratio (defined as the DA peak height divided by the average of the absolute value of the difference between each pair of immediately adjacent timepoints for all fifty timepoints in the pre-stimulus period), it was apparent that all parameter values exhibited considerably more variability at relatively low S/N ratios, but that much of this variability vanished at higher S/N ratios.

Figure 31. Apparent Effect of Noise On RD Model Parameters
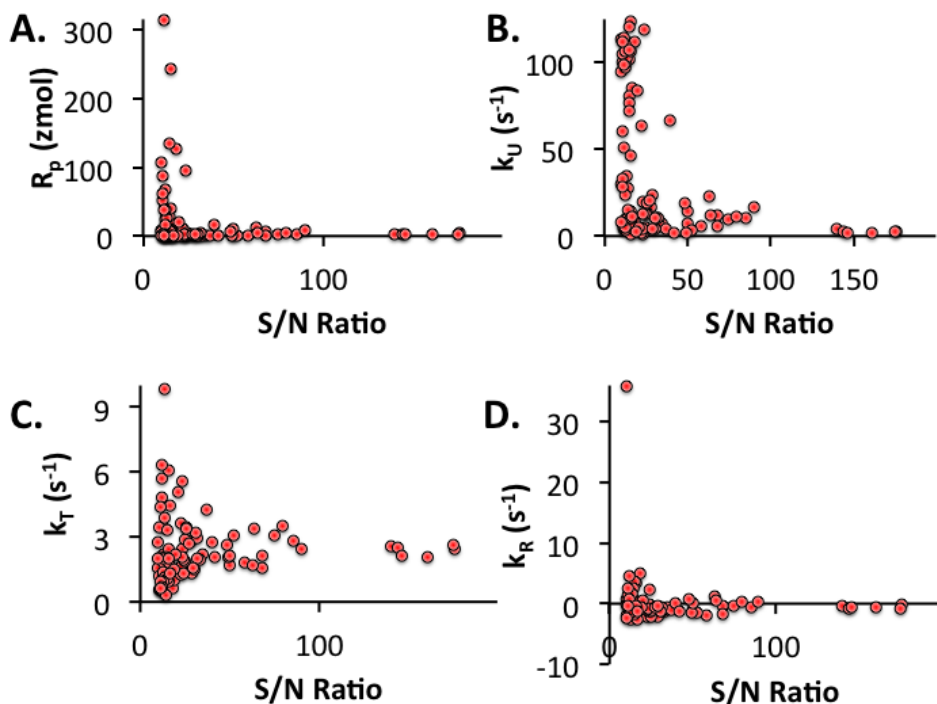
Fig 31: Apparent effect of noise on parameters obtained by model fitting. Parameter values from 100 evoked DA responses (250 uA, 60 pulses, 60 Hz) plotted against S/N ratio. Fits to noisier signals are associated with increased variability in the parameters. Because all of the parameters except kR cannot have negative values, this increased variability manifests as larger average values of release and uptake at the lower signal to noise ratios. No responses with S/N ratio < 10 were fit. In this figure, S/N ratio was defined as the peak DA concentration divided by the average of the absolute value of the difference between each pair of immediately adjacent timepoints for all fifty timepoints in the pre-stimulus period.

The sample standard deviation of the noise was 63% of the average noise amplitude (check with full set of 100) overall, for the 100 responses with S/N ratio >10, while the correlation coefficient of the relationship of peak signal amplitude to S/N ratio was 0.68 (check with full set of 100). Thus, signal to noise ratio was strongly related to signal amplitude, but

variability in the noise was also a component of variability in the S/N ratio. The noise was significantly (highly significant) higher in the lateral striatum compared to the medial striatum, across all animals. This was not localized to the DLS; the DLS and VLS showed identical levels of noise. The increased electrical noise observed in the lateral striatum is therefore a feature of the lateral striatum. This did not prevent measurement of DA in the lateral striatum, as 68% of the signals with S/N > 10 came from this region.

Since it seemed possible that the decreased signal to noise ratio was causing the larger variability in the parameters, we tested for this in the following way. A set of dopamine responses was constructed, using 6 different sets of parameters intended to provide archetypes of the kinetic possibilities for DA responses. To these 6 dopamine responses, 8 random noise components were added to produce n = 8 noise patterns for each of the 6 dopamine responses. These responses were also added together to produce an average, which was also modeled. Each random noise component consisted of a sine wave with a period of ~6 s and random phase, summed with gaussian noise normally distributed around 0. These random noise components were then scaled to S/N ratio of: 3, 5, 10, 15, 20, 25, 50, and 100. This yielded a total of 448 simulated DA responses with added noise to be modeled (including the averages). Since the DA responses were constructed, the parameters which made them up were known, and this allowed direct assessment of the effect of noise on the accuracy of the parameters arrived at by our fitting algorithm.

Figure 32. Effect of Artificial Noise On RD Model Parameters
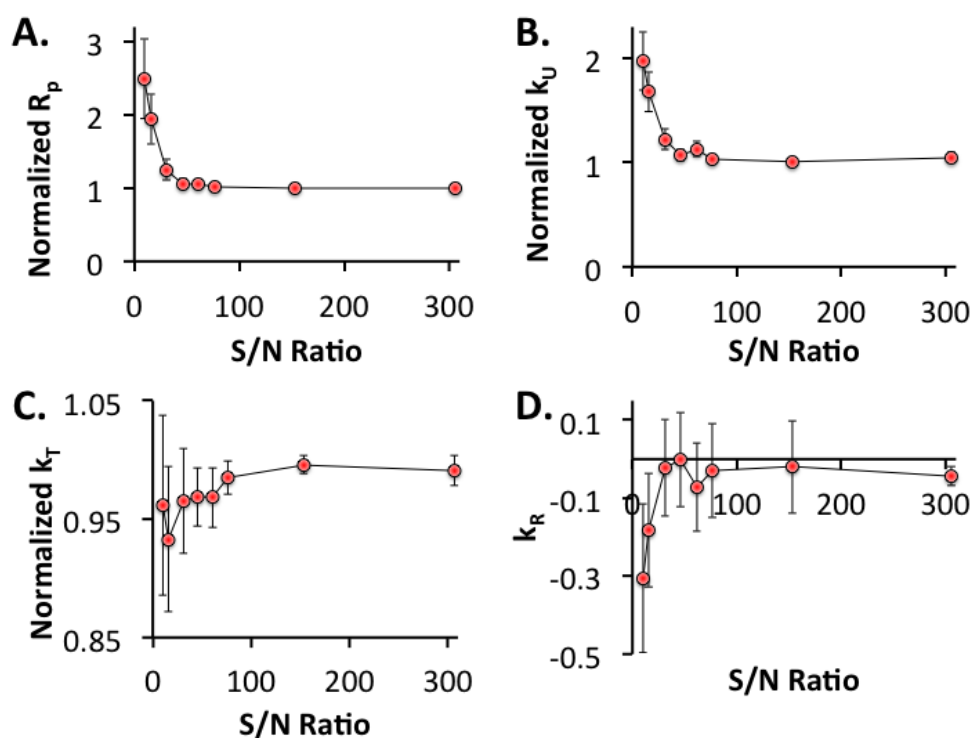
Fig 32: Effect of artificial noise on accuracy of model fitting, for S/N values ~10-300. In **A**, **B**, and **C**, averaged parameter values are normalized to the actual average; in **D** this is not possible because the actual average is zero. Decreased signal to noise ratio causes marked deviation of the averaged parameters obtained by fitting from the true parameter values. In the case of DA release per pulse (**A**) and DA uptake (**B**), this results in a substantial upward boost of both values. The first order mass transport parameter k_T expands in variability but the average is not affected dramatically (**C**), although it is slightly decreased. The rate of change of release per pulse, kR, is least affected by noise (**D**). The simulations that Figure 5 is based on, for each point at a given S/N ratio, used 8 random-noise replicates of the following 6 parameter sets {R_p, k_U, k_T, k_R}: {10, 20, 2, 1}; {10, 20, 2, 0}; {10, 20, 2, -1}; {10, 1, 2, 1}; {10, 1, 2, 0}; {10, 1, 2, -1}. This yielded a total of 48 replicates per S/N ratio. SEM error bars are reported for every data point, but too small to see in some cases. S/N ratio was defined in the same way as for Figure S1.

It was observed that a decreased signal to noise ratio affected the accuracy of parameter assignment in all test cases, but the effect was uneven and dependent on the actual value of the

105

parameters, as well as on the specific instance of noise. DA responses with a positive k_R seemed to handle noise more robustly, as did DA responses with slower uptake (shown in supplementary information). All signal to noise ratios of 25 and above produced good agreement with the actual data for all kinds of responses tested. This is in good agreement with the large reduction in variability above S/N = 25 in real data. Our *in vivo* detection limit was ~100 nM for a response peak, and thus response peaks of over 0.8 uM are typically required, at a minimum, for accurate assignment of parameters in all cases. The very most sensitive kinds of DA detection discovered to date, at a LOD of ~10 nM, would in contrast be able to resolve kinetic parameters from DA peaks of just over 80 nM, under ideal conditions.

The information learned about the effects of signal to noise ratio was applied to the DA kinetic parameters obtained from each studied striatal subregion. In cases where a substantial number of robust signals of S/N > 25 was available (8 or more), only the parameters obtained from fitting those signals were included in the reported average parameter values in figure 8. This was the case with fast sites in the DLS, VLS, and DMS. VMS fast sites also had large S/N ratios but were not common enough for this approach. Only 5 total slow sites had S/N ratio > 25. In the VMS fast sites, and in the slow sites in all 4 striatal subregions, the parameter values obtained by modeling the average were themselves averaged with the average of the parameter values obtained by modeling the S/N > 25 responses, as a compromise. Comprehensive parameter values are reported in Table 12.

Table 12. RD Model Parameter Values of Fast & Slow Sites in the DLS, DMS, VLS, and VMS

106

	Model of Average					AVG of S/N > 10					AVG of S/N > 25			
Brain Region	R_p	k_U	k_T	k_R	n	R_p	k_U	k_T	k_R	n	R_p	k_U	k_T	k_R
DLS Fast	8.0	33	2.1	0.1	36	40	49	2.6	1.7	10	7.3	21	2.7	0.2
VLS Fast	2.1	8.6	1.7	-0.7	13	6.5	25	2.9	-0.5	8	1.9	8.1	2.8	-0.9
DMS Fast	1.4	2.6	2.5	-0.5	12	2.9	22	2.2	-0.9	10	2.1	6.2	2.3	-0.8
VMS Fast	1.5	3.1	1.7	-0.5	2	1.8	4.6	1.9	-0.8	2	1.8	4.6	1.9	-0.8
DLS Slow	3.4	18	1.4	-0.9	13	11	44	1.9	-1.1	1	2.1	10	1.5	-1.3
VLS Slow	1.2	6.3	1.5	-0.9	6	5.8	42	2.7	-1.1	2	1.0	3.3	2.6	-1.1
DMS Slow	0.6	8.4	1.0	-1.7	15	1.6	30	2.0	-1.8	2	0.8	15	1.6	-1.7
VMS Slow	0.6	4.4	0.7	-1.0	3	3.0	47	1.1	-0.9	0	-	-	-	-

Figure 33. Signal to Noise Ratio In Real and Generated Data
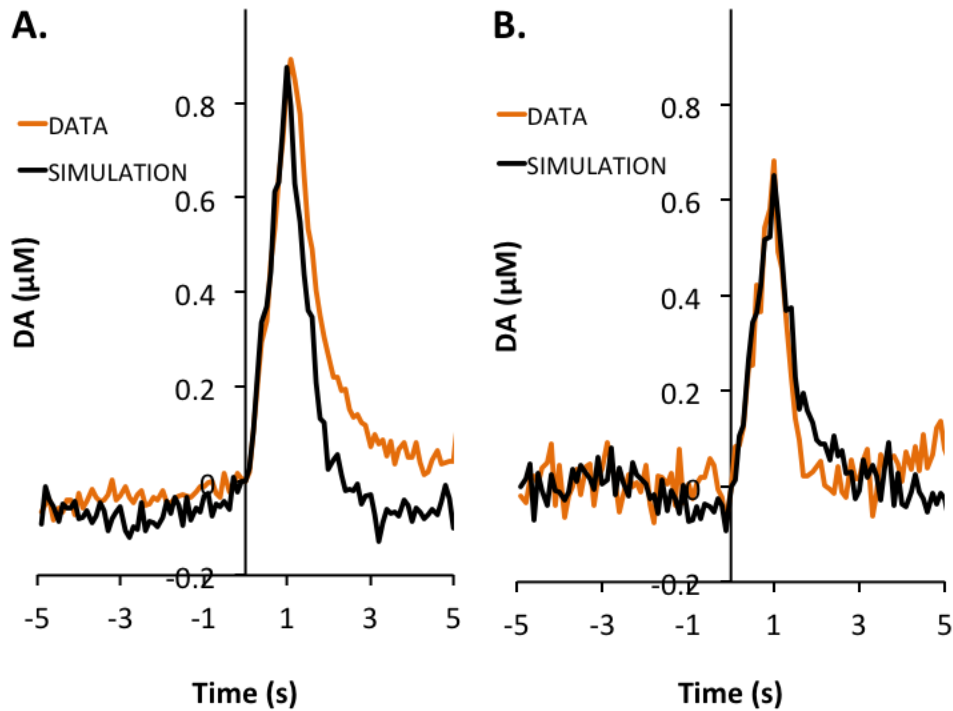
Figure 33: Experimental and generated examples of S/N ratios above and below the threshold for potentially accurate determination of biophysical parameters from kinetic modeling. **A.** At ~35 S/N ratio, both the real and simulated signal are considered adequate for determination of parameters kinetic modeling. **B.** At ~17 S/N ratio, the simulated and real signal are considered inadequate for accurate determination of parameters by means of

107

kinetic modeling. Signal averaging is a straightforward means of surmounting this issue, and improves the signal to noise ratio by a factor of the square root of the number of averaged measurements.

Independent Verification of the Restricted Diffusion Model By Linking Kinetic Modeling to Exocytotic and Ultrastructural Information, And The Action of Silent DA Terminals in Kinetic Diversity

Equation 19: Biophysical Subdivision of Release per Pulse

$$R_p = DApV \cdot TVP \cdot fFV \cdot fVE$$

The main text states that there is an upper bound on the value of R_p at 28 zmol. This figure is arrived at by multiplying dopamine per vesicle (*DApV*), the total vesicle pool (*TVP*) present in the arbitary outer compartment volume that scales R_p, the fraction of fusing vesicles (*fFV*) in reponse to a stimulus, and the fraction of vesicle emptying upon a stimulus (*fVE*).

DApV, *fFV*, and *fVE* are independent of the number of vesicles considered. In PC12 cells, *DApV* has been found to be 33,000, as has *fVE* been found to be 0.40 – both by Omiatek and coworkers, from the Ewing lab. The value of fVE was determined for DA vesicles in PC12 cells, which are approximately 3X the diameter of striatal DA vesicles. It is therefore possible that fVE is somewhat higher than 0.40 for striatal DA vesicles, as the diffusion distance in shorter than in the larger vesicles. However, our findings, and the findings of others, make it mathematically necessary that DA vesicles be reused, as even over 1 second of 60 Hz stimulus, the product of ffV*(number of stimulus pulses) > 1. Since vesicles take 30 seconds to be reformed, the vesicles must be reused for this observation to be possible. This effect is even more obvious if silent terminals are considered, as well as considering that evoked DA overflow in

108

response to 60 Hz MFB stimulus can continue to increase for well more than 1 second (5-10 seconds is common). Rooney and Wallace used a computational modeling approach to specify that at most, 25% of a single vesicle per DA varicosity would be required to be released per firing event. This means that at most 6.3% of the total DA in each varicosity would be released per firing event, since there are 4 DA vesicles per varicosity on average, according to the recent report by Lohr et al. This implies (from *fVE*) that, at most, 16% of the vesicles per terminal (on average) would fuse in response to a stimulus.

$$R_p \leq \frac{10E21 \; zeptomoles \; DA}{6.022E23 \; molecules \; DA} \cdot 33,000 \; \frac{DA \; molecules}{vesicle} \cdot 8 \; vesicles \cdot 0.16 \cdot 0.40$$

$$R_p \leq 28 \; zmol$$

The recent report of Pereria et al that only ~17% of DA terminals were found to be actively engaged in release in response to a stimulus allows us to calculate an upper bound for R_p in a slightly different way:

$$R_p = DApV \cdot TVP \cdot 0.17 \; active \; terminals \cdot fVE$$

$$R_p \leq 30 \; zmol$$

This also means that the terminals which are active must be fusing all of their vesicles at the upper bound of R_p, while the terminals which are not active of course fuse none of their vesicles even at the upper bound of R_p. At values of R_p below the upper bound, it is possible

either that entire DA terminals "go offline", or that some fraction of vesicles are activated with every pulse.

In maximally or close to maximally active sites, the rate of uptake is a constraint on the rate of vesicle refilling. We would therefore predict that combining high rates of release with lowered DA uptake would result in a positive k_R, as the ability of the DA vesicles to continue releasing is depleted with time. Thus, the k_R parameter yields composite information about vesicle refilling rates, progressive activation of vesicles/terminals over time with continued MFB stimulation, and any other components which might influence the release rate.

Thus, the k_R parameter is capable of yielding useful information about the composite effect of subsecond changes to DA release. It is clear that the actual release per pulse at any given time is a balance between vesicle refilling rate, DA autoinhibition and increase in activation over time. The k_R parameter allows quantitative information to be obtained about the net effect of this process at any recording site in the brain, and indicates that the regulation of release favors an equilibrium state of suppression of DA release at all subdivisions of the striatum except for the DLS fast sites.

The substantially larger values of R_p in the DLS as compared to the DMS, VMS, and VLS, indicate that a larger percentage of DLS dopamine terminals must fire synchronously in response to MFB stimulus. The average value for R_p within a region varies between 0.6 zmol and 8 zmol; the maximum recorded value (S/N>25 data) for R_p over the entire set of experiments was 17 zmol. These data mean that, on average, 0.3% to 4.6% of vesicles in a sampling volume are actively engaged in release on average in response to an initial stimulus pulse. This in turn means that as few as 0.3% (DMS and VMS slow) to 4.6% (DLS fast) (and as many as 1.2%

(DMS slow and VMS slow) to 18.4% (DLS fast) of terminals release DA in response to a single stimulus pulse *in vivo*. Assuming that ~6,400 DA terminals reside within the sampling volume of our carbon fiber microelectrodes, this implies that as few as 19 terminals may be responsible for the initial signal at DMS and VMS slow sites, assuming that all of the active terminals have all their vesicles active, and the the *fVE* value of 0.40 holds.

Figure 34. Physiological Predictions from The RD Model I
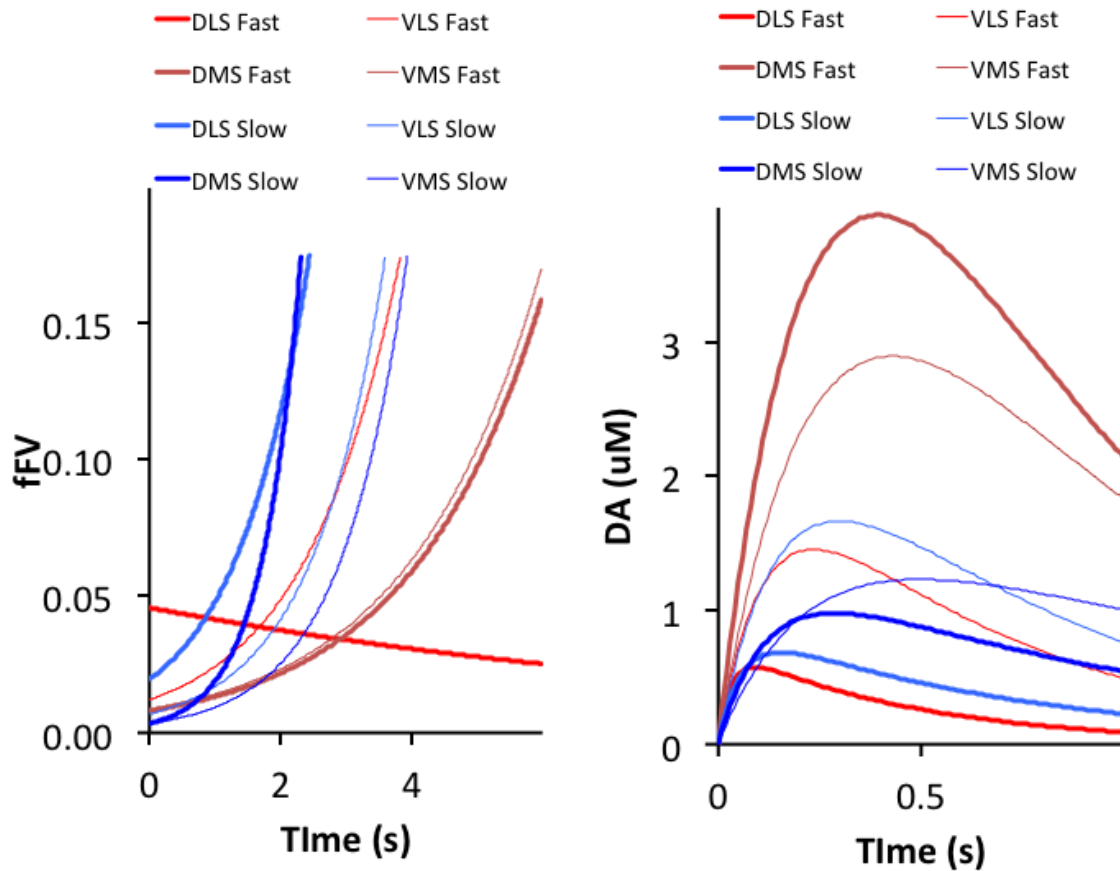
Figure 34: Physiological Extrapolations from the Restricted Diffusion Model: Simulated physiological extrapolations of fast and slow sites from the four studied striatal subregions. **A:** Modeled prediction of the average fraction of fusing vesicles (fFV) over time. The modeling shows several points where it is progressively less likely to be reliable: When average fFV > 1, when average fFV > 0.16, and when average fFV > 0.046. None of the simulations exceeds fFV > 0.046 at 1s of stimulation, which is how all of the experiments in this study were done. Decribing k_R with a simple exponential in many stimulations much longer than 1s may not be not valid, as fFV rapidly exceeds plausible and even possible values. **B:** Based on the initial fFV at each site, single pulse models have been extrapolated to give an idea of the concentrations that would develop at individual terminals in response to a single action potential. Fickian diffusion to and away from the terminal is not accounted for in **B**, because we have no information about the distribution of terminals, under the measured average. All responses in B are overestimates of the concentration increasingly with increasing time, because diffusion will clear the local sites, but more densely packed active terminal fields will be less affected by this, as DA from adjacent terminals will diffuse into the site in question to replace what was lost by diffusional clearance.

Fast DA sites are those DA sites in which the balance of release regulation is biased towards high DA release when the stimulus begins, while slow DA sites are suppressed in balance, although this suppression can be overcome with time. In some cases (the silent sites), the time to meaningfully overcome this suppression exceeds 1 second of stimulation at 60 pulses.

Physiological Extrapolations from the RD Model

Figure 35. Physiological Predictions from The RD Model II
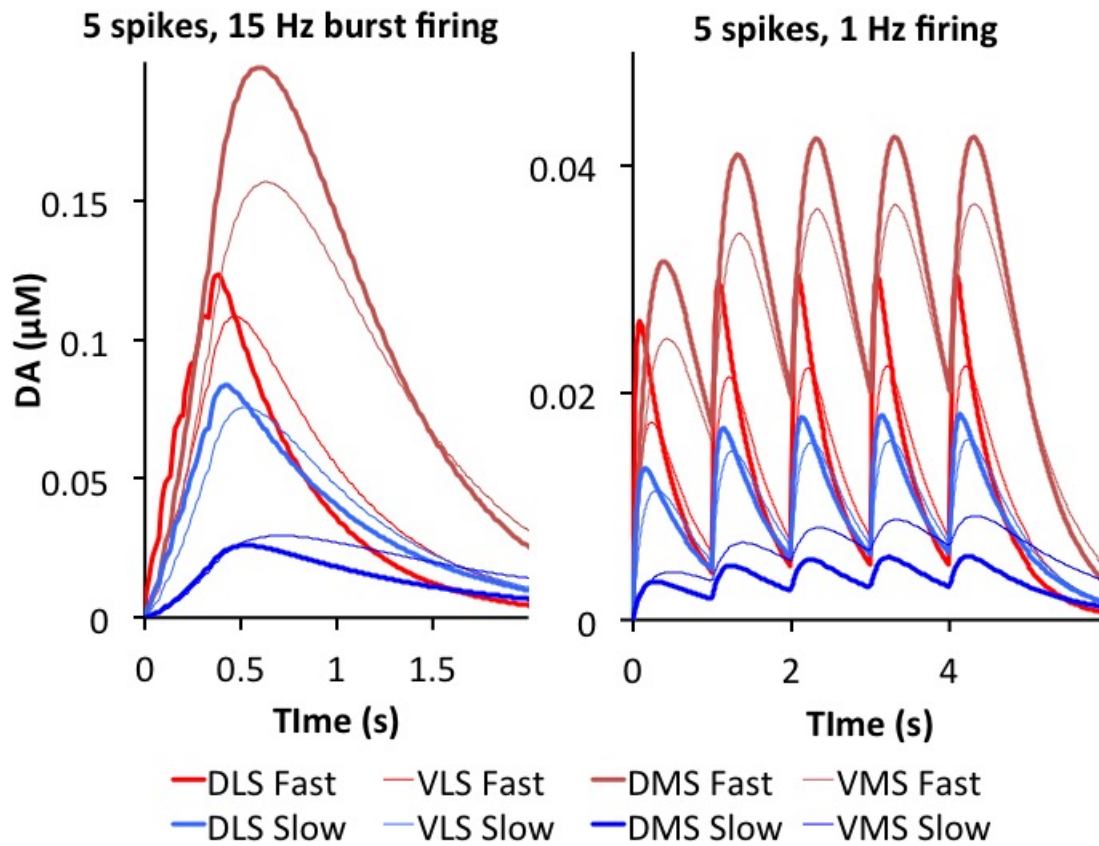
Figure 35: Physiological Extrapolations from the Restricted Diffusion Model: Restricted Diffusion Makes Frequency Based DA Signal Transduction Impossible Above ~1 Hz. Simulated physiological extrapolations of fast and slow sites from the four studied striatal subregions. **A:** 5 spike, 15 Hz signals fail to exhibit meaningful peak differentiation at any level of uptake, and thus do not directly transduce data on the phasic DA firing rate to postsynaptic receptors. However, the signal amplitudes are considerably increased over single, differentiated spikes as seen in **B:** 5 spike, 1 Hz signals exhibit peak differention and so are capable of directly transducing DAergic neuron firing frequency to postsynaptic receptors.

8.0   REFLECTION AND FURTHER DEVELOPMENT OF THE RD MODEL

8.1   SUMMARY OF CONCLUSIONS REACHED FROM THIS WORK

Evoked dopamine responses, if arising from a sufficiently short stimulus, can be reproduced in perfect mathematical detail by a restricted diffusion model which contains only three adjustable parameters. The parameter values of release, uptake, and mass transport are biophysically meaningful. The kinetics of evoked dopamine responses are minimally influenced by normal mode adsorption. However, there is a second mode of adsorption which causes the hangup feature commonly observed in FSCV measurements of dopamine. This adsorption can easily be corrected for in order to obtain a more accurate representation of the concentration over time. While increasing the parameterization of the model in general allows for better fits to longer stimuli, it appears that short term plasticity of release is able to meaningfully explain many of the characteristic, kinetically diverse DA patterns that are seen when the brain is subjected to longer stimuli. When the release is modified by a simple exponential, this four parameter version of the RD model is able to fit the hangup-corrected data perfectly in almost every case for stimulations lasting three seconds or less. This gives insight into the dynamic nature of DA overflow over a subsecond timescale. It is also notable that nomifensine, an uptake inhibitor, can be seen to alter the plasticity of DA overflow over the subsecond timescale. This

114

is also seen with buproprion, another uptake inhibitor used as an antidepressant. In particular, buproprion appears to diminish the magnitude of DA release over time, while the initial DA release is unaffected. This is in good agreement with vesicle refilling being required for maximal continued release according to the kiss-and-run fusion model of DA exocytosis, but the initial release being unaffected seems to stand in constrast to other uptake inhibitors such as cocaine and MDPV, which are thought to increase DA release. This may represent a mechanistic difference between DAT-blocking drugs of abuse and DAT-blocking drugs that have little to no abuse potential. When the brain is spatially mapped, sites recorded in the lateral striatum are found to be significantly more likely to be of the fast type than sites in the medial striatum, and sites recorded in the ventral striatum are found to be significantly more likely to be silent (nonresponsive to an MFB stimulus within the first second) than sites recorded in the dorsal striatum. In addition, fast sites recorded in the dorsolateral striatum are significantly different from other fast sites, with the difference being largely due to a difference in the rate of uptake. The higher rate of uptake in the dorsolateral striatum cannot increase the DA signaling bandwidth appreciably - as restricted diffusion becomes a rate-limiting step in the disappearance of the DA overflow, rapid rates of uptake are unable to clear the signal any more rapidly than somewhat slower rates of uptake. This leads to the conclusion that the high rate of uptake in the DLS is likely present to create more signal processing capacity in space, as high uptake has no effect on the amount of signal bandwidth for a given brain volume. It was also determined that noise present in the FSCV data introduces systematic errors into the parameter values obtained by RD modeling, making the R_p and k_U larger, and introducing random error into the k_T. A signal to noise ratio of better than about 25 is required to minimize this issue. Finally, it appears

to be possible to subdivide the parameters obained by RD Modeling, and in particular we have subdivided the release parameter, in order to compare the values obtained for Rp to values coming from the exocytosis literature. These values are in good agreement, which builds further confidence in the correctness of the model.

8.2   VALIDATING ACCURACY OF THE SIMPLEST RD MODEL

The 3 parameter version of the RD model makes truly excellent fits in reponse to all short stimuli, even and perhaps even especially when uptake has been inhibited. This is especially impressive because all of the release can be made to occur in a single data point, while the model is able to fit all of the subsequent 40-100 data points with ease. Furthermore, the release parameter R_p acts only as a scaling factor and has no impact on the shape. It also appears to me from studying the results of many hundreds of model fittings that the mass transport parameter k_T is constant with a value approximately equal to 2. Therefore, the different shapes of every FSCV curve following a short stimulus are defined almost completely by the first order rate of uptake, k_U. The fact that the model contains a number of parameters only equal to the three basic phenomena that must be accounted for is highly encouraging as to its potential accuracy but not a proof of correctness. For example, it has been suggested that release of DA continues after the end of the stimulus[23] and that this, rather than mass transport from an inner compartment, explains the existence of overshoots. However, if this is the case, it might imply that this creates a pattern of DA release exactly equal to what we have considered as transport from an inner compartment - and also that the effects of mass transport are negligible, and that the DA terminal

116

field in the vicinity of the carbon fiber microcylinder can be treated on average as a radially homogenous field. However, there are also still other possibilities, which would mostly involve complex scenarios that just happened to be fit by an underparameterized model. Given current knowledge, I do advocate the use of the three parameter RD model to analyze evoked DA overflows, especially in cases involving characterizing the effects of short stimuli. It is however quite desirable to know that it is restricted mass transport, as opposed to delayed release or some other combination of factors, which is actually responsible for the observed overshoot. Construction of a parsimonious model which describes the data with high fidelity is an important step, but the nature of restricted diffusion should be confirmed by further experiment.

8.3   EXPLORING THE NATURE OF RESTRICTED DIFFUSION

I have conducted Monte Carlo simulations of confined volumes of various topologies with exits that occupy only a small portion of the surface areas of the volume. As the exit becomes very small, the diffusional egress from the confined volume becomes first order and unidirectional, which confirms that physically restricted diffusion from a physical inner compartment is a plausible explanation. However, it is important to test this with an experiment. The only experiment that I can envision that would provide satisfactory evidence to this question is microscopy designed to measure DA or some surrogate for DA with high spatial and temporal resolution. Combined with FSCV data, this should be capable of providing full experimental confirmation of the theorized Inner Compartment.

8.4 PLASTICITY AND PARAMETER TIME INCONSISTENCY

The model provides very satisfying fits to evoked DA responses that arise due to short stimuli of a few pulses. However, when longer stimuli are applied, a wide variety of responses arise due to differences in local kinetics. These responses require, at a minimum, at least one additional parameter to fit them. Because release, uptake, and mass transport have all been accounted for by the first three parameters, and because the 3 parameter model fits all known DA responses arising from short stimulations, it is reasonable to assume that at least one of the parameters ought to be made to vary with time or some other factor. We have chosen to assume that it is the release parameter that varies with time, and have thus multiplied the release by an exponential. This is able to make very good fits to almost all stimulations of 180 pulses and 3 seconds or less, however there are two issues that this presents. While in some cases (such as in slow domains after nomifensine), the 4 parameter set is relatively time invariant (meaning that the same or very close to the same parameters can describe the results of stimulations at the same location but conducted for different lengths of time, such as 12 pulses and 180 pulses for example,) in many other cases the 4 parameter set is not time invariant. This is not entirely surprising, as any exponential modifying any other parameter either collapses to zero or increases to infinity with time. While an exponential modifying the release per pulse is a simple and perhaps adequate approximation of short term plasticity of release, it is by definition at least partially inaccurate. A more sophisticated and more accurate representation is desirable; however, this will require both more data from experiments other than FSCV, and additional model parameters.

8.5   PARAMETER SUBDIVISION

I have made rudimentary progress on subdividing the release parameter into other parameters which have meaning with respect to cellular activity. This is highly promising, because it means that sufficient knowledge about the system might allow us to analyze individual cellular parameters in real time, given a sufficient set of experiments. This could eventually provide a compelling link between the basic biophysical functions of the dopamine neurons and the physiological functions in which dopamine is involved. Critically, it might be possible to see exactly what about the cellular signaling is affected in disease states, drug addictions, and various normal physiological functions. This could yield unique insights which could drive new therapies and new technological developments. However, while progress on this aspect of study may be made in parallel with the previously mentioned issues in this chapter, progress in this area will also require resolution of the previous issues as a necessary but not sufficient condition.

BIBLIOGRAPHY

1.   Ponchon, J. L., Cespuglio, R., Gonon, F., Jouvet, M. & Pujol, J. F. Normal pulse polarography with carbon fiber electrodes for in vitro and in vivo determination of catecholamines. *Anal. Chem.* **51,** 1483–1486 (1979).

2.   Ewing, A. G., Bigelow, J. C. & Wightman, R. M. Direct in vivo monitoring of dopamine released from two striatal compartments in the rat. *Science (80-.).* **221,** 169–171 (1983).

3.   Wightman, R. M. *et al.* Real-time characterization of dopamine overflow and uptake in the rat striatum. *Neuroscience* **25,** 513–23 (1988).

4.   Engstrom, R. C., Wightman, R. M. & Kristensen, E. W. Diffusional distortion in the monitoring of dynamic events. *Anal. Chem.* **60,** 652–656 (1988).

5.   Wu, Q., Reith, M. E., Wightman, R. M., Kawagoe, K. T. & Garris, P. A. Determination of release and uptake parameters from electrically evoked dopamine dynamics measured by real-time voltammetry. *J. Neurosci. Methods* **112,** 119–133 (2001).

6.   Kristensen, E. W., Kuhr, W. G. & Wightman, R. M. Temporal characterization of perfluorinated ion exchange coated microvoltammetric electrodes for in vivo use. *Anal. Chem.* **59,** 1752–1757 (1987).

7.   Wu, Q., Reith, M. E., Wightman, R. M., Kawagoe, K. T. & Garris, P. A. Determination of release and uptake parameters from electrically evoked dopamine dynamics measured by real-time voltammetry. *J. Neurosci. Methods* **112,** 119–33 (2001).

8.   Garris, P. A., Ciolkowski, E. L. & Wightman, R. M. Heterogeneity of evoked dopamine overflow wihin the striatal and striatoamygdaloid regions. *Neuroscience* **59,** 417–427 (1994).

9.   Garris, P. A., Ciolkowski, E. L., Pastore, P. & Wightman, R. M. Efflux of dopamine from the synaptic cleft in the nucleus accumbens of the rat brain. *J. Neurosci.* **14,** 6084–6093 (1994).

10.   Garris, P. A. & Wightman, R. M. Different kinetics govern dopaminergic transmission in the amygdala, prefrontal cortex, and striatum: an in vivo voltammetric study. *J. Neurosci.* **14,** 442–450 (1994).

11.   Bath, B. D. *et al.* Subsecond adsorption and desorption of dopamine at carbon-fiber microelectrodes. *Anal. Chem.* **72,** 5994–6002 (2000).

12.   Bath, B. D., Martin, H. B., Wightman, R. M. & Anderson, M. R. Dopamine Adsorption at Surface Modified Carbon-Fiber Electrodes. *Langmuir* **17,** 7032–7039 (2001).

13.   Venton, B. J., Troyer, K. P. & Wightman, R. M. Response times of carbon fiber microelectrodes to dynamic changes in catecholamine concentration. *Anal. Chem.* **74,** 539–546 (2002).

14.   Atcherley, C. W. *et al.* Improved Calibration of Voltammetric Sensors for Studying Pharmacological Effects on Dopamine Transporter Kinetics in Vivo. *ACS Chem. Neurosci.* (2014). doi:10.1021/cn500020s

15.   Venton, B. J. *et al.* Real-time decoding of dopamine concentration changes in the caudate-putamen during tonic and phasic firing. *J. Neurochem.* **87,** 1284–95 (2003).

16.   Montague, P. R. *et al.* Dynamic gain control of dopamine delivery in freely moving animals. *J. Neurosci.* **24,** 1754–1759 (2004).

17.   Heien, M. L. a V, Johnson, M. a & Wightman, R. M. Resolving neurotransmitters detected by fast-scan cyclic voltammetry. *Anal. Chem.* **76,** 5697–704 (2004).

18.   Willuhn, I., Burgeno, L. M., Groblewski, P. a & Phillips, P. E. M. Excessive cocaine use results from decreased phasic dopamine signaling in the striatum. *Nat. Neurosci.* **17,** 704–9 (2014).

19.   Howe, M. W., Tierney, P. L., Sandberg, S. G., Phillips, P. E. M. & Graybiel, A. M. Prolonged dopamine signalling in striatum signals proximity and value of distant rewards. *Nature* **500,** 575–9 (2013).

20.   Hollon, N. G., Arnold, M. M., Gan, J. O., Walton, M. E. & Phillips, P. E. M. Dopamine-associated cached values are not sufficient as the basis for action selection. *Proc. Natl. Acad. Sci. U. S. A.* **111,** 18357–62 (2014).

21.   Rodeberg, N. T. *et al.* Construction of Training Sets for Valid Calibration of in Vivo Cyclic Voltammetric Data by Principal Component Analysis. *Anal. Chem.* **87,** 11484–11491 (2015).

22.   Johnson, J. A., Rodeberg, N. T. & Wightman, R. M. Failure of Standard Training Sets in the Analysis of Fast-Scan Cyclic Voltammetry Data. *ACS Chem. Neurosci.* **7,** 349–59 (2016).

23.   Harun, R., Grassi, C. M., Munoz, M. J., Torres, G. E. & Wagner, A. K. Neurobiological model of stimulated dopamine neurotransmission to interpret fast-scan cyclic voltammetry data. *Brain Res.* **1599,** 67–84 (2015).

24.   Schultz, W. Multiple dopamine functions at different time courses. *Annu. Rev. Neurosci.* **30,** 259–88 (2007).

25.   Abi-Dargham, A. *et al.* Increased baseline occupancy of D2 receptors by dopamine in schizophrenia. *Proc. Natl. Acad. Sci. U. S. A.* **97,** 8104–9 (2000).

26.   Schultz, W. Depletion of dopamine in the striatum as an experimental model of parkinsonism: direct effects and adaptive mechanisms. *Prog. Neurobiol.* **18,** 121–166 (1982).

27.   Sagvolden, T., Johansen, E. B., Aase, H. & Russell, V. A. A dynamic developmental theory of attention-deficit/hyperactivity disorder (ADHD) predominantly hyperactive/impulsive and combined subtypes. *Behav. Brain Sci.* **28,** 397–419 (2005).

28.   Carlsson, A., Lindquist, M., Magnusson, T. & Waldeck, B. On the presence of 3-hydroxytyramine in brain. *Science* **127,** 471 (1958).

29.   May, L. J., Kuhr, W. G. & Wightman, R. M. Differentiation of dopamine overflow and uptake processes in the extracellular fluid of the rat caudate nucleus with fast-scan in vivo voltammetry. *J. Neurochem.* **51,** 1060–9 (1988).

30.   Iversen, L. L. Role of transmitter uptake mechanisms in synaptic neurotransmission. *Br. J. Pharmacol.* **41,** 571–91 (1971).

31.   Sharp, T., Zetterström, T. & Ungerstedt, U. An in vivo study of dopamine release and metabolism in rat brain regions using intracerebral dialysis. *J. Neurochem.* **47,** 113–22 (1986).

32.   Nicholson, C. Interaction between diffusion and Michaelis-Menten uptake of dopamine after iontophoresis in striatum. *Biophys. J.* **68,** 1699–1715 (1995).

33.   Rice, M. E., Oke, A. F., Bradberry, C. W. & Adams, R. N. Simultaneous voltammetric and chemical monitoring of dopamine release in situ. *Brain Res.* **340,** 151–155 (1985).

34.   Moquin, K. F. & Michael, A. C. Tonic autoinhibition contributes to the heterogeneity of evoked dopamine release in the rat striatum. *J. Neurochem.* **110,** 1491–1501 (2009).

35. Mitch Taylor, I., Jaquins-Gerstl, A., Sesack, S. R. & Michael, A. C. Domain-dependent effects of DAT inhibition in the rat dorsal striatum. *J. Neurochem.* **122,** 283–294 (2012).

36. Taylor, I. M., Ilitchev, A. I. & Michael, A. C. Restricted diffusion of dopamine in the rat dorsal striatum. *ACS Chem. Neurosci.* **4,** 870–878 (2013).

37. Shu, Z., Taylor, I. M. & Michael, A. C. The dopamine patchwork of the rat nucleus accumbens core. *Eur. J. Neurosci.* **38,** 3221–9 (2013).

38. Shu, Z., Taylor, I. M., Walters, S. H. & Michael, A. C. Region- and domain-dependent action of nomifensine. *Eur. J. Neurosci.* **40,** 2320–2328 (2014).

39. Taylor, I. M. *et al.* Kinetic diversity of dopamine transmission in the dorsal striatum. *J. Neurochem.* n/a–n/a (2015). doi:10.1111/jnc.13059

40. Walters, S. H., Robbins, E. M. & Michael, A. C. The Kinetic Diversity of Striatal Dopamine: Evidence from a Novel Protocol for Voltammetry. *ACS Chem. Neurosci.* (2016). doi:10.1021/acschemneuro.6b00020

41. Kawagoe, K. T., Garris, P. a, Wiedemann, D. J. & Wightman, R. M. Regulation of transient dopamine concentration gradients in the microenvironment surrounding nerve terminals in the rat striatum. *Neuroscience* **51,** 55–64 (1992).

42. Mitch Taylor, I., Jaquins-Gerstl, A., Sesack, S. R. & Michael, A. C. Domain-dependent effects of DAT inhibition in the rat dorsal striatum. *J. Neurochem.* **122,** 283–294 (2012).

43. Walters, S. H., Taylor, I. M., Shu, Z. & Michael, A. C. A Novel Restricted Diffusion Model of Evoked Dopamine. *ACS Chem. Neurosci.* (2014). doi:10.1021/cn5000666

44. Hrabetová, S. & Nicholson, C. Contribution of dead-space microdomains to tortuosity of brain extracellular space. *Neurochem. Int.* **45,** 467–77 (2004).

45. Ogston, A. G., Preston, B. N. & Wells, J. D. On the Transport of Compact Particles Through Solutions of Chain-Polymers. *Proc. R. Soc. A Math. Phys. Eng. Sci.* **333,** 297–316 (1973).

46. Johnson, E. M., Berk, D. a, Jain, R. K. & Deen, W. M. Hindered diffusion in agarose gels: Test of effective medium model. *Biophys. J.* **70,** 1017–1023 (1996).

47. Hrabetová, S., Masri, D., Tao, L., Xiao, F. & Nicholson, C. Calcium diffusion enhanced after cleavage of negatively charged components of brain extracellular matrix by chondroitinase. ABC. *J. Physiol.* **587,** 4029–49 (2009).

48. Nicholson, C. & Rice, M. E. *Volume Transmission in the Brain*. (1991).

49. Moss, J. & Bolam, J. P. A dopaminergic axon lattice in the striatum and its relationship with cortical and thalamic terminals. *J. Neurosci.* **28,** 11221–11230 (2008).

50. Stamford, J. A., Kruk, Z. L., Palij, P. & Millar, J. Diffusion and uptake of dopamine in rat caudate and nucleus accumbens compared using fast cyclic voltammetry. *Brain Res.* **448,** 381–5 (1988).

51. Cass, W. A., Gerhardt, G. A., Mayfield, R. D., Curella, P. & Zahniser, N. R. Differences in dopamine clearance and diffusion in rat striatum and nucleus accumbens following systemic cocaine administration. *J. Neurochem.* **59,** 259–266 (1992).

52. Wu, Q., Reith, M. E., Kuhar, M. J., Carroll, F. I. & Garris, P. A. Preferential increases in nucleus accumbens dopamine after systemic cocaine administration are caused by unique characteristics of dopamine neurotransmission. *J. Neurosci.* **21,** 6338–6347 (2001).

53. Jones, S. R., Garris, P. a & Wightman, R. M. Different effects of cocaine and nomifensine on dopamine uptake in the caudate-putamen and nucleus accumbens. *J. Pharmacol.Exp.Ther.* **274,** 396–403 (1995).

54. Kawagoe, K. T., Garris, P. A., Wiedemann, D. J. & Wightman, R. M. Regulation of transient dopamine concentration gradients in the microenvironment surrounding nerve terminals in the rat striatum. *Neuroscience* **51,** 55–64 (1992).

55. Moquin, K. F. & Michael, A. C. An inverse correlation between the apparent rate of dopamine clearance and tonic autoinhibition in subdomains of the rat striatum: A possible role of transporter-mediated dopamine efflux. *J. Neurochem.* **117,** 133–142 (2011).

56. Kile, B. M. *et al.* Optimizing the temporal resolution of fast-scan cyclic voltammetry. *ACS Chem. Neurosci.* **3,** 285–292 (2012).

57. Bath, B. D. *et al.* Subsecond adsorption and desorption of dopamine at carbon-fiber microelectrodes. *Anal. Chem.* **72,** 5994–6002 (2000).

58. Kume-Kick, J. & Rice, M. E. Dependence of dopamine calibration factors on media Ca^{2+} and Mg^{2+} at carbon-fiber microelectrodes used with fast-scan cyclic voltammetry. *J. Neurosci. Methods* **84,** 55–62 (1998).

59. Kovach, P. M., Ewing, A. G., Wilson, R. L. & Wightman, R. M. In vitro comparison of the selectivity of electrodes for in vivo electrochemistry. *J. Neurosci. Methods* **10,** 215–227 (1984).

60.   Gonon, F. G., Fombarlet, C. M., Buda, M. J. & Pujol, J. F. Electrochemical treatment of pyrolytic carbon fiber electrodes. *Anal. Chem.* **53,** 1386–1389 (1981).

61.   Stamford, J. A. Effect of electrocatalytic and nucleophilic reactions on fast voltammetric measurements of dopamine at carbon fiber microelectrodes. *Anal. Chem.* **58,** 1033–6 (1986).

62.   Gerhardt, G. a. & Hoffman, a. F. Effects of recording media composition on the responses of Nafion-coated carbon fiber microelectrodes measured using high-speed chronoamperometry. *J. Neurosci. Methods* **109,** 13–21 (2001).

63.   Hafizi, S., Kruk, Z. L. & Stamford, J. a. Fast cyclic voltammetry: Improved sensitivity to dopamine with extended oxidation scan limits. *J. Neurosci. Methods* **33,** 41–49 (1990).

64.   Heien, M. L. a V, Phillips, P. E. M., Stuber, G. D., Seipel, A. T. & Wightman, R. M. Overoxidation of carbon-fiber microelectrodes enhances dopamine adsorption and increases sensitivity. *Analyst* **128,** 1413–1419 (2003).

65.   Walters, S. H., Robbins, E. M. & Michael, A. C. Modeling the Kinetic Diversity of Dopamine in the Dorsal Striatum. *ACS Chem. Neurosci.* (2015). doi:10.1021/acschemneuro.5b00128

66.   Bard, A. J. & Faulkner, L. R. *Electrochemical Methods: Fundamentals and Applications.* **6,** (Wiley, 2000).

67.   Quantitative Chemical Analysis - 8th edition. at <http://documents.pageflip-   flap.com/27l3fpUKJ0kyCB36#.VqFgaWBh2u4=&p=0>

68.   Kile, B. M. *et al.* Optimizing the Temporal Resolution of Fast-Scan Cyclic Voltammetry. *ACS   Chem. Neurosci.* **3,** 285–292 (2012).

69.   Dissertation   of   Adrian   Michael.   at <http://cseweb.ucsd.edu/~swanson/papers/AdrianThesis.pdf>

70.   Claudel, C. E., Cho, M. H. & McDonald, R. D. Effect of amphetamine and catecholamines on startle response and general motor activity of albino rats. *Nature* **210,** 864–5 (1966).

71.   Smith, J. E., Co, C., Freeman, M. E., Sands, M. P. & Lane, J. D. Neurotransmitter turnover in rat striatum is correlated with morphine self-administration. *Nature* **287,** 152–4 (1980).

72.   Tempel, B. L., Livingstone, M. S. & Quinn, W. G. Mutations in the dopa decarboxylase gene affect learning in Drosophila. *Proc. Natl. Acad. Sci. U. S. A.* **81,** 3577–81 (1984).

73.   Turjanski, N. *et al.* PET studies of the presynaptic and postsynaptic dopaminergic system in Tourette's syndrome. *J. Neurol. Neurosurg. Psychiatry* **57,** 688–92 (1994).

74.   Chen, J. Y., Wang, E. A., Cepeda, C. & Levine, M. S. Dopamine imbalance in Huntington's disease: a mechanism for the lack of behavioral flexibility. *Front. Neurosci.* **7,** 114 (2013).

75.   Starr, M. S. The role of dopamine in epilepsy. *Synapse* **22,** 159–94 (1996).

76.   Andén, N. E. *et al.* Oral L-dopa treatment of parkinsonism. *Acta Med. Scand.* **187,** 247–55 (1970).

77.   Carlsson, A. Does dopamine play a role in schizophrenia? *Psychol. Med.* **7,** 583–97 (1977).

78.   Shaw, P. *et al.* Polymorphisms of the dopamine D4 receptor, clinical outcome, and cortical structure in attention-deficit/hyperactivity disorder. *Arch. Gen. Psychiatry* **64,** 921–31 (2007).

79.   Ritz, M. C., Lamb, R. J., Goldberg, S. R. & Kuhar, M. J. Cocaine self-administration appears to be mediated by dopamine uptake inhibition. *Prog. Neuropsychopharmacol. Biol. Psychiatry* **12,** 233–9 (1988).

80.   Ostlund, S. B., Leblanc, K. H., Kosheleff, A. R., Wassum, K. M. & Maidment, N. T. Phasic Mesolimbic Dopamine Signaling Encodes the Facilitation of Incentive Motivation Produced by Repeated Cocaine Exposure. *Neuropsychopharmacology* **39,** 2441–2449 (2014).

81.   Brimblecombe, K. R. & Cragg, S. Ni(2+) affects dopamine uptake which limits suitability as inhibitor of T-type voltage-gated Ca(2+) channels. *ACS Chem. Neurosci.* (2014). doi:10.1021/cn500274g

82.   Cheer, J. F. *et al.* Phasic dopamine release evoked by abused substances requires cannabinoid receptor activation. *J. Neurosci.* **27,** 791–795 (2007).

83.   Hashemi, P. *et al.* Brain dopamine and serotonin differ in regulation and its consequences. *Proc. Natl. Acad. Sci. U. S. A.* **109,** 11510–5 (2012).

84.   Huang, E. Y.-K. *et al.* Amantadine ameliorates dopamine-releasing deficits and behavioral deficits in rats after fluid percussion injury. *PLoS One* **9,** e86354 (2014).

85.   Peters, J. L. & Michael, A. C. Changes in the kinetics of dopamine release and uptake have differential effects on the spatial distribution of extracellular dopamine concentration in rat striatum. *J. Neurochem.* **74,** 1563–73 (2000).

86.   May, L. J. & Wightman, R. M. Effects of D-2 antagonists on frequency-dependent stimulated dopamine overflow in nucleus accumbens and caudate-putamen. *J. Neurochem.* **53,** 898–906 (1989).

87.   May, L. J. & Wightman, R. M. Heterogeneity of stimulated dopamine overflow within rat striatum as observed with in vivo voltammetry. *Brain Res.* **487,** 311–20 (1989).

88.   Furini, C. R. G., Myskiw, J. C., Schmidt, B. E., Marcondes, L. A. & Izquierdo, I. D1 and D5 dopamine receptors participate on the consolidation of two different memories. *Behav. Brain Res.* **271,** 212–217 (2014).

89.   Salimpoor, V. N., Benovoy, M., Larcher, K., Dagher, A. & Zatorre, R. J. Anatomically distinct dopamine release during anticipation and experience of peak emotion to music. *Nat. Neurosci.* **14,** 257–62 (2011).

90.   Eshel, N. *et al.* Arithmetic and local circuitry underlying dopamine prediction errors. *Nature* **525,** 243–246 (2015).

91.   Zalocusky, K. A. *et al.* Nucleus accumbens D2R cells signal prior outcomes and control risky decision-making. *Nature* **531,** 642–6 (2016).

92.   Dodson, P. D. *et al.* Representation of spontaneous movement by dopaminergic neurons is cell-type selective and disrupted in parkinsonism. *Proc. Natl. Acad. Sci.* 201515941 (2016). doi:10.1073/pnas.1515941113

93.   Buckholtz, J. W. *et al.* Mesolimbic dopamine reward system hypersensitivity in individuals with psychopathic traits. *Nat. Neurosci.* **13,** 419–21 (2010).

94.   Salinas, A. G., Nguyen, C. T. Q., Ahmadi-Tehrani, D. & Morrisett, R. A. Reduced ethanol consumption and preference in cocaine- and amphetamine-regulated transcript (CART) knockout mice. *Addict. Biol.* **19,** 175–84 (2014).

95.   Boyden, E. S., Zhang, F., Bamberg, E., Nagel, G. & Deisseroth, K. Millisecond-timescale, genetically targeted optical control of neural activity. *Nat. Neurosci.* **8,** 1263–8 (2005).

96.   Chen, R., Romero, G., Christiansen, M. G., Mohr, A. & Anikeeva, P. Wireless magnetothermal deep brain stimulation. *Science* **347,** 1477–80 (2015).

97. Robinson, D. L. *et al.* Sub-second changes in accumbal dopamine during sexual behavior in male rats. *Neuroreport* **12,** 2549–2552 (2001).

98. Jones, S. R., Garris, P. A., Kilts, C. D. & Wightman, R. M. Comparison of dopamine uptake in the basolateral amygdaloid nucleus, caudate-putamen, and nucleus accumbens of the rat. *J. Neurochem.* **64,** 2581–2589 (1995).

99. Garris, P. A. & Wightman, R. M. Distinct pharmacological regulation of evoked dopamine efflux in the amygdala and striatum of the rat in vivo. *Synapse* **20,** 269–279 (1995).

100. Moquin, K. F., Jaquins-Gerstl, A. & Michael, A. C. A method for the intracranial delivery of reagents to voltammetric recording sites. *J. Neurosci. Methods* **208,** 101–107 (2012).

101. Pereira, D. B. *et al.* Fluorescent false neurotransmitter reveals functionally silent dopamine vesicle clusters in the striatum. *Nat. Neurosci.* **19,** 578–586 (2016).

102. Hoffman, A. F., Spivak, C. E. & Lupica, C. R. Enhanced Dopamine Release by Dopamine Transport Inhibitors Described by a Restricted Diffusion Model and Fast-Scan Cyclic Voltammetry. *ACS Chem. Neurosci.* (2016). doi:10.1021/acschemneuro.5b00277

103. Yin, H. H., Knowlton, B. J. & Balleine, B. W. Lesions of dorsolateral striatum preserve outcome expectancy but disrupt habit formation in instrumental learning. *Eur. J. Neurosci.* **19,** 181–189 (2004).

104. Yin, H. H. & Knowlton, B. J. Contributions of Striatal Subregions to Place and Response Learning. *Learn. Mem.* **11,** 459–463 (2004).

105. Lerner, T. N. *et al.* Intact-Brain Analyses Reveal Distinct Information Carried by SNc Dopamine Subcircuits. *Cell* **162,** 635–647 (2015).

106. Omiatek, D. M. *et al.* The real catecholamine content of secretory vesicles in the CNS revealed by electrochemical cytometry. *Sci. Rep.* **3,** 1447 (2013).

107. Omiatek, D. M., Dong, Y., Heien, M. L. & Ewing, A. G. Only a fraction of quantal content is released during exocytosis as revealed by electrochemical cytometry of secretory vesicles. *ACS Chem. Neurosci.* **1,** 234–245 (2010).

108. Rooney, K. E. & Wallace, L. J. Computational modeling of extracellular dopamine kinetics suggests low probability of neurotransmitter release. *Synapse* **69,** 515–525 (2015).

109. Lohr, K. M. *et al.* Increased vesicular monoamine transporter enhances dopamine release and opposes Parkinson disease-related neurodegeneration in vivo. *Pnas* **111,** 9977–82 (2014).

110. Calipari, E. S., Huggins, K. N., Mathews, T. A. & Jones, S. R. Conserved dorsal-ventral gradient of dopamine release and uptake rate in mice, rats and rhesus macaques. *Neurochem. Int.* **61,** 986–991 (2012).

111. Cragg, S. J., Hille, C. J. & Greenfield, S. a. Functional domains in dorsal striatum of the nonhuman primate are defined by the dynamic behavior of dopamine. *J. Neurosci.* **22,** 5705–5712 (2002).

112. Cragg, S. J., Hille, C. J. & Greenfield, S. a. Dopamine release and uptake dynamics within nonhuman primate striatum in vitro. *J. Neurosci.* **20,** 8209–8217 (2000).

113. Sesack, S. R., Hawrylak, V. A., Matus, C., Guido, M. A. & Levey, A. I. Dopamine axon varicosities in the prelimbic division of the rat prefrontal cortex exhibit sparse immunoreactivity for the dopamine transporter. *J. Neurosci.* **18,** 2697–708 (1998).

114. Marcott, P. F., Mamaligas, A. A. & Ford, C. P. Phasic Dopamine Release Drives Rapid Activation of Striatal D2-Receptors. *Neuron* **84,** 164–176 (2014).

115. Strand, A. M. & Venton, B. J. Flame etching enhances the sensitivity of carbon-fiber microelectrodes. *Anal. Chem.* **80,** 3708–3715 (2008).

116. Zhang, H. & Sulzer, D. Frequency-dependent modulation of dopamine release by nicotine. *Nat. Neurosci.* **7,** 581–582 (2004).